



NTNU – Trondheim
Norwegian University of
Science and Technology

Thrust allocation for DP in ice

Henrik Emil Wold

Master of Science in Engineering Cybernetics

Submission date: June 2013

Supervisor: Lars Imsland, ITK

Co-supervisor: Øivind Kåre Kjerstad, IMT
Roger Skjetne, IMT

Norwegian University of Science and Technology
Department of Engineering Cybernetics

PROJECT DESCRIPTION SHEET**Name of the candidate:** Henrik Emil Wold**Thesis title (Norwegian):****Thesis title (English):** Thrust allocation for DP in ice**Background**

As offshore oil- and gas production enters arctic seas, the presence of ice becomes a substantial challenge in station-keeping operations. Ice affects most aspects of the operation, and also the DP control system, including thrust allocation. This master study should investigate thrust allocation in ice, its capacity to withstand ice environmental forces, and its use for “ice clearance”. The study builds on project work fall 2012.

Work Description

1. Give a brief overview of ice management operations, and the role of the DP system in this regard. Give a brief account of DP system and components, with emphasis on thruster allocation.
2. Implement a thrust allocation system based on numerical optimization (for a “typical”/given vessel). As thruster dynamics may be important for allocation performance, suggest ways to incorporate such dynamic constraints.
3. Thrust capability: Suggest methodology for checking, and informative illustrations for, thrust capabilities with respect to ice forces. Use ice force data from towing tests in ice to illustrate.
4. Extend thrust allocation with “ice clearance by thruster wake”, that is, define (possibly time-varying) minimum thruster forces in given directions.
5. Implement prioritization of degrees of freedom relevant for DP in ice, to achieve “graceful”/predictable degradation of allocation performance when ice loads are too high.
6. If time permits: How can a possible drift-off be predicted from ice force data (from towing tests, in conjunction with thruster allocation)? Is it possible to use some sort of energy analysis, that is, do the forces integrated over time contain too much energy for the thrust allocation to withstand?
7. Make illustrative simulations, and discuss and conclude on findings.

Start date: January 14th 2013**Due date:** June 10th 2013**Supervisor:** Lars Imsland**Co-advisor(s):** Øivind Kåre Kjerstad and Roger Skjetne, IMT NTNU

Trondheim, __28.02.2013_____

**Lars Imsland**
Supervisor

AddressSem Sælandsvei 5
NO-7491 Trondheim**Org.no.** 974 767 880E-mail:
postmottak@itk.ntnu.no
<http://www.itk.ntnu.no>**Location**O.S. Bragstads plass 2D
NO-7034 Trondheim**Phone**

+ 47 73 59 43 76

Fax

+ 47 73 59 45 99

Phone: + 47 47 23 19 49

Abstract

The commercial industry has initiated work on how to make it feasible to enter the Arctic seas. Ice loads affects most aspects of the Arctic operation, and the marine crafts must be able to handle them all. The DP control system, and thus the thrust allocation, is not designed to handle ice loads and will not work properly [24].

The main purpose of this master thesis is to enhance the thrust allocation for handling ice loads. This is done by including thruster dynamics and adding thruster ice clearance by thruster wake. When the ice loads are too high for the DP system to handle, a prioritization of the degrees of freedom is included to achieve predictable degradation of performance. To predict possible drift-offs, energy analysis will be used to investigate if the control forces integrated over time contain enough energy to withstand the ice loads.

The thrust allocation is based on numerical optimization and implemented in *Matlab*. To make the thrust allocation more realistic, thruster dynamics are added. The first method is to low-pass filter the control forces, and the second is to add restrictions on the change of control forces. To clear the ice away from the hull, thruster ice clearance is implemented. The first solution is to let the algorithm calculate the azimuth angles within predefined sectors, and secondly to force the azimuth thrusters to follow predefined references in control forces and azimuth angles.

A case study is done to investigate the performance of the thrust allocation algorithm, where towing tank measurement data from CIV Arctic is used as input. To measure the performance of the thrust allocation, the magnitude of the slack term, $\mathbf{s}^\top \mathbf{Q} \mathbf{s}$, gives a first impression. For further investigation, the error between the forces and moments from the ice loads and the achieved forces and moments from the thrust allocation is used.

The results from the case study indicated that when the ice loads were high, the prioritization of degrees of freedom was followed. Both with and without thruster dynamics the error in produced thrust was less than 8 [%] for small ice conditions, but increased rapidly for 1.2 [m] of ice. The thruster dynamics did not increase the error significantly, except an increase in yaw error for light ice conditions when the low-pass filter was applied. By adding thruster ice clearance, the error in produced thrust increased. Corresponding results were found for the energy considerations.

The chosen thrust allocation algorithm gave satisfactory results. By decreasing the ice concentrations, for instance by using ice management, the performance was improved. Adding restrictions on the change of control forces was found to be the best way of including thruster dynamics, because then the restrictions were implicit in the thrust

allocation algorithm. Two solutions were also proposed for implementing thruster ice clearance. By letting the thrust allocation find the azimuth angles, the performance of the algorithm was better than by forcing the control forces and azimuth angles to follow predefined references. In spite of this, the second solution was found to be the best in practice because the vessel operator has more control over the thrusters. Some recommendations for future work are to include all the components of the DP control system, do a more advanced implementation of the thruster dynamics and a more detailed energy analysis.

Sammendrag

Den kommersielle industrien har igangsatt arbeid om hvordan det skal muliggjøres å gå inn i arktiske havområder. Isen berører de fleste aspektene ved arktiske operasjoner, og de marine fartøyene må kunne håndtere det. DP-systemet, og dermed thrust-allokeringen, er ikke laget for å håndtere is og vil ikke fungere ordentlig [24].

Hovedformålet med denne masteroppgaven er å forbedre thrust-allokeringen for å håndtere is. Dette gjøres ved å inkludere thruster-dynamikk og thruster-is-klarering ved hjelp av kjølvannet til azimuth-thrusterne. Når iskreftene er for store til at DP-systemet kan håndtere dem, vil en prioritering av frihetsgradene gi en forutsigbar reduksjon av ytelsen. For å kunne forutsi mulig drift-offs, brukes energianalyse for å undersøke om kreftene fra thrusterne over tid inneholder nok energi til å motstå iskreftene.

Thrust-allokeringen er basert på numerisk optimalisering og implementert i *Matlab*. For å gjøre thrust-allokeringen mer realisk er det lagt til thruster-dynamikk. Den første metoden for å løse dette er å lavpassfiltrere kreftene, og den andre er å legge til restriksjoner på endring av krefter. For å hindre at is fester seg til skroget er det implementert thruster-is-klarering. Den første løsningen for å legge til thruster-is-klarering er å la algoritmen kalkulere azimuth-vinklene innenfor forhåndsdefinerte sektorer. Den andre er å tvinge azimuth-thrusterne til å følge forhåndsdefinerte referanser for krefter og azimuth-vinkler.

Det er gjennomført et case-studie for å undersøke ytelsen til thrust-allokeringsalgoritmen, hvor måledata fra en slepetanktest fra CIV Arctic er brukt som inndata. For å måle ytelsen til thrust-allokering brukes slakken for å gi et førsteinntrykk. For videre undersøkelser sammenlignes feilen mellom kreftene og momentene fra isen og de faktiske produserte kreftene og momentene fra thrust-allokeringen.

Resultatene fra case-studiet indikerte at når iskreftene blir for store følges prioriteringen av frihetsgrader. Både med og uten thruster-dynamikk er feilen i produsert thrust mindre enn 8 [%] for små iskrefter, men økte raskt for 1.2 [m] is. Thruster-dynamikken økte ikke feilen betydelig, bortsett fra en økning i gir for små iskrefter når lavpassfilteret ble brukt. Ved å legge til thruster-is-klarering øker feilen i produsert thrust. Tilsvarende resultater ble funnet for energianalysen.

Den valgte thrust-allokeringsalgoritmen ga tilfredstillende resultater. Ved å redusere iskonsentrasjonen, for eksempel ved hjelp av ishåndtering, ble ytelsen forbedret. Det å legge til restriksjoner i endring av krefter er betraktet som den beste måten å legge til thruster-dynamikk, fordi da er begrensingene tatt med implisitt i algoritmen. Det ble foreslått to løsninger for å implementere thruster-is-klarering. Ved å la thrust-allokeringen

finne azimuth-vinklene ble ytelsen til algoritmen bedre enn ved å tvinge kreftene og azimuth-vinklene til å følge forhåndsdefinerte referanser. Til tross for dette var den andre løsningen ansett å være best i praksis, fordi operatøren da har da mer kontroll over thrusterne. Noen anbefalinger for videre arbeid er å sette samme alle komponentene i DP-kontrollsystemet, gjøre en mer avansert implementering av thruster-dynamikken og en mer detaljert energianalyse.

Preface

The work of this thesis has been done in the spring of 2013 and makes the course TTK4990 Master thesis for Engineering Cybernetics at NTNU. It counts for 30 credits and aims to use the knowledge acquired during 5 years of education at the university to do research in collaboration with supervisors.

This project has been conducted in close collaboration with the Research Council of Norway project no. 199567 "Arctic DP" and its consortium partners Statoil, Kongsberg Maritime and Det Norske Veritas. I also wish to thank the Research Council of Norway project no. 188913 "CIV Arctic" and its consortium partners for providing me with the towing tank measurement data for the case study.

I would like to show my gratitude to my supervisor, Professor Lars Imsland, for finding interesting topics of Arctic DP for my master thesis and all the help during the semester.

A special thanks to Ph.D. candidate Øivind Kåre Kjerstad for being my co-supervisor, for providing me with great ideas on how to enhance the thrust allocation for Arctic environments and for always having the office door open when I had questions.

Thanks to my second co-supervisor, Professor Roger Skjetne, for introducing me to interesting research topic in Arctic DP and specifically ideas on how thrust allocation can be enhanced to handle the Arctic.

I must also thank my office colleagues and my friends through the studies for a good working environment and good discussions. Finally, thanks to my girlfriend, Anne-Guro, for always standing by my side.

Henrik Emil Wold
Trondheim, June 2013

Contents

Project Description	iii
Abstract	v
Sammendrag	vii
Preface	ix
List of Figures	xv
List of Tables	xix
Nomenclature	xxi
1 Introduction	1
1.1 Dynamic Positioning	2
1.2 Arctic DP	2
1.3 The DP Control System	3
1.4 Scope of Work	4
1.5 Outline	5
2 Theory	7
2.1 Literature Study	7
2.1.1 Definitions	7
2.1.2 Previous Work on Thrust Allocation	8
2.2 Quadratic Programming	10
2.3 Normalization	11
2.4 Froude Scaling	12
2.5 Low-Pass Filter	12
2.6 Energy Calculation	12
3 Thruster Dynamics	15
3.1 Low-Pass Filter Approach	15
3.2 Restriction on Change of Control Forces	16
4 Thruster Ice Clearance	19
4.1 Background	19

4.2	Implementation Aspects	20
4.2.1	Solution 1	20
4.2.2	Solution 2	21
5	Energy Considerations	25
5.1	Capability Plot	25
5.2	Peek Over Capability	25
6	Case Study	29
6.1	Thrust Allocation Algorithm	29
6.2	CIV Arctic Vessel	29
6.3	Thruster Configuration	30
6.4	Bollard Pull	32
6.5	Azimuth Thrusters	32
6.6	Towing Tank Measurement Data	33
6.7	Reference Signals	35
6.8	Cases	36
6.9	Performance Methodology	36
7	Simulations	39
7.1	Implementation in <i>Matlab</i>	39
7.1.1	Optimization Vector	39
7.1.2	Objective Function	39
7.1.3	Constraints	40
7.1.4	Numerical Differentiation	40
7.1.5	Prioritization of Degrees of Freedom	41
7.1.6	Choice of Parameters	41
7.2	Results Case Study	42
7.2.1	Thrust Allocation	43
7.2.2	Thrust Allocation with Thruster Dynamics	45
7.2.3	Thrust Allocation with Thruster Ice Clearance	47
7.3	Results Energy Considerations	52
8	Discussion	57
8.1	General Discussion	57
8.2	Thrust Allocation	60
8.3	Thrust Allocation with Thruster Dynamics	60
8.4	Thrust Allocation with Thruster Ice Clearance	62
8.5	Energy Considerations	63
9	Conclusion	65
9.1	Concluding Remarks	65
9.1.1	Thrust Allocation	65
9.1.2	Thrust Allocation with Thruster Dynamics	66
9.1.3	Thrust Allocation with Thruster Ice Clearance	66
9.1.4	Energy Considerations	66
9.2	Future Work	67

Bibliography	69
A <i>quadprog</i> Matrices	73
B Appendix Results	75
B.1 Thrust Allocation with Thruster Dynamics	75
B.2 Thrust Allocation with Thruster Ice Clearance	79
C Energy Consideration Tables	85

List of Figures

1.1	Motion of a vessel in 6 DOF. Courtesy of Fossen [8].	2
1.2	DP software modules, with PMS. Courtesy of Sørensen [33].	4
2.1	DP control system.	7
2.2	Butterworth filter, with $T = 20$	13
3.1	Low-pass filtered step.	16
3.2	Step with restrictions on change of control forces, $\Delta \mathbf{f}$	17
4.1	Vessel with TIC.	20
4.2	Reference signals for azimuth angles, $\boldsymbol{\alpha}_{ref}$, for azimuth two (bottom) and four (top).	22
4.3	Two ways of flushing with azimuth thrusters two and four. Top: forces vectors point away from each other. Bottom: Butterfly shape.	23
5.1	DP capability plot. Courtesy of MARINTEK [18].	26
6.1	The CIV Arctic vessel. Courtesy of CIV Arctic.	30
6.2	Thruster configuration for case study vessel.	31
6.3	Change of azimuth angles.	33
6.4	Illustration of model test.	34
6.5	Ice loads for towing tank measurement data.	35
6.6	Measure of performance.	37
7.1	Pendulum analogy.	41
7.2	Results from Case I: $\mathbf{s}^\top \mathbf{Q} \mathbf{s}$, $C = 90$ [%].	44
7.3	Results from Case I: $\mathbf{s}^\top \mathbf{Q} \mathbf{s}$, $C = 100$ [%].	44
7.4	Results from Case I: Error sorted by h_i , $C = 90$ [%]. — Surge, — Sway, — Yaw.	45
7.5	Results from Case I: Error sorted by h_i , $C = 100$ [%]. — Surge, — Sway, — Yaw.	46
7.6	Results from Case I: Error sorted by DOF, $C = 90$ [%]. - - $h_i = 0.5$ [m], — $h_i = 0.8$ [m], \cdots $h_i = 1.2$ [m].	47
7.7	Results from Case I: Error sorted by DOF, $C = 100$ [%]. - - $h_i = 0.5$ [m], — $h_i = 0.8$ [m], \cdots $h_i = 1.2$ [m].	48
7.8	Results from Case II: Error sorted by h_i , $C = 100$ [%]. — Surge, — Sway, — Yaw.	49

7.9	Results from Case III: $\mathbf{s}^\top \mathbf{Q} \mathbf{s}$, $C = 90$ [%].	49
7.10	Results from Case III: Error sorted by DOF, $C = 90$ [%]. - - $h_i = 0.5$ [m], — $h_i = 0.8$ [m], \cdots $h_i = 1.2$ [m].	50
7.11	Results from Case IV: $\mathbf{s}^\top \mathbf{Q} \mathbf{s}$, $C = 100$ [%].	50
7.12	Results from Case IV: Error sorted by h_i , $C = 100$ [%]. — Surge, — Sway, — Yaw.	51
7.13	Results from Case IV: Error sorted by DOF, $C = 90$ [%]. - - $h_i = 0.5$ [m], — $h_i = 0.8$ [m], \cdots $h_i = 1.2$ [m].	52
7.14	Results from Case V: Error sorted by DOF, $C = 90$ [%]. - - $h_i = 0.5$ [m], — $h_i = 0.8$ [m], \cdots $h_i = 1.2$ [m].	53
7.15	Energy of \mathbf{f}_{diff} subtracted energy of $\boldsymbol{\tau}_{diff}$ for lightest ice condition, surge direction.	54
7.16	Frequency analysis of the energy of \mathbf{f}_{diff} and $\boldsymbol{\tau}_{diff}$ for the lightest ice condition, surge direction.	55
7.17	Energy of \mathbf{f}_{diff} subtracted energy of $\boldsymbol{\tau}_{diff}$ for toughest ice condition, surge direction.	55
7.18	Frequency analysis of the energy of \mathbf{f}_{diff} and $\boldsymbol{\tau}_{diff}$ for the toughest ice condition, surge direction.	56
8.1	$\boldsymbol{\tau}_{ice}$ and $\boldsymbol{\tau}_{act}$ for Case I with $C = 100$ [%], $h_i = 1.2$ [m] and $\theta = 10$ [deg]. . .	58
8.2	Initial values for the case study vessel.	59
8.3	$\boldsymbol{\tau}_{ice}$ and $\boldsymbol{\tau}_{act}$ between 870 [s] and 1250 [s] for Case I with $C = 100$ [%], $h_i = 0.5$ [m] and $\theta = 5$ [deg].	61
B.1	Results from Case II: Error sorted by h_i , $C = 90$ [%]. — Surge, — Sway, — Yaw.	75
B.2	Results from Case II: Error sorted by DOF, $C = 90$ [%]. - - $h_i = 0.5$ [m], — $h_i = 0.8$ [m], \cdots $h_i = 1.2$ [m].	76
B.3	Results from Case II: Error sorted by DOF, $C = 100$ [%]. - - $h_i = 0.5$ [m], — $h_i = 0.8$ [m], \cdots $h_i = 1.2$ [m].	76
B.4	Results from Case III: $\mathbf{s}^\top \mathbf{Q} \mathbf{s}$, $C = 100$ [%].	77
B.5	Results from Case III: Error sorted by h_i , $C = 90$ [%]. — Surge, — Sway, — Yaw.	77
B.6	Results from Case III: Error sorted by h_i , $C = 100$ [%]. — Surge, — Sway, — Yaw.	78
B.7	Results from Case III: Error sorted by DOF, $C = 100$ [%]. - - $h_i = 0.5$ [m], — $h_i = 0.8$ [m], \cdots $h_i = 1.2$ [m].	78
B.8	Results from Case IV: $\mathbf{s}^\top \mathbf{Q} \mathbf{s}$, $C = 90$ [%].	79
B.9	Results from Case IV: Error sorted by h_i , $C = 90$ [%]. — Surge, — Sway, — Yaw.	80
B.10	Results from Case IV: Error sorted by DOF, $C = 100$ [%]. - - $h_i = 0.5$ [m], — $h_i = 0.8$ [m], \cdots $h_i = 1.2$ [m].	80
B.11	Results from Case V: $\mathbf{s}^\top \mathbf{Q} \mathbf{s}$, $C = 90$ [%].	81
B.12	Results from Case V: $\mathbf{s}^\top \mathbf{Q} \mathbf{s}$, $C = 100$ [%].	81
B.13	Results from Case V: Error sorted by h_i , $C = 90$ [%]. — Surge, — Sway, — Yaw.	82

B.14 Results from Case V: Error sorted by h_i , $C = 100$ [%]. — Surge, — Sway, — Yaw.	82
B.15 Results from Case V: Error sorted by DOF, $C = 100$ [%]. - - $h_i = 0.5$ [m], — $h_i = 0.8$ [m], \cdots $h_i = 1.2$ [m].	83

List of Tables

1.1	The SNAME notation for marine vessels.	3
2.1	Normalization variables for the bis system.	11
6.1	Moment arm in yaw for the thrusters [39].	31
6.2	Conversion from power to forces.	32
6.3	The parameters used from the CIV Arctic towing tank measurement data.	35
7.1	Possible drift-offs in sway, Case V.	53
C.1	Results energy considerations, Case I.	86
C.2	Results energy considerations, Case II.	87
C.3	Results energy considerations, Case III.	87
C.4	Results energy considerations, Case IV.	88
C.5	Results energy considerations, Case V.	88

Nomenclature

List of Acronyms

- CO Center of origin. Usually a point midships in the water plane.
- DNV Det Norske Veritas.
- DOF Degree of freedom: the set of independent displacements and rotations that specify the displaced position and orientation of the vessel.
- DP Dynamic positioning: a computer-controlled system used to maintain a vessel's position and heading exclusively by use of thrusters.
- GUI Graphical user interface.
- IM Ice management: the sum of all activities where the objective is to reduce or avoid actions from any kind of ice features [7].
- LP Low-pass filter.
- PMS Power management system. The purpose of PMS is to ensure enough available power at all times.
- PSD Power spectral density.
- QP Quadratic programming: an optimization problem with a quadratic objective function and linear constraints [25].
- TA Thrust allocation. The purpose of TA is to convert the generalized forces and moments to forces and directions for the actuators.
- TIC Thruster ice clearance.

List of Variables

- β Scalar weight for the difference in control forces.
- α Azimuth angles.
- α_0 Azimuth angles from previous iteration.
- α_{ref} Reference for azimuth angles.
- ν Generalized velocities.
- Ω Weighting matrix for the change in azimuth angles.

$\boldsymbol{\tau}$	Generalized forces and moments.
$\boldsymbol{\tau}_{act}$	The forces and moments produced by the TA.
$\boldsymbol{\tau}_{diff}$	Ice loads the TA was not able to withstand.
$\boldsymbol{\tau}_{env}$	Environmental forces and moments.
$\boldsymbol{\tau}_{ice}$	Ice loads from the towing tank measurement data from CIV Arctic.
\boldsymbol{D}	Damping matrix.
\boldsymbol{e}_i	i th unit vector.
\boldsymbol{f}	Control forces.
\boldsymbol{f}_0	Control forces from previous iteration.
\boldsymbol{f}_{act}	Control forces which is output from the TA.
\boldsymbol{f}_{diff}	Superfluous control forces from the TA.
\boldsymbol{f}_{max}	Maximum control forces.
\boldsymbol{f}_{ref}	Reference for control forces.
\boldsymbol{K}	Force coefficient matrix.
\boldsymbol{M}	Inertia matrix.
\boldsymbol{P}	Weighting matrix for the control forces.
\boldsymbol{Q}	Weighting matrix for the slack variables.
\boldsymbol{s}	Slack variables.
$\boldsymbol{T}(\boldsymbol{\alpha})$	Thrust configuration matrix.
\boldsymbol{t}_i	Column vectors in the thrust configuration matrix, $\boldsymbol{T}(\boldsymbol{\alpha})$.
\boldsymbol{u}	Vector of control inputs.
\boldsymbol{W}	Weighting matrix for the control forces in singularity avoidance.
\boldsymbol{x}	State vector.
$\Delta\boldsymbol{\alpha}$	Change in azimuth angles.
$\Delta\boldsymbol{f}$	Change in control forces.
ϵ	Scalar for numerical differentiation.
γ	Scalar weight for the difference in azimuth angles.
λ	Scaling factor for Froude scaling.
μ	Body mass density ratio.
∇	Volume of displaced water.
ρ	Water density.

τ_N	Surge and sway part of $\boldsymbol{\tau}$, with denomination [N].
τ_{Nm}	Yaw part of $\boldsymbol{\tau}$, with denomination [Nm].
E_N	Energy for surge and sway.
E_{Nm}	Energy for yaw.
θ	Drift angle in yaw.
ε	Small, positive scalar introduced to avoid division by zero.
ϱ	Scalar weight in singularity avoidance term that affects the relationship between manoeuvrability and power consumption.
a	Linear acceleration.
B	Beam of the vessel.
b_i	Transversal length from center of origin to thruster i .
C	Ice concentration.
h_i	Ice thickness.
I	Moment of inertia.
J	Cost function for the quadratic programming problem.
L_f	Length of full scale vessel.
l_i	Longitudinal length from center of origin to thruster i .
L_m	Length of model vessel.
L_{oa}	Overall length of the vessel.
L_{pp}	Length between perpendiculars.
L_{WL}	Length of the water line of the vessel.
m	Mass of fully laden vessel.
n	Number of degrees of freedom.
p	Number of azimuth thrusters.
r	Number of actuators.
t	Time.
V	Ice drift speed.
x	Linear displacement.
g	Earth's gravity.

Chapter 1

Introduction

In 2008, the United States Geological Survey performed a study to prove the potential for oil and gas exploration north of the Arctic Circle [37]. This study estimated a potential of 90 billion barrels of oil, 47 trillion cubic meters of natural gas and 44 billion barrels of natural gas liquids to be extracted from these areas. This accounts for 22 % of the undiscovered, recoverable resources in the world. By today prices [38], both the oil and natural gas can give an income of nearly USD 16 trillion.

As the polar ice is melting, the Arctic regions are more accessible. The potential for oil and gas exploration is just one example of the many possibilities for these areas. One can imagine that most operation performed in open-water today can be done in the Arctic in the future. This includes everything from offshore supply and oil and gas extraction, to tourism, research and shipping.

Even though the ice is retreating, it will pose a challenge for future Arctic marine operations. The ice loads are large and rapidly varying, making it difficult to predict how they will affect the dynamics of the marine craft. Because the ice is rigid, it will affect the marine craft differently than the other environmental loads, such as wind, waves and ocean currents. The weather at these remote places can be harsh, with low temperatures and high winds. All these challenges need to be handled to make it feasible to go into the Arctic areas. Therefore, research is required to obtain robust and safe technology. As an example, Statoil has tripled their Arctic research budget to NOK 250 million in 2013 [35].

This master thesis is a part of the research project KMB Arctic DP [26] at the Norwegian University of Science and Technology, NTNU. The research project is a collaboration between NTNU and several industrial partners, and the main purposes are to develop both technology and competence for Arctic challenges.

1.1 Dynamic Positioning

Station keeping is an essential part of many marine operations, such as hydrocarbon extraction, platform supply vessels, cruise ships and cable-laying. When the waters are deep, such that mooring is not an option, dynamic positioning (DP) is the only way to maintain the desired position and orientation of the marine craft. The Norwegian classification society, Det Norske Veritas (DNV), defines a DP vessel as [6]:

...a vessel which automatically maintains its position and heading (fixed location or pre-determined track) exclusively by means of thruster force.

To specify the displaced position and orientation of the vessel, degrees of freedom (DOF) is used. The vessel has maximum 6 DOFs, with 3 translational and 3 rotational components. The motions along the x_b , y_b and z_b axes in Figure 1.1 are referred to as surge, sway and heave. The rotations about these axes are referred to as roll, pitch and yaw. This convention follows the SNAME notation [32], given in Table 1.1.

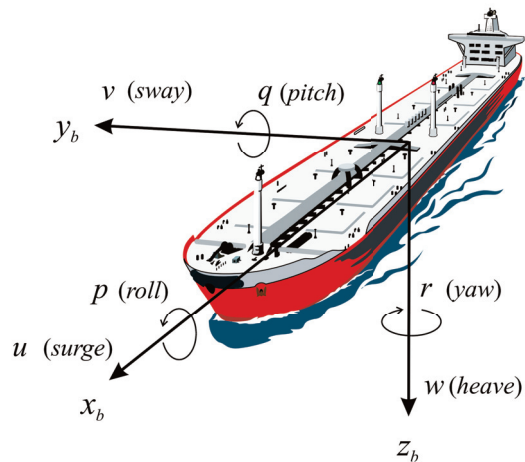


Figure 1.1: Motion of a vessel in 6 DOF. Courtesy of Fossen [8].

DP applications for ships are often simplified to 3 DOFs, including surge, sway and yaw. This is because it is possible to decouple the motion in the horizontal and the vertical plane [8]. On the other hand, sometimes it is desirable to include damping in roll and pitch as well. For instance on semi-submersible oil platforms, cruise ships and operation requiring small roll movement. This increases the level of complexity, but it might be necessary if the vessel is intended to operate in harsh and demanding conditions.

1.2 Arctic DP

Today, DP systems for open-water applications are commercialized and well developed [8, 33]. However, using such systems in the Arctic environment have shown to be infeasible, as they are not designed for handling the ice loads and the induced dynamics [24]. Some

Table 1.1: The SNAME notation for marine vessels.

DOF		Forces and Moments	Linear and Angular Velocities	Positions and Euler Angles
1	Motion in x direction (surge)	X	u	x
2	Motion in y direction (sway)	Y	v	y
3	Motion in z direction (heave)	Z	w	z
4	Rotation about x direction (roll)	K	p	ϕ
5	Rotation about y direction (pitch)	M	q	θ
6	Rotation about z direction (yaw)	N	r	ψ

research areas have been covered, for instance design of ice going vessels [29, 41] and power requirements [14], but DP systems for the Arctic are not well developed. Even though some research has briefly covered the general problems with Arctic DP and the use of azimuth thrusters to improve the DP system [11, 42], no literature was found treating applications of thrust allocation (TA) in Arctic regions.

The large and rapidly varying ice loads acting on the vessel are some of the major challenges with Arctic DP. To argue why this is the case, the DP model is presented [8]:

$$\mathbf{M}\dot{\boldsymbol{\nu}} + \mathbf{D}\boldsymbol{\nu} = \boldsymbol{\tau} + \boldsymbol{\tau}_{env} \quad (1.1)$$

where \mathbf{M} is the inertia matrix, \mathbf{D} is the damping matrix, $\boldsymbol{\nu}$ are generalized velocities, $\boldsymbol{\tau}$ are the generalized forces and moments and $\boldsymbol{\tau}_{env}$ are the environmental forces and moments. The inertia matrix and the damping matrix are constant matrices, and designed for open-water applications. When operating in ice it is believed that both matrices change due to the interaction with the rigid ice loads [16]. The larger the ice loads, the more the open-water model, Equation (1.1), deviates from the real world. In turn, performance of the DP system will be reduced. With a deviating model, the deduction of the appropriate generalized forces and moments, $\boldsymbol{\tau}$, will be slower and less accurate.

Another important aspect is that the integral effect in the DP control law cannot be too aggressive. The relation between input and response is not as distinct as in open-water and might result in undesirable behaviour and poor performance.

1.3 The DP Control System

The overall goal of any DP system is to calculate the required thruster forces and moments in order to maintain the desired position and orientation of the vessel. The software doing this is typically divided into several modules, as illustrated in Figure 1.2. The reason for the modularization is that it is easier to use, maintain and replace modules.

The most important modules in Figure 1.2 are signal processing, observer, controller and TA. An adaptive law can be included to update the parameters in the observer and the controller, if that is necessary. The power management system (PMS) is not a part

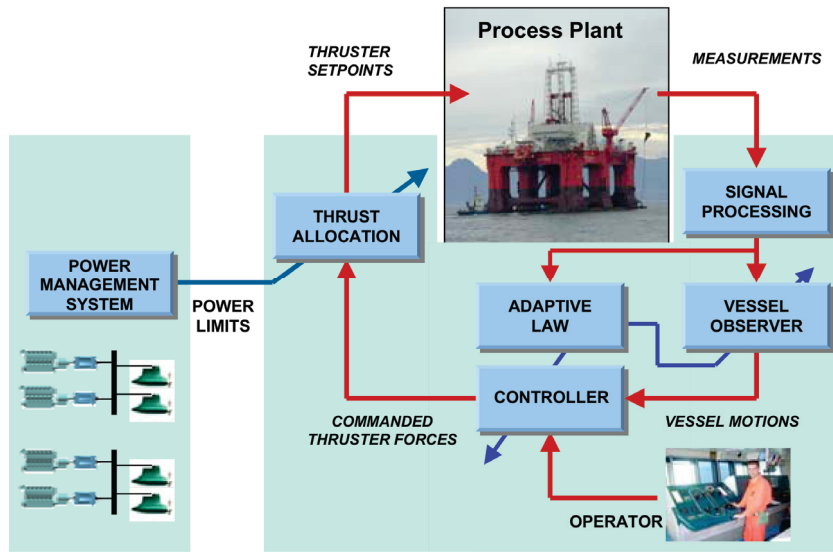


Figure 1.2: DP software modules, with PMS. Courtesy of Sørensen [33].

of the DP control system, but is necessary in practice to ensure sufficient power levels. The first module, signal processing, analyses and handles the input measurements to provide feasible signals to the observer. This can include noise reduction, signal checks and voting. The observer estimates unmeasured signals, for instance velocity, and filter measured signals. The control law compares the output from the observer with a reference to determine how much the vessel needs to move in surge, sway and yaw to keep the desired position and orientation. At last, the TA distributes the generalized forces and moments from the control law to forces and directions for each of the thrusters.

1.4 Scope of Work

This master thesis will focus on the TA module in Figure 1.2, and investigate how this can be enhanced to handle operations in ice. It is assumed that the other modules in Figure 1.2 are in place and functioning properly. The ice conditions subject to investigation are managed ice, which usually is produced by one or more icebreakers performing ice management (IM) upstream from the DP vessel [24].

The motivation of this work is to investigate how the TA can be optimized for marine operations in the Arctic. This includes examining whether the ice loads can be reduced and the manoeuvrability can be increased by actively using the thrusters, for instance by using the azimuth thrusters to clear the ice away from the hull. When the TA is not able to counteract for all the ice loads, a prioritization of DOFs can be included to achieve predictable degradation of the TA. The TA algorithm is implemented and a case study, using towing tank measurement data from CIV Arctic, is carried out. Because of the ice's nature it is necessary to also look at the thruster dynamics.

1.5 Outline

In Chapter 2, theory and background material will be presented. Chapter 3 contains a brief discussion on why thruster dynamics should be incorporated in the TA, and two ways of solving this problem is suggested. An introduction to thruster ice clearance and aspects of practical implementation is presented in Chapter 4. Two tools for indicating when the vessel is not able to keep position and heading is described in Chapter 5. In Chapter 6 a case study is presented. The results from this is presented in Chapter 7, in addition to aspects of implementation in *Matlab*. A discussion of the findings from the case study is given in Chapter 8, and finally some concluding remarks and recommendations for further work are given in Chapter 9.

This thesis is a continuation of the project work presented in [43]. It is chosen to make this report as extensive as possible, and therefore some of the sections are based on work from [43]. Sections 4.1, 6.1, 6.4, 7.1.1, 7.1.3 and 7.1.4 are copied from the project report, and sections 2.1, 2.2, 4.2, 4.2.1, 6.3, 7.1.2 and 7.1.6 are based on material from the report.

Chapter 2

Theory

This chapter will give a review of important background theory. Some important variables for the TA are defined, and then previous work on TA will be presented. After that, quadratic programming, normalization, adjustment for model scaling of the vessel, low-pass filtering and energy calculations will briefly be presented.

2.1 Literature Study

The modularization of the simplified DP control system in Figure 1.2 provides opportunities to replace one or more of the modules. In this project the TA module is extracted to analyse and make modifications for Arctic operations.

Extracting the middle module of Figure 2.1, the TA can be treated as a stand-alone system with the generalized forces and moments, $\boldsymbol{\tau}$, as input and the control forces, \boldsymbol{f} , as output. If azimuth thrusters are applied, the azimuth angles, $\boldsymbol{\alpha}$, may as well be outputs of the TA. Assuming that the TA always produces outputs adequately fast, such that the bandwidth of the DP control system is not affected, this simplification should hold.

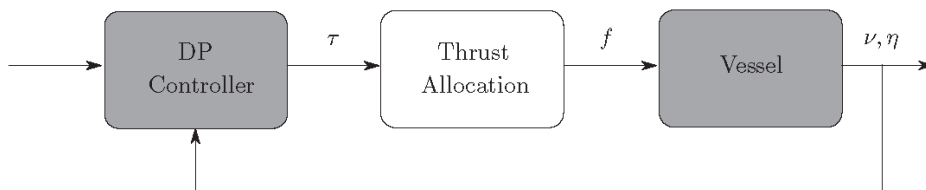


Figure 2.1: DP control system.

2.1.1 Definitions

Before presenting the TA algorithms, some basic terms must be defined. n is the number of DOFs, r is the number of actuators and p is the number of azimuth thrusters. The following definitions are provided by [8].

The control forces, $\mathbf{f} = [f_1, \dots, f_r]^\top \in \mathbb{R}^r$, are defined as:

$$\mathbf{f} = \mathbf{K}\mathbf{u} \quad (2.1)$$

where $\mathbf{K} \in \mathbb{R}^{r \times r}$ is the diagonal force coefficient matrix and $\mathbf{u} = [u_1, \dots, u_r]^\top \in \mathbb{R}^r$ are the control inputs to the actuators.

The relationship between the generalized forces and moments, $\boldsymbol{\tau} = [\tau_1, \dots, \tau_n]^\top \in \mathbb{R}^n$, and the control forces, \mathbf{f} , is given by:

$$\boldsymbol{\tau} = \mathbf{T}(\boldsymbol{\alpha})\mathbf{f} \quad (2.2)$$

where $\mathbf{T}(\boldsymbol{\alpha}) \in \mathbb{R}^{n \times r}$ is the thrust configuration matrix and $\boldsymbol{\alpha} = [\alpha_1, \dots, \alpha_p]^\top \in \mathbb{R}^p$ are the azimuth angles. Equation (2.2) is the primary constraint in all the TA algorithms.

The thrust configuration matrix, $\mathbf{T}(\boldsymbol{\alpha})$, is defined as:

$$\mathbf{T}(\boldsymbol{\alpha}) = [\mathbf{t}_1, \dots, \mathbf{t}_r] \quad (2.3)$$

where $\mathbf{t}_i \in \mathbb{R}^n$ are column vectors. For azimuth thrusters and tunnel thrusters the column vectors, in 3 DOF, is gives as:

$$\mathbf{t}_i = [\cos(\alpha_i), \sin(\alpha_i), l_i \sin(\alpha_i) - b_i \cos(\alpha_i)]^\top \quad (2.4)$$

$$\mathbf{t}_i = [0, 1, l_i]^\top \quad (2.5)$$

where l_i and b_i denotes the lengths from the center of origin (CO) to thruster i , in longitudinal and transverse direction, respectively, and α_i is the azimuth angle for thruster i .

It is preferred to use the control forces, \mathbf{f} , instead of the control inputs, \mathbf{u} , as the output of the TA module. The denomination for the control forces, \mathbf{f} , are Newton [N]. For the control inputs, \mathbf{u} , the denominations are either pitch or revolutions per minute of the thruster blades. When interpreting the results it is more convenient to use Newton as the denomination because it is more practical and closer related to power consumption. This way it is easier to analyse the efficiency of the TA algorithm.

2.1.2 Previous Work on Thrust Allocation

Typical for TA problems in DP applications are that they are over-actuated, $r > n$. In practice, this means that there are more control inputs than controllable DOFs. Because of this, the problem is to distribute the generalized forces and moments to each of the thrusters in an optimal manner. This may be important because the available resources, such as fuel and the thrusters themselves, should be distributed in the best possible way. The over-actuated TA problem is formulated as an optimization problem with respect to physical restrictions, such as power consumption and wear and tear of the thrusters.

Overview of Thrust Allocation Algorithms

The simplest form of TA is power minimization, with no state constraints. An explicit solution is found using the geometric inverse of Equation (2.2).

In real life, the actuators do not have infinite amount of available power. Therefore, it is natural to have constraints on the control forces applied to the thrusters. A more sophisticated version of the TA will include the constraints on the control forces.

Using azimuth thrusters as actuators, constraints on the azimuth angles and azimuth angle rates can be introduced. It can be desirable to restrict the azimuth angles so that challenges with superfluous rotations are avoided. Azimuth thrusters can be enormous, the propeller diameter can be up to 7.8 [m] [1], so the azimuth angle rates are limited. In the most sophisticated TA presented in [8], the restrictions on azimuth angles and azimuth angle rates are included. Also, a singularity avoidance term is added in the cost function to penalize singularity configurations [12]. The reason for penalizing singularity configuration is to avoid linearly dependent thrusters. For azimuth thrusters it means that several thrusters have equal azimuth angles. If a sudden change in ice loads occurs, the possibility for a drift-off is present because the thruster may not be able to change azimuth angles fast enough. If the TA is able to avoid near-singular thruster configurations the thrusters may be better distributed around 360 [deg], and it is more likely that changes in ice loads can be counteracted for.

Thrust Allocation with Singularity Avoidance

In the last 20 years the use of azimuth thrusters on ice going vessels has increased rapidly [9]. Compared to traditional propulsion, using main propeller with rudder, azimuth thrusters can offer better manoeuvrability when performing operations on ice. Therefore, using a TA algorithm that utilizes azimuth thrusters are a natural choice when enhancing the TA to operate in Arctic environments. Singularity configurations of the azimuth thrusters may result in a non-optimal solution resulting in higher power consumption and less manoeuvrability [12]. Therefore, it is desirable to include the singularity avoidance term in the cost function.

Formulated as a convex optimization problem, this TA algorithm is given as [8]:

$$J = \min_{\Delta \mathbf{f}, \Delta \boldsymbol{\alpha}, \mathbf{s}} \{ (\mathbf{f}_0 + \Delta \mathbf{f})^\top \mathbf{P} (\mathbf{f}_0 + \Delta \mathbf{f}) + \mathbf{s}^\top \mathbf{Q} \mathbf{s} + \Delta \boldsymbol{\alpha}^\top \boldsymbol{\Omega} \Delta \boldsymbol{\alpha} + \left. \frac{\partial}{\partial \boldsymbol{\alpha}} \left(\frac{\rho}{\varepsilon + \det(\mathbf{T}(\boldsymbol{\alpha}) \mathbf{W}^{-1} \mathbf{T}^\top(\boldsymbol{\alpha}))} \right) \right|_{\boldsymbol{\alpha}=\boldsymbol{\alpha}_0} \Delta \boldsymbol{\alpha} \} \quad (2.6)$$

subject to:

$$\mathbf{s} + \mathbf{T}(\boldsymbol{\alpha}_0) \Delta \mathbf{f} + \left. \frac{\partial}{\partial \boldsymbol{\alpha}} (\mathbf{T}(\boldsymbol{\alpha}) \mathbf{f}) \right|_{\boldsymbol{\alpha}=\boldsymbol{\alpha}_0, \mathbf{f}=\mathbf{f}_0} \Delta \boldsymbol{\alpha} = \boldsymbol{\tau} - \mathbf{T}(\boldsymbol{\alpha}_0) \mathbf{f}_0 \quad (2.7)$$

$$\mathbf{f}_{min} - \mathbf{f}_0 \leq \Delta \mathbf{f} \leq \mathbf{f}_{max} - \mathbf{f}_0 \quad (2.8)$$

$$\boldsymbol{\alpha}_{min} - \boldsymbol{\alpha}_0 \leq \Delta \boldsymbol{\alpha} \leq \boldsymbol{\alpha}_{max} - \boldsymbol{\alpha}_0 \quad (2.9)$$

$$\Delta \boldsymbol{\alpha}_{min} \leq \Delta \boldsymbol{\alpha} \leq \Delta \boldsymbol{\alpha}_{max} \quad (2.10)$$

where \mathbf{f}_0 and $\boldsymbol{\alpha}_0$ are the control forces and azimuth angles from the previous iteration, $\Delta\mathbf{f}$ and $\Delta\boldsymbol{\alpha}$ are the change in control forces and azimuth angles, $\mathbf{s} \in \mathbb{R}^n$ are the slack variables, $\mathbf{P} \in \mathbb{R}^{r \times r}$, $\mathbf{Q} \in \mathbb{R}^{n \times n}$ and $\boldsymbol{\Omega} \in \mathbb{R}^{p \times p}$ are positive definite weighting matrices for the states, $\varrho > 0$ is a scalar weight that influences the relationship between manoeuvrability and power consumption, $\varepsilon > 0$ is a small number to avoid division by zero and $\mathbf{W} \in \mathbb{R}^{r \times r}$ is a positive definite weighting matrix for the control forces in the singularity avoidance term.

In the derivation of the optimization problem, equations (2.6) - (2.10), some simplifications must be introduced. First of all, the power consumption is in reality proportional to $\mathbf{f}^{3/2}$ [34], but is locally approximated to a quadratic term in \mathbf{f} such that $\mathbf{f} = \mathbf{f}_0 + \Delta\mathbf{f}$. The singularity avoidance term introduces a non-convex term that can be locally approximated by a linear term around the last azimuth angle, $\boldsymbol{\alpha}_0$, such that $\boldsymbol{\alpha} = \boldsymbol{\alpha}_0 + \Delta\boldsymbol{\alpha}$. Making these approximations yields a convex optimization problem, equations (2.6) - (2.10), which can be solved using standard software for numerical optimization.

2.2 Quadratic Programming

The TA algorithm, equations (2.6) - (2.10), is formulated as an optimization problem with a quadratic objective function subject to linear constraints. This type of optimization problem is the definition of quadratic programming (QP) [25]. Using the m-file function *quadprog* [22] in the Optimization ToolboxTM in *Matlab*, the optimization problem can be rewritten on matrix form:

$$\min_{\mathbf{x}} \quad \left\{ \frac{1}{2} \mathbf{x}^\top \mathbf{H} \mathbf{x} + \mathbf{g}^\top \mathbf{x} \right\} \quad (2.11)$$

subject to:

$$\mathbf{A} \mathbf{x} \leq \mathbf{b} \quad (2.12)$$

$$\mathbf{A}_{eq} \mathbf{x} = \mathbf{b}_{eq} \quad (2.13)$$

$$\mathbf{lb} \leq \mathbf{x} \leq \mathbf{ub} \quad (2.14)$$

Note that in the objective function, \mathbf{g} is used as the vector of linear terms instead of \mathbf{f} , which is the standard *quadprog* notation. This is to avoid confusion with the vector of control forces in Equation (2.1).

The active set method is used to solve the QP problem. It is an old and well proven algorithm and works well for most of minor optimization problem [25], compared to the interior point method. Briefly speaking, the active set method searches along the active set of constraints, which is the equality constraints and the inequality constraints that are equal to zero for the given state [25], to find the optimal solution of the QP problem. In short, the general structure of the primal active set algorithm, for convex optimization problems, can be given as:

```

Find a feasible initial point and the active set.
for  $i = 0, 1, 2, \dots$ 
Solve QP with equality constraints for active set, to find step.
  if(step = 0)
    Compute Lagrange multipliers for active set.
    if(Lagrangian multiplier = 0)
      Optimal solution is found.
    else
      Remove constraints with most negative Lagrange multiplier.
  else (step  $\neq 0$ )
    Compute step length.
    Move the solution in desired direction.
    if(blocking constraints)
      Add blocking constraint in active set.
end

```

The reader is referred to [25] for more detailed description of the active set method and definitions of the Lagrange multipliers.

2.3 Normalization

According to [8], two of the most commonly used normalization systems are the prime system and the bis system. The prime system is mostly used in ship manoeuvring, and not applicable for DP application due to zero division. The bis system, on the other hand, avoids the division of speed by using $\sqrt{\frac{L_{pp}}{g}}$ as the time unit. Therefore, for DP applications the bis system is the preferred normalization system, as well as for high speed applications.

The bis system is chosen for this purpose because the problems with zero division are avoided. Table 2.1 summarizes the normalization variables used in this report. The variables used in Table 2.1 are: $\mu = \frac{m}{\rho \nabla}$ is the body mass density ratio ($\mu = 1$ for floating vessels), ρ is the water density, g is the acceleration of gravity, ∇ is the volume of displaced water and L_{pp} is the length between perpendiculars.

Table 2.1: Normalization variables for the bis system.

Unit	Bis normalization
Force	$\mu \rho g \nabla$
Moment	$\mu \rho g \nabla L_{pp}$
Angle	1

2.4 Froude Scaling

The forces and moments in the CIV Arctic towing tank measurement data, described in Section 6.6, are scaled to full scale. Froude scaling must therefore be applied to adjust for the scaling of the vessel used in the model test.

The scaling factor is given as [10]:

$$\lambda = \frac{L_f}{L_m} \quad (2.15)$$

where L_f is the full scale length and L_m is the model length of the vessel. λ represents how much larger the full scale vessel is compared to the model.

Applying the scaling factor, λ , in Equation (2.15), the time, t , is scaled according to [10]:

$$\sqrt{\lambda} \cdot t \quad (2.16)$$

2.5 Low-Pass Filter

A low-pass filter (LP) is designed to remove frequencies above a certain frequency, the cut-off frequency, ω_c . For ideal LP filters the frequencies below ω_c will pass through the filter.

For this project it is chosen to use the Butterworth filter as a LP filter. The Butterworth filter is designed to have a maximally flat magnitude in the passband and monotonically descend in the stopband [28]. Using the syntax in the m-file function *butter* [20], of first order, in the Signal Processing ToolboxTM in *Matlab* the digital domain transfer function is given as:

$$H(z) = \frac{b_1 + b_2 z^{-1}}{1 + a_2 z^{-1}} \quad (2.17)$$

where a_2 , b_1 and b_2 are the filter coefficients.

Applying the filter coefficients in the Butterworth filter, Equation (2.17), as well as the vector to be LP filtered into the m-file function *filter* [21] in *Matlab* yields the LP filtered input vector.

A Bode diagram showing the magnitude and phase of the LP filter is given in Figure 2.2, where $T = 20$ is the time constant.

2.6 Energy Calculation

The denomination of energy is joule (J). One joule is defined to be the work done by applying one unit of force [N] to move a point one meter [27]. One joule is therefore equal to one newton times one meter.

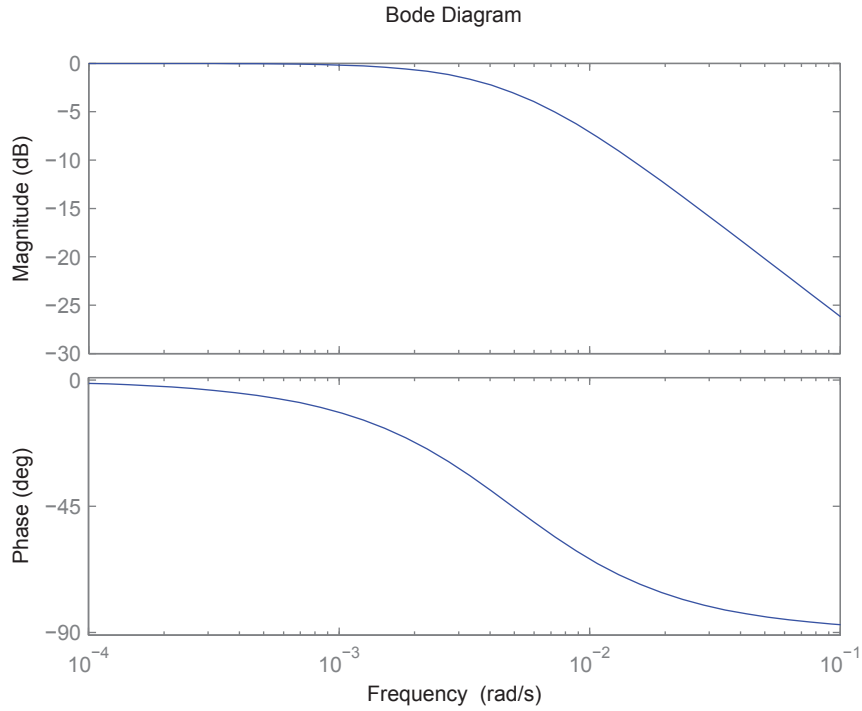


Figure 2.2: Butterworth filter, with $T = 20$.

Calculations of the energy of the forces in surge and sway is given as:

$$\begin{aligned}
 E_N &= \tau_N \cdot x \\
 &= \tau_N \cdot \frac{1}{2} \cdot a \cdot t^2 \\
 &= \tau_N \cdot \frac{1}{2} \cdot \frac{\tau_N}{m} \cdot t^2 \\
 &= \frac{1}{2m} \cdot \tau_N^2 \cdot t^2
 \end{aligned} \tag{2.18}$$

where τ_N is the surge and sway part of τ , x is the linear displacement, a is the linear acceleration, t is the time and m is the mass of the fully laden vessel. The acceleration, a , is calculated using Newton's second law.

According to [27], the denomination of yaw is [Nm], which can be given as energy per angle. In other words, $[Nm] = \frac{[J]}{[rad]}$. By reshuffling this equation, the energy of the yaw component of τ can be calculated as:

$$\begin{aligned}
 E_{Nm} &= \tau_{Nm} \cdot \theta_r \\
 &= \tau_{Nm} \cdot \frac{1}{2} \cdot \alpha \cdot t^2 \\
 &= \tau_{Nm} \cdot \frac{1}{2} \cdot \frac{\tau_{Nm}}{I} \cdot t^2 \\
 &= \frac{1}{2I} \cdot \tau_{Nm}^2 \cdot t^2
 \end{aligned} \tag{2.19}$$

where τ_{Nm} is the sway part of τ , θ is the drift angle, α is the angular acceleration, t is the time and I is the moment of inertia. The moment of inertia is given as [39]:

$$I = \left(\frac{L_{WL}}{4} \right)^2 \cdot m$$

where L_{WL} is the length of the water line of the vessel and m is the mass.

Chapter 3

Thruster Dynamics

It is assumed that the thruster dynamics are more important for the performance of the TA in ice compared to open-water, because of the induced dynamics of the ice loads. In open-water, the environmental forces acting on the vessel changes relatively slow. Because of the nature of the ice, an impact between the vessel and the ice loads yields large forces and moments for the DP control system to withstand. If, for instance, the vessel crushed the ice, the forces to withstand dropped quickly. To be able to withstand these ice loads, the control forces must change quickly and frequently. In real life applications some time is needed to adjust for new thruster levels, and a new engine might need to be started [39]. To make the TA algorithm more realistic for operations in ice, some way of incorporate constraints on the thruster dynamics should be included.

This chapter will present two possible solutions for including thruster dynamics in the TA algorithm. First, a LP filter approach where the control forces are LP after the optimization. The second approach is to include restrictions on the change of control forces, $\Delta \mathbf{f}$, implicitly in the TA.

3.1 Low-Pass Filter Approach

As a first thought, the time needed to adjust the pitch or propeller speed on the thrusters can be achieved by approximating the control forces, \mathbf{f} , using a LP filter. In this project it is chosen to do this off-line using a first-order Butterworth filter, as described in Section 2.5.

The time constant for adjusting the control forces is guesstimated to be approximately 65 [s]. By trial and error, 65 [s] gave satisfactory results in terms of comparing the LP filtered control forces with the original control forces. This parameter is specific for each thruster and engine, and it is not critical to have the exact value for this project. Finding the exact time constant is not the main focus of this report and no further effort will be put into finding more a more realistic value. Applying the LP filter, given in Figure 2.2, to a step from zero to one yields the result given in Figure 3.1.

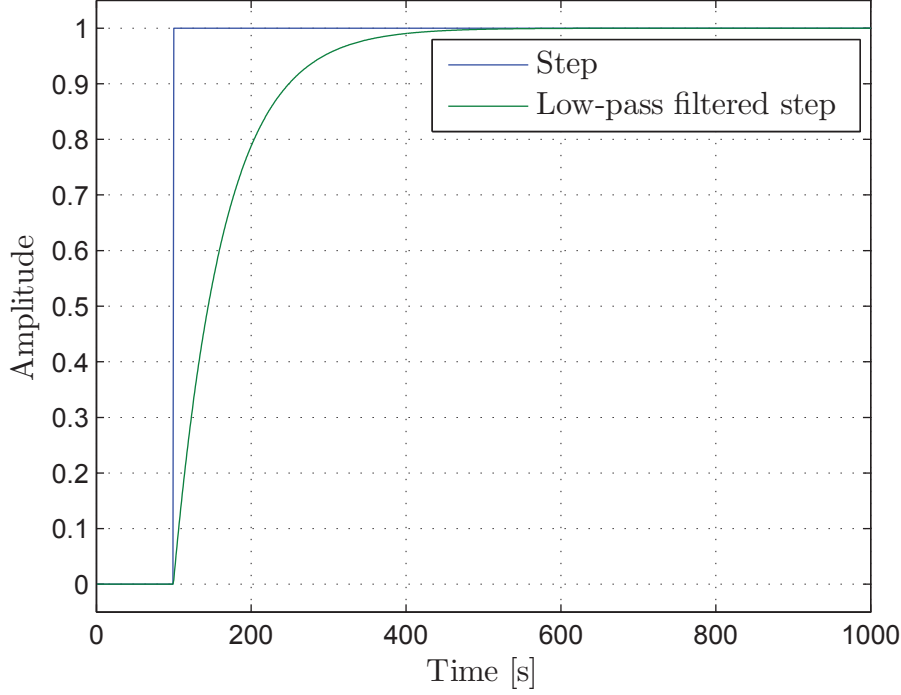


Figure 3.1: Low-pass filtered step.

3.2 Restriction on Change of Control Forces

Another way of solving the problem of adding thruster dynamics is to add restrictions to the TA algorithm, equations (2.6) - (2.10). Equivalent to the restriction on change of azimuth angles, $\Delta\alpha$, in Equation (2.10), a restriction on change of control forces, $\Delta\mathbf{f}$, can be added:

$$\Delta\mathbf{f}_{min} \leq \Delta\mathbf{f} \leq \Delta\mathbf{f}_{max} \quad (3.1)$$

The TA algorithm including the restriction on change of control forces, in Equation (3.1), is given by:

$$J = \min_{\Delta\mathbf{f}, \Delta\alpha, s} \left\{ (\mathbf{f}_0 + \Delta\mathbf{f})^\top \mathbf{P} (\mathbf{f}_0 + \Delta\mathbf{f}) + \mathbf{s}^\top \mathbf{Q} \mathbf{s} + \Delta\alpha^\top \Omega \Delta\alpha + \frac{\partial}{\partial \alpha} \left(\frac{\varrho}{\varepsilon + \det(\mathbf{T}(\alpha) \mathbf{W}^{-1} \mathbf{T}^\top(\alpha))} \right) \Big|_{\alpha=\alpha_0} \Delta\alpha \right\} \quad (3.2)$$

subject to:

$$\mathbf{s} + \mathbf{T}(\alpha_0) \Delta\mathbf{f} + \frac{\partial}{\partial \alpha} (\mathbf{T}(\alpha) \mathbf{f}) \Big|_{\alpha=\alpha_0, \mathbf{f}=\mathbf{f}_0} \Delta\alpha = \boldsymbol{\tau} - \mathbf{T}(\alpha_0) \mathbf{f}_0 \quad (3.3)$$

$$\mathbf{f}_{min} - \mathbf{f}_0 \leq \Delta\mathbf{f} \leq \mathbf{f}_{max} - \mathbf{f}_0 \quad (3.4)$$

$$\alpha_{min} - \alpha_0 \leq \Delta\alpha \leq \alpha_{max} - \alpha_0 \quad (3.5)$$

$$\Delta\mathbf{f}_{min} \leq \Delta\mathbf{f} \leq \Delta\mathbf{f}_{max} \quad (3.6)$$

$$\Delta\alpha_{min} \leq \Delta\alpha \leq \Delta\alpha_{max} \quad (3.7)$$

A disadvantage of using the LP filter to approximate the thruster dynamics is that the control forces, \mathbf{f} , is filtered after optimization. The TA algorithm does not know of the thruster dynamics and the results may become non-optimal. The results may be more accurate if the LP filtering is done on-line, but will not be optimal before the restrictions are included in the TA algorithm. It is therefore believed that the best choice is to include restrictions in the TA algorithm.

The rate restrictions, $\Delta \mathbf{f}_{min}$ and $\Delta \mathbf{f}_{max}$, are for instance dependent on the engines, the thrusters and the PMS, because of physical limitations and to protect the equipment from large steps in working points. For these reasons, the minimum and maximum limits are in real life dependent on the engine and thruster state. According to conversations [40] with Ph.D. candidate Aleksander Veksler at NTNU and Mr. Helge Asle Lundeberg, from Scana Mar-El, using diesel-mechanical propulsion limitation on the control forces should be on minimum 20 to 30 [s] from 0 [%] to 100 [%] of thrust. In real life, the step from 0 [%] to 100 [%] thrust is divided in three stages, i.e. $[0, 60)$, $[60, 90)$ and $[90, 100]$, with approximately 10 [s] in every interval. As a simplification these three intervals are added together and one time constant is used for 0 [%] to 100 [%] of thrust. When the vessel is using diesel-electric propulsion the time constant can be smaller, probably close to half, relative to diesel-mechanic propulsion. Therefore, for diesel-electric propulsion, the time for 0 [%] to 100 [%] is chosen to be 20 [s].

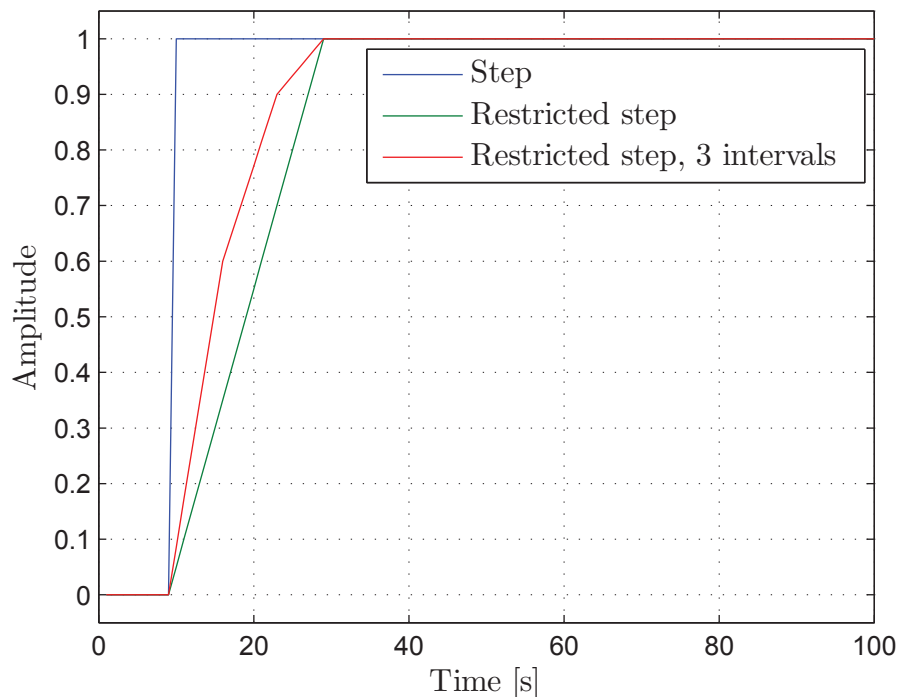


Figure 3.2: Step with restrictions on change of control forces, $\Delta \mathbf{f}$.

The concept of restricting the change of control forces is illustrated in Figure 3.2. As an illustrative example, a step from zero to one is applied at time $t = 10$ [s]. Restricting the control forces from 0 to 100 [%] to 20 [s], as described above, the restricted step will reach

one at time $t = 30$ [s]. Dividing the restricted step in 3 intervals, $[0, 60)$, $[60, 90)$ and $[90, 100]$, with 6.67 [s] ($\frac{20}{3} \approx 6.67$) in each interval yields a steeper slope in the interval $[0, 60)$ and a gentler slope in the interval $[90, 100]$. Approximating the three intervals into one interval, $[0, 100]$, the slope will be $\frac{1}{20}$ [$\frac{1}{s}$]. As seen in Figure 3.2, dividing the restricted step in 3 intervals will give a faster rise in the interval $[0, 60)$, but to make it as easy as possible the approximation of one interval is chosen for this project.

Chapter 4

Thruster Ice Clearance

Thruster ice clearance (TIC) is a mode for clearing ice from the hull by use of azimuth thrusters. Using the wakes of the azimuth thrusters to clear the ice has shown to give positive results in real life [3, 15]. It is believed that it can be useful for IM, to change the vessel's position and/or heading and to prevent the vessel from getting stuck in the ice.

The crew on board the Finnish icebreaker "MSV Fennica", operating in the Chukchi Sea, found the wakes of the thrusters so powerful that they were used to clear the ice away [3]. As the ice drifted past the vessel, the thruster wakes broke the ice and left a clear passage behind for other vessels to operate in.

This chapter will motivate TIC and aspects regarding practical implementation. Two possible solutions for implementation will be presented. Some focus will be given to how to make it user friendly for the vessel operator who actually might use this in real life.

4.1 Background

When operating in Arctic environments, ice might adhere on the vessel and the possibility for getting stuck increases. Between the late 1960s and early 1990s, several vessels used an air bubble system to prevent this [41]. It was quite efficient, but additional equipment was needed, such as compressors, valves and piping. The extra equipment needed space on the vessel, it consumed extra energy and modification had to be made on the hull.

As stated in Chapter 2.1.2, the use of azimuth thrusters for marine vessels operating in the Arctic has increased considerably in the past 20 years. With the flexibility of changing the force direction, the azimuth thrusters can replace the air bubble system as a self IM system. The wake of the azimuth thrusters is powerful and used for both breaking the ice and clearing it away from the hull [15]. The ice clearance can be very useful to prevent the ice adhere the vessel and reduce the ice resistance along the hull.

Using azimuth thrusters instead of the air bubble system releases a lot of space and no extra equipment is needed. A disadvantage of using the azimuth thrusters as a self IM solution is that more effort is required to keep desired position and orientation. On the

other hand, the alternative equipment for clearing the ice uses extra power. Therefore, the extra power consumption due to the azimuth thrusters might not be substantial.

The idea of using the azimuth thrusters for self IM is not entirely new [11, 31, 42], but more research needs to be done in order to incorporate it into the TA algorithm.

4.2 Implementation Aspects

Two solutions for implementing TIC are presented sections 4.2.1 and 4.2.2. Some focus will be given to how to make it user friendly for the vessel operator. First, some aspects applying for both ideas will be covered.

For a vessel to be able to apply TIC, it must be equipped with a set of thrusters such that some of them can be used for the DP operation and some can be used for TIC. Figure 4.1 shows a vessel where TIC can be applied. For this vessel, the two front azimuth thrusters are used for TIC and the two rear azimuth thrusters are used for keeping desired position and heading. The vessel is in addition equipped with bow thrusters, which can be used to help keeping the desired position and heading if necessary. If the ice concentration in the area is high, it might be advantageous not to use the tunnel thrusters. This is because ice can get sucked into the tunnel thrusters and break them.

The blue sectors in Figure 4.1 indicates how and where the TIC can work. The azimuth thrusters will apply forces within these sectors, for instance at constant azimuth angles or continuously flush back and forth. The indicated sectors in Figure 4.1 are examples of how they can look like. More research has to be done to find the optimal sectors, and how the TIC is resolved in an optimal manner. In this report the TIC concept in Figure 4.1 will be used.

The top priority for the DP system is to keep the desired position and heading. If the rear azimuth thrusters are not able to counteract for the extra forces and moments introduced by the TIC, the clearing of ice must be stopped. Even though this topic is important, it will not be discussed further.

4.2.1 Solution 1

The first way of solving TIC is to restrict the azimuth angles to be within the blue sectors in Figure 4.1, and let the TA algorithm find the optimal azimuth angles within these.

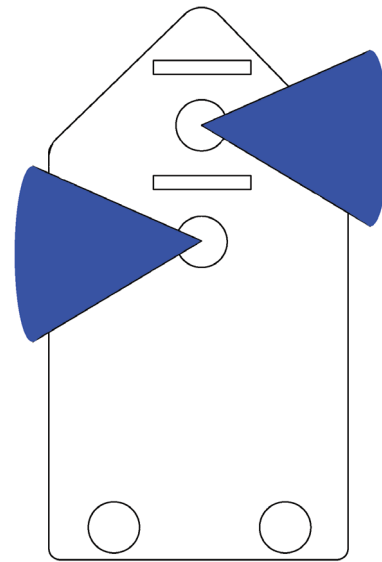


Figure 4.1: Vessel with TIC.

Sometimes, the TA algorithm can give non-optimal azimuth angles for azimuth thruster two and four. This can be because it might not be optimal to apply forces in the directions of the azimuth thrusters within these sectors. If so, the control forces for these azimuth angles will be zero, and TIC will not be applied. This can be solved by forcing the TA to apply control forces to azimuth thruster two and four by setting the minimum control forces, \mathbf{f}_{min} , to be positive values. One way of finding these positive values is to run the TA algorithm without TIC. The average value of the control forces, \mathbf{f} , are then used as minimum control forces, \mathbf{f}_{min} , for azimuth thruster two and four.

Using this way of solving TIC, the TA algorithm will decide which azimuth angles, within the restricted sectors, that resists the ice loads, $\boldsymbol{\tau}_{ice}$, in the best possible way.

From the vessel operator's perspective, it can be useful to have a simple graphical user interface (GUI) where the TIC mode can be activated and possibly some simple specifications can be made. It can be desirable for the vessel operator to be able to specify the minimum control forces, \mathbf{f}_{min} and the width of the sectors. To make it simple, the vessel operator can for instance choose between "little", "middle" and "high" level of minimum control forces, and corresponding for the sectors. If the ice conditions is estimated, the minimum control forces, \mathbf{f}_{min} , can be set automatically based on mathematical models.

4.2.2 Solution 2

Solution 1 leaves little control for the vessel operator to decide which directions to point the azimuth thrusters used for TIC. The second solution aims to give the vessel operator more freedom to point the azimuth thrusters where it is desirable. To achieve this, azimuth thruster two and four are extracted from the first and third term in the objective function, Equation (2.6). To be able to let the vessel operator control the behaviour of the azimuth thrusters, two quadratic terms are added to force azimuth thruster two and four to follow predefined references in control forces, \mathbf{f}_{ref} , and azimuth angles, $\boldsymbol{\alpha}_{ref}$. β and γ are scalar weights for the difference in control forces and azimuth angles, respectively. The optimization algorithm, with the quadratic deviation terms, is given as:

$$J = \min_{\Delta \mathbf{f}, \Delta \boldsymbol{\alpha}, \mathbf{s}} \{ (\mathbf{f}_0 + \Delta \mathbf{f})_{1,3,5,6}^\top \mathbf{P}_{1,3,5,6} (\mathbf{f}_0 + \Delta \mathbf{f})_{1,3,5,6} + \mathbf{s}^\top \mathbf{Q} \mathbf{s} + \Delta \boldsymbol{\alpha}_{5,6}^\top \boldsymbol{\Omega}_{5,6} \Delta \boldsymbol{\alpha}_{5,6} + \frac{\partial}{\partial \boldsymbol{\alpha}} \left(\frac{\rho}{\varepsilon + \det(\mathbf{T}(\boldsymbol{\alpha}) \mathbf{W}^{-1} \mathbf{T}^\top(\boldsymbol{\alpha}))} \right) \Big|_{\boldsymbol{\alpha}=\boldsymbol{\alpha}_0} \Delta \boldsymbol{\alpha} + \beta (\mathbf{f}_{2,4} - \mathbf{f}_{ref})^\top (\mathbf{f}_{2,4} - \mathbf{f}_{ref}) + \gamma (\boldsymbol{\alpha}_{2,4} - \boldsymbol{\alpha}_{ref})^\top (\boldsymbol{\alpha}_{2,4} - \boldsymbol{\alpha}_{ref}) \} \quad (4.1)$$

subject to:

$$\mathbf{s} + \mathbf{T}(\boldsymbol{\alpha}_0) \Delta \mathbf{f} + \frac{\partial}{\partial \boldsymbol{\alpha}} (\mathbf{T}(\boldsymbol{\alpha}) \mathbf{f}) \Big|_{\boldsymbol{\alpha}=\boldsymbol{\alpha}_0, \mathbf{f}=\mathbf{f}_0} \Delta \boldsymbol{\alpha} = \boldsymbol{\tau} - \mathbf{T}(\boldsymbol{\alpha}_0) \mathbf{f}_0 \quad (4.2)$$

$$\mathbf{f}_{min} - \mathbf{f}_0 \leq \Delta \mathbf{f} \leq \mathbf{f}_{max} - \mathbf{f}_0 \quad (4.3)$$

$$\boldsymbol{\alpha}_{min} - \boldsymbol{\alpha}_0 \leq \Delta \boldsymbol{\alpha} \leq \boldsymbol{\alpha}_{max} - \boldsymbol{\alpha}_0 \quad (4.4)$$

$$\Delta \boldsymbol{\alpha}_{min} \leq \Delta \boldsymbol{\alpha} \leq \Delta \boldsymbol{\alpha}_{max} \quad (4.5)$$

Azimuth thruster two and four are not extracted from the singularity avoidance term in the objective function, Equation (2.6), and the constraints, equations (2.7) - (2.10), because these equations must be calculated using all the thrusters.

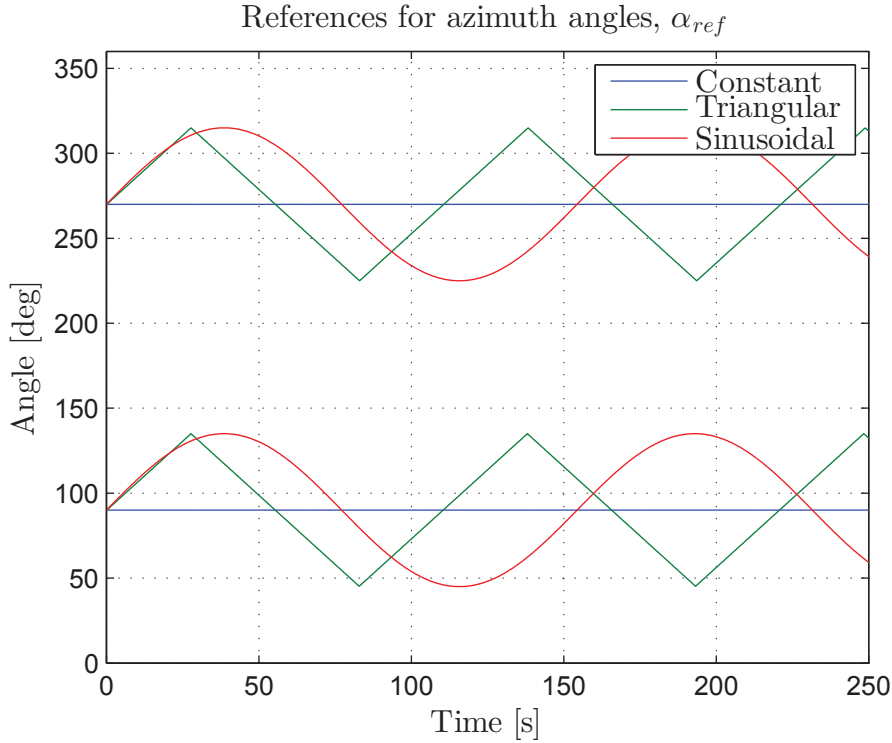


Figure 4.2: Reference signals for azimuth angles, α_{ref} , for azimuth two (bottom) and four (top).

From the vessel operator's perspective, the two interesting parameters are the references in control forces, \mathbf{f}_{ref} , and azimuth angles, α_{ref} . For the reference in the control forces, \mathbf{f}_{ref} , the same applies as for the minimum control forces, \mathbf{f}_{min} , described in the latter part of Section 4.2.1. For the reference in azimuth angles, α_{ref} , the GUI can display different choices of reference signals for the vessel operator. Figure 4.2 displays three different examples of reference signals for azimuth angles that can be applied. First keeping a constant angle, then a triangular signal and at last a sinusoidal signal. The lower part of Figure 4.2 is the reference for azimuth thruster two and the upper part is for azimuth thruster four. The period of the signals are not equal, and is just meant to illustrate possible reference signals for the azimuth angles. The simplest reference is to keep a constant azimuth angle, α , where the vessel operator can specify the azimuth angle. The more advanced reference is to let the azimuth thrusters, used for TIC, to flush back and forth, using triangular or sinusoidal signals. The triangular signal can be easier to imagine and a first choice, but it is discontinuous when reaching the ends of the sectors. The sinusoidal signal is smooth and continuously differentiable, and therefore a more suitable signal to use in practice. Using the sinusoidal signal, there will be less wear and tear of the thrusters because there are no sudden changes in the azimuth angles. Parameters for the vessel operator to choose are the width of the flushing sectors, as in Figure 4.1, and how fast to flush.

To make it easier for the vessel operator, some specific choices of reference signals can be standard. The vessel operator can then change parameters, as the width of the sectors and the speed of flushing, if desired. In the beginning, the vessel operator must activate the TIC mode manually. Later, if some system to decide when to activate TIC is developed, it can be done automatically.

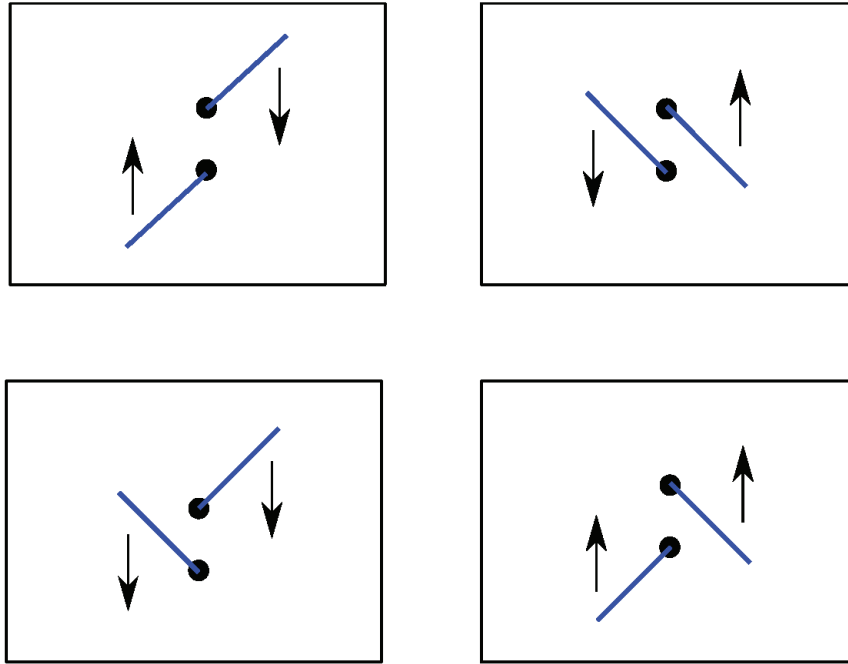


Figure 4.3: Two ways of flushing with azimuth thrusters two and four. Top: forces vectors point away from each other. Bottom: Butterfly shape.

For the triangular and the sinusoidal reference it is chosen to always let force vectors of azimuth thrusters two and four point away from each other, as in the top part of Figure 4.3. This is like the roll motion on an aircraft, when the wings represent the force vectors of the azimuth thrusters. The other way of flushing the azimuth thrusters in TIC mode is as a bird flapping with its wings, called the butterfly shape in the bottom part Figure 4.3. It is believed that pointing the azimuth thrusters from each other, such that the force vectors always will be close to 180 [deg] between each other, will induce less moment compared to the butterfly shape. This because the butterfly shape will force the vessel to move a little back and forth while flushing. By pointing the control forces away from each other, it is believed that if the azimuth thrusters are close enough such that the induced moment will be small, and probably negligible.

Chapter 5

Energy Considerations

This chapter will give a brief introduction to why DP capability plots are not, at least with today's mathematical models, suitable for predicting possible drift-offs for vessels operating in the Arctic. An alternative method using energy analysis will be presented.

5.1 Capability Plot

A DP capability plot is, according to DNV [5], defined as a

...graphic illustration of vessel's position and heading keeping capacity in a specified vessel condition and specified environmental condition.

The vessel condition involves for instance the thrusters, and the environmental conditions involve wind, waves and current [2]. An example of a DP capability plot is given in Figure 5.1. The vessel is in the middle and for this particular example the green line is the maximum limit of wind the vessel is able to withstand for a given heading. If DP capability plots are to be used for vessels operating in the Arctic, ice loads must also be included in this guideline.

In open-water, the environmental forces and moments are calculated using experimental results [8], but this is not the case for ice loads. Mathematical models of ice are not well developed because of the quantity of ice parameters and ice properties [23]. The ice loads are also fluctuating and it can be difficult to model how and when the ice loads will affect the vessel. In [36], some work on DP capability plot including ice loads is done, but the problem is to get realistic models for the ice loads. Therefore, another solution to predict the DP capability for vessels operating in the Arctic is presented.

5.2 Peek Over Capability

An alternative way of predicting possible drift-offs can be to investigate if the ice loads, integrated over time, contain too much energy for the TA to withstand. To do this, two

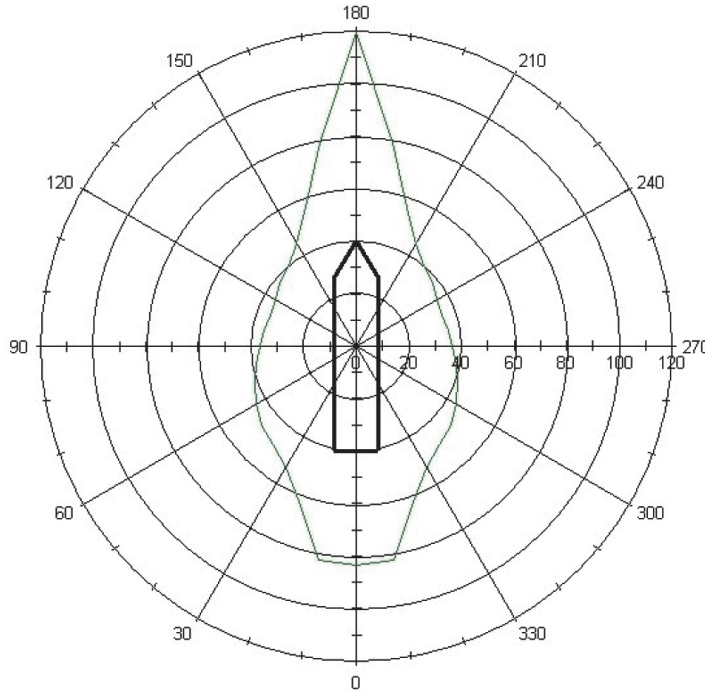


Figure 5.1: DP capability plot. Courtesy of MARINTEK [18].

variables are defined. First, the superfluous control forces are defined as:

$$\mathbf{f}_{diff} = \mathbf{f}_{max} - \mathbf{f}_{act} \geq 0 \quad (5.1)$$

which is how much of the control forces the TA did not need to withstand the ice loads. Then, the variable peek over capability is defined as [17]:

$$\boldsymbol{\tau}_{diff} = -\boldsymbol{\tau}_{ice} - \mathbf{T}(\boldsymbol{\alpha})\mathbf{f}_{act} \quad (5.2)$$

which is how much of the ice loads the TA was not able to counteract for. $\boldsymbol{\tau}_{ice}$ are the measurements of the ice loads from the towing tank test. They are negative because $\boldsymbol{\tau}_{ice}$ are the generalized forces and moments from the ice acting on the vessel. Input to the TA must be the other way around, the generalized forces and moments from the vessel to counteract for the ice loads.

Large peeks in ice loads may result in drift-offs and it is therefore interesting to investigate if the vessel is able to come back to its original position and heading after the peek has passed, and how much time it will take. When the TA is able to withstand all the ice loads perfectly, $\boldsymbol{\tau}_{diff}$ is equal to zero. If it becomes positive, meaning that the ice loads are larger than what the TA is able to withstand, \mathbf{f}_{diff} must be investigated to see if the vessel is able to come back to the desired position and heading in a sufficiently short period of time. If \mathbf{f}_{diff} is equal to zero, the TA uses all the available control forces and has nothing more to give if the vessel loses position. For the vessel to be able to come back in the original position, \mathbf{f}_{diff} must be positive for a sufficiently large time after the drift-off. Analysing the energy of these two variables can give an indication of possible drift-offs. If the vessel is required to be on DP, the energy of \mathbf{f}_{diff} must be larger than

the energy of τ_{diff} . The energy of f_{diff} and τ_{diff} is calculated according to practises described in Section 2.6, using equations (2.18) and (2.19). In the frequency plane the area of f_{diff} must be larger than the area of τ_{diff} to accomplish the same.

Chapter 6

Case Study

The material presented in chapters 2.1, 3, 4 and 5 are general and applies for all types of marine crafts. To demonstrate the performance of the TA, a case study of an intervention vessel is carried out.

This chapter will present the case study vessel, discuss the appurtenant values, briefly discuss the towing tank measurement data from CIV Arctic, discuss the reference signals for TIC, present the cases for the case study and finally suggest a methodology for checking the performance of the TA.

6.1 Thrust Allocation Algorithm

Based on the argumentation in Section 2.1.2, the thrust allocation algorithm, given in equations (2.6) - (2.10), is chosen for the case study. This is the most sophisticated TA algorithm and it accounts for many of the practical aspects, like restrictions on control forces, azimuth angles and azimuth angle rates.

6.2 CIV Arctic Vessel

CIV Arctic KMB [19] has been a project at MARINTEK, in the period 2008 to 2012, for which the objective was to extend the operating season into seasonal ice for construction and intervention vessels. The CIV Arctic project has designed an Arctic construction and intervention vessel, the CIV Arctic vessel. The vessel was designed for operation in the Norwegian parts of the Barents Sea, with high operability in both open-water and first year ice up to 0.7 [m] [4].

The CIV Arctic vessel, pictured in Figure 6.1, is chosen as the case study vessel in the project. The vessel is designed using the double acting concept [13], and can be used both bow first for DP operations and open-water applications and stern first for ice breaking.

In stern first mode, the two rear Azipods are often used as main propulsion units, while in DP mode all six thrusters might be used.

The overall length, L_{oa} , of the CIV Arctic vessel is 121.8 [m], the length between perpendiculars, L_{pp} , is 109.3 [m] and the beam, B , of the vessel is 24.0 [m]. The maximum power is 5 [MW] for the two rear Azipods and 1.5 [MW] for the two front retractable azimuth thrusters and the two tunnel thrusters. The propulsion system includes these six thrusters and four diesel generators at 4 [MW] each, adding up to a total of 16 [MW] of power.



Figure 6.1: The CIV Arctic vessel. Courtesy of CIV Arctic.

6.3 Thruster Configuration

The CIV Arctic vessel is, as described above, equipped with two main Azipods in the stern and two retractable azimuth thrusters in the bow, in addition to two tunnel thrusters in the bow. A detailed sketch of the thruster configuration, with all the appurtenant variables, can be seen in Figure 6.2. f_i denotes the control force for thruster i , α_i denotes the azimuth angle for azimuth thruster i and l_i and b_i denotes the lengths from CO to thruster i , in longitudinal and transverse direction, respectively.

Provided the notation in Figure 6.2 and the definitions in equations (2.3) - (2.5), the thruster configuration matrix, $\mathbf{T}(\boldsymbol{\alpha})$, is given by:

$$\mathbf{T}(\boldsymbol{\alpha}) = \begin{bmatrix} 0 & \cos(\alpha_2) & 0 & \cos(\alpha_4) & \cos(\alpha_5) & \cos(\alpha_6) \\ 1 & \sin(\alpha_2) & 1 & \sin(\alpha_4) & \sin(\alpha_5) & \sin(\alpha_6) \\ l_1 & l_2 \sin(\alpha_2) & l_3 & l_4 \sin(\alpha_4) & -l_5 \sin(\alpha_5) & -l_6 \sin(\alpha_6) \\ & & & & -b_5 \cos(\alpha_5) & +b_6 \cos(\alpha_6) \end{bmatrix} \quad (6.1)$$

where l_i and b_i is given in Table 6.1, f_i is the control force for thruster i and α_i is the angle between x_b and f_i . Both f_i and α_i are outputs of the optimization problem given in equations (2.6) - (2.10).

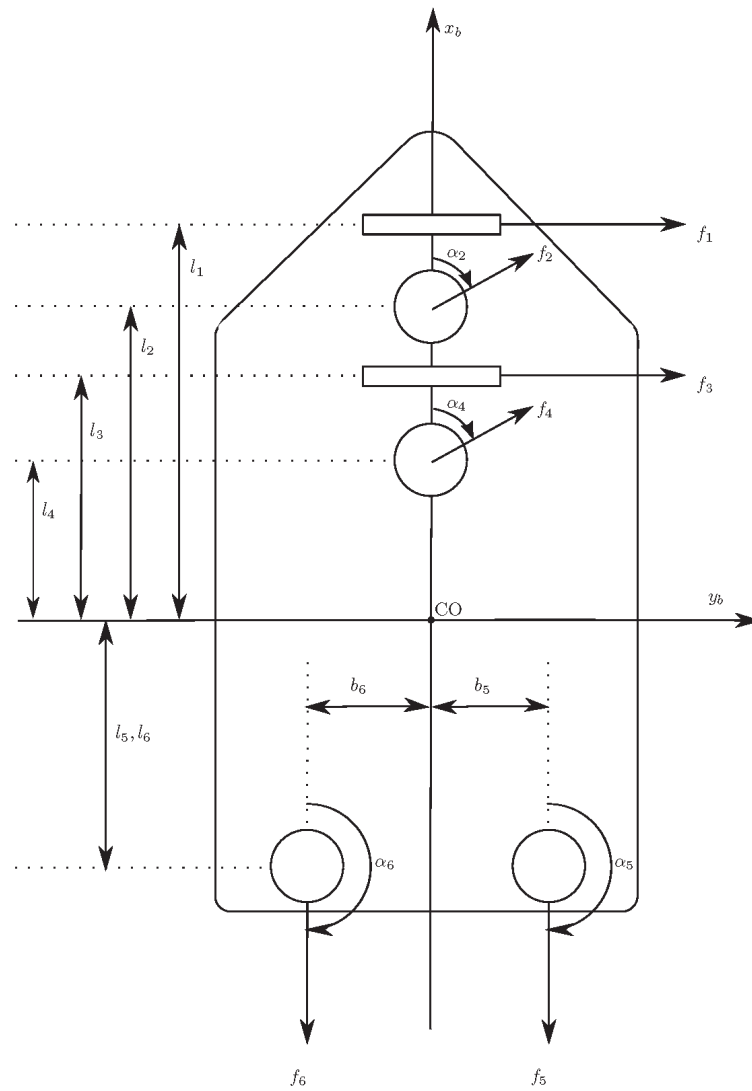


Figure 6.2: Thruster configuration for case study vessel.

Table 6.1: Moment arm in yaw for the thrusters [39].

Distance from CO
$l_1 = 49.9$ [m]
$l_2 = 45.9$ [m]
$l_3 = 42.3$ [m]
$l_4 = 38.3$ [m]
$l_5 = 52.5$ [m]
$l_6 = 52.5$ [m]
$b_5 = 6$ [m]
$b_6 = 6$ [m]

6.4 Bollard Pull

Section 6.2 provided information on the maximum power of the thrusters for the CIV Arctic vessel. To find the maximum control forces, f_{max} , the thruster power is converted from [MW] to [kN] by calculating the bollard pull.

As a rule of thumb [44], the bollard pull is given by:

$$\text{Bollard Pull} = \frac{0.9 \cdot c \cdot \text{BHP}}{100} \cdot 1000 \cdot 9.81[\text{N}] \quad (6.2)$$

where c is a constant, dependent on fixed/controllable pitch propeller and Kort nozzle, and BHP is break horse power (1 [kW] \approx 1.34 [HP]). The multiplication with $1000 \cdot 9.81$ is done to convert the bollard pull from metric tonnes to [N]. Assuming that all the azimuth thrusters have fixed pitch propeller without Kort nozzle, then $c = 1.10$. The results are given in Table 6.2.

Table 6.2: Conversion from power to forces.

Thruster power	Control forces
5 [MW]	651 [kN]
1.5 [MW]	195 [kN]

It is important to notice that Equation (6.2) is an empirical formula which gives rough estimates of the bollard pull. It is chosen for this work because it is not critical that the maximum control forces, f_{max} , are exact.

Only positive thrust for the azimuth thrusters are allowed because they are often optimized for producing thrust in one direction [30]. It is chosen to let the tunnel thrusters apply thrust in both positive and negative direction, which is defined in Figure 6.2, meaning that the minimum control forces, f_{min} , are negative of the maximum control forces, f_{max} .

6.5 Azimuth Thrusters

The azimuth thrusters are not able to rotate infinitely fast, partly because of what was discussed in Section 2.1.2. In the report describing the towing tank measurement data from the CIV Arctic vessel [39], it is stated that the azimuth thrusters can rotate 24 [deg/s], in model scale. To adjust for the model scaling, Froude scaling must be applied. Looking at the unit for the azimuth angles rates, [deg/s], the numerator is scaled with 1 and the denominator with the square root of λ according to Equation (2.16). The scaling factor, λ , for the CIV Arctic vessel, defined in Equation (2.15), is given as:

$$\lambda = 24.138 \quad (6.3)$$

The resulting azimuth angle rates, $\Delta\alpha$, are:

$$\Delta\alpha = 24 \cdot \frac{1}{\sqrt{\lambda}} \left[\frac{\text{deg}}{\text{s}} \right] = \frac{24}{\sqrt{24.138}} \left[\frac{\text{deg}}{\text{s}} \right] = \frac{24}{4.913} \left[\frac{\text{deg}}{\text{s}} \right] = 4.885 \left[\frac{\text{deg}}{\text{s}} \right] \quad (6.4)$$

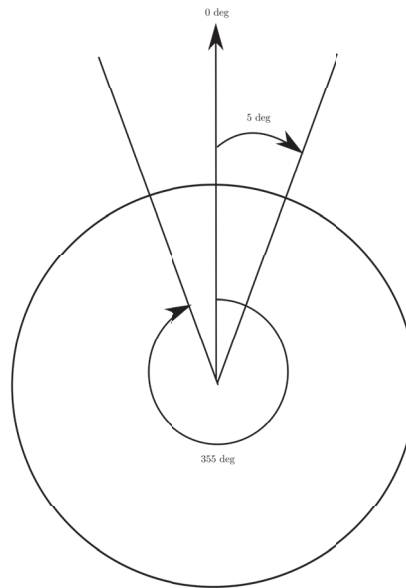


Figure 6.3: Change of azimuth angles.

The azimuth thrusters can rotate 360 [deg] around. If the azimuth thrusters are allowed to rotate around and around, the azimuth angles might grow to infinity. To prevent this from happening, it is chosen to constraint the azimuth angles between 0 [deg] and 360 [deg]. A problem then arises in the transaction between 0 and 360 [deg]. An example is if the azimuth angles are to change from 355 [deg] to 5 [deg]. It is not optimal to do a full rotation, because the angles can be changed only 10 [deg] crossing 0 [deg], see Figure 6.3. Note that the figure is illustrative and the angles might not correspond 5 [deg] and 355 [deg]. A solution could be to map the azimuth angles from 360 to 0 [deg] when crossing 360 [deg]. In that way, the azimuth thrusters can change the angles from 355 [deg] to 360 [deg] and since 360 [deg] equals 0 [deg], another rotation on 5 [deg] can be done to reach 5 [deg]. Also, if the azimuth angles becomes below 0 [deg], the azimuth angles are mapped to 360 [deg].

6.6 Towing Tank Measurement Data

As input to the TA algorithm, towing tank measurement data from CIV Arctic [39] is used. These data were gathered in May 2011 in the Aker Arctic test facility in Helsinki, Finland. The best data comes from full scale test from real life tests, but this is expensive. It can also be difficult to gather real life data for a wide variety of parameters, so a towing tank test is most likely the best way of measuring the ice loads acting on the vessel [11].

The CIV Arctic vessel was towed, without any propulsion, through a stationary ice sheet at constant speed with a fixed drift angle, as illustrated in Figure 6.4. The dark blue area is open-water and the light blue squares on the top are ice floes. The vessel is attached to the light grey test carriage via a 6-component balance, and towed through the ice. The forces acting on the vessel is measured, and converted to full scale forces and moments in

surge, sway and yaw, according to standard practices [39]. The measurement data were trimmed to exclude the parts when the vessel was not completely inside the ice sheet. These parts include the beginning, when the vessel entered the ice sheet, and the end of the model basin when the ice was packed together. The ice was prefabricated in desired square floe size and concentration. To remove effects from carriage vibrations and natural frequencies from the vessel and the 6-component balance, a 1 [Hz], 8th order Butterworth LP filter was applied to remove the noise.

Several tests were done varying the ice thickness, h_i , ice concentration, C , drift speed, V and drift angle, θ .

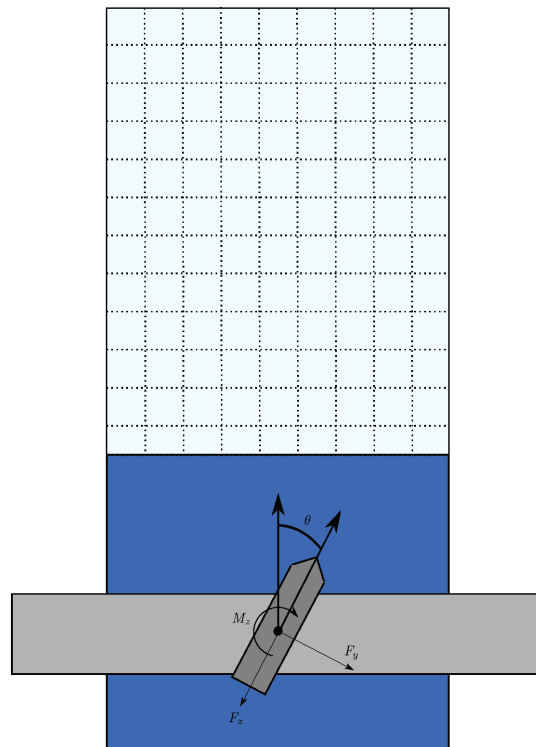


Figure 6.4: Illustration of model test.

To exemplify how the towing tank measurement data can look like, an example using the toughest ice conditions is presented in Figure 6.5. Note that these data are normalized, using his normalization from Section 2.3. As seen in the figure, the forces in sway are in average 3 times as large as the forces in surge. The moment in yaw seems to be small, because the normalization, but in reality it is nearly an average of 10 times as large as the forces in surge.

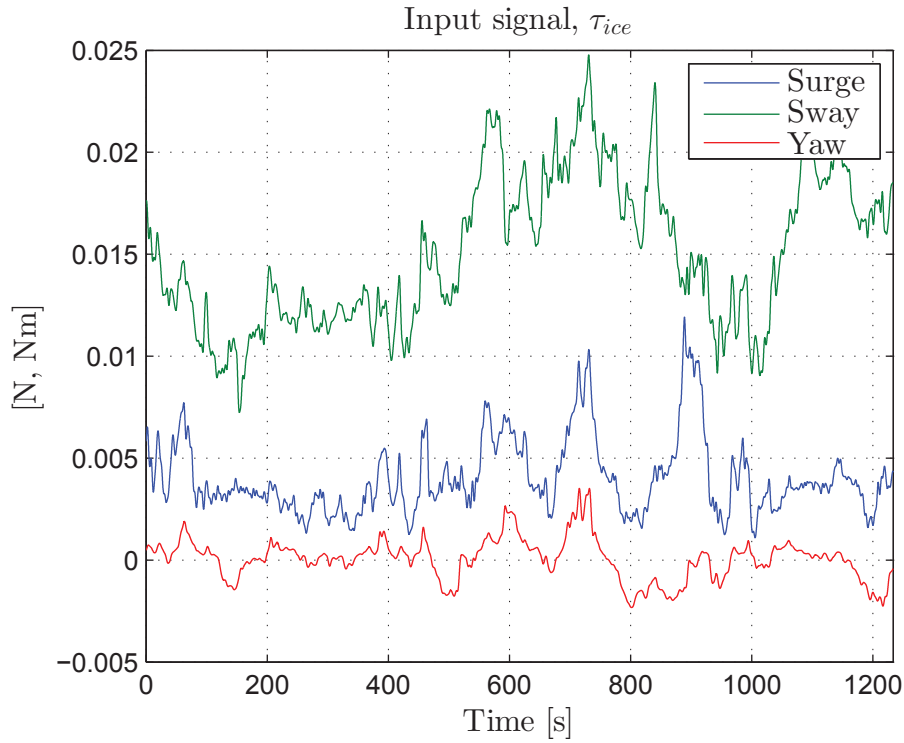


Figure 6.5: Ice loads for towing tank measurement data.

The sets of data from the towing tank are extensive and not all the data sets are used for this case study. Table 6.3 summarizes the relevant parameters for this case study, where V is the drift speed of the ice, C is the ice concentration, h_i is the ice thickness and θ is the drift angle of the vessel. The towing tank measurement data are combinations of all these parameters, except for $h_i = 0.8$ [m] with $\theta = 10$ [deg].

Table 6.3: The parameters used from the CIV Arctic towing tank measurement data.

V [m/s]	h_i [m]			C [%]		θ [deg]			
0.2	0.5	0.8	1.2	90	100	0	5	10	20

6.7 Reference Signals

The magnitude of the ice loads, presented in the previous section, is significantly different from the lightest to the toughest ice conditions. Experiences from [43] shows that the control forces applied to the azimuth thrusters, used for TIC, can not be equal for different ice conditions. If the control forces are large, compared with the ice loads, they will be dominating. Therefore, the control forces for the azimuth thrusters, used for TIC, must have the same magnitude as the ice loads. To find appropriate values, the towing tank measurement data from CIV Arctic was applied to the original TA algorithm, given in equations (2.6) - (2.10). Then, the average of the control forces for azimuth thruster two and four was used as references.

For TIC solution 1, the reference in control forces, \mathbf{f}_{ref} , was chosen as the minimum control forces, \mathbf{f}_{min} . This because the minimum control forces, \mathbf{f}_{min} , must be greater than zero for the TA to apply any control forces to azimuth thruster two and four.

In addition to choosing a reference for the control forces, \mathbf{f}_{ref} , for TIC solution 2, a reference in azimuth angles, $\boldsymbol{\alpha}_{ref}$, must also be chosen. The basis for selecting reference for azimuth angles, $\boldsymbol{\alpha}_{ref}$, is the three references in Figure 4.2. Keeping a constant azimuth angle is a simple solution. To be able to flush the ice away in a wider area it is chosen a time varying reference signal. Due to the discontinuities in the triangular reference signal it is chosen to use the sinusoidal reference signal as reference for the azimuth angles, $\boldsymbol{\alpha}_{ref}$. In the simulation, a frequency of 0.005 [Hz] was found to be appropriate. This is equal to the sinusoidal signal illustrated in Figure 4.2.

6.8 Cases

The case study consists of five cases. Case I is the original TA algorithm, without thruster dynamics and TIC. In Cases II and III thruster dynamics is added, with LP filter and restrictions on change of control forces, $\Delta\mathbf{f}$, respectively. In Cases IV and V TIC is added to the original TA, using solution 1 and 2 respectively.

It is chosen not to include thruster dynamics in Cases IV and V. This is a simplification to assume instantaneous change of control forces, \mathbf{f} , but the simulations are only meant to give indications on how the TIC affects the performance of the TA. That way, it is easier to give indications on how well the TA performs with and without thruster dynamics and TIC.

6.9 Performance Methodology

An important part of the case study is to measure the thrust capability of the TA algorithm. It is important to present the results in a way such that it is easy to investigate for which ice conditions the TA is able to keep desired position and heading. Two ways of displaying the thrust capability of the TA will be presented. First, by using the slack variables as an initial indication. Then, the error in thrust is used to investigate for which ice thickness the TA is not able to produce sufficient amount of thrust to withstand the ice loads, $\boldsymbol{\tau}_{ice}$.

As an overall performance indication of the TA algorithm the slack term, $\mathbf{s}^\top \mathbf{Q} \mathbf{s}$, in the objective function, Equation (2.6), is plotted for each case described in Section 6.8. It is believed that $\mathbf{s}^\top \mathbf{Q} \mathbf{s}$ can give a first impression of the thrust capability in all 3 DOFs in one number, and by that an indication whether the vessel is able to be on DP. A large slack term means that the TA is not able to distribute all the ice loads to the thrusters for a given set of thruster forces and azimuth angles.

Secondly, the performance is related to produced thrust, $\boldsymbol{\tau}_{act}$. Input to the TA is $-\boldsymbol{\tau}_{ice}$, where the minus is explained in Section 5.2, and the outputs are control forces, \mathbf{f} , and

azimuth angles, α . The idea is to use the difference between the ice loads, τ_{ice} , and the forces and moments actually produced by the TA, τ_{act} , to measure the performance. The control forces and azimuth angles from the TA are used to calculate the corresponding forces and moments, by using Equation (2.2). The error between desired thrust, $-\tau_{ice}$, and achieved thrust, τ_{act} , is denoted τ_{diff} , as defined in Equation (5.2). The concept is illustrated in Figure 6.6. The error in thrust is given by:

$$Error = \frac{-\tau_{ice} - \tau_{act}}{\tau_{ice}} = \frac{\tau_{diff}}{\tau_{ice}} \quad (6.5)$$

Multiplying the *Error* with 100 will give the error in thrust in percent.

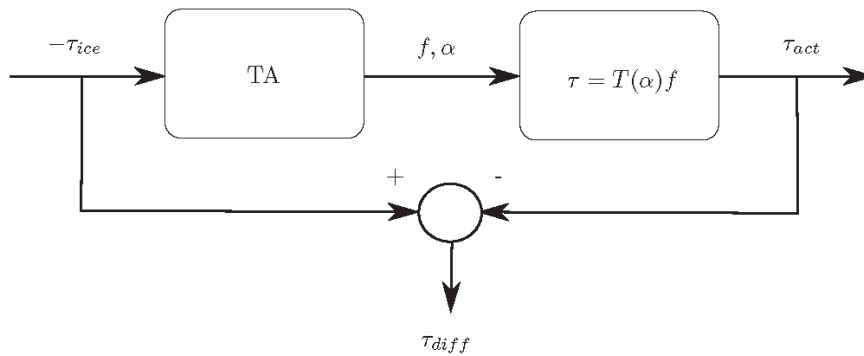


Figure 6.6: Measure of performance.

Compared to $\mathbf{s}^\top \mathbf{Q} \mathbf{s}$, this error, defined in Equation (6.5), gives the error for the 3 DOFs separately. The error will be plotted both sorted by ice thickness, h_i , and DOFs to investigate how the error develops with different variables. This provides opportunities to compare the results both in terms of ice thickness and DOF.

Chapter 7

Simulations

This chapter will first present how the TA algorithm was implemented and argue why the chosen parameters are reasonable. Then, results from the case study are presented. Finally, some samples of the energy analysis will be presented, with the lightest and toughest ice conditions as examples.

7.1 Implementation in *Matlab*

To implement the TA in *Matlab*, the modifications in sections 7.1.2 - 7.1.4 were performed to convert the TA algorithm to *quadprog* syntax. Using the weighting matrix for the slack variables to prioritize degradation of the performance of the TA is discussed in Section 7.1.5. Finally, Section 7.1.6 provides some guidelines on how to determine satisfactorily parameters for the TA algorithm.

7.1.1 Optimization Vector

To convert the optimization problem, equations (2.6) - (2.10), to *quadprog* syntax, equations (2.11) - (2.14), an optimization vector, \mathbf{x} , must to be defined. Based on the optimization problem, it is easy to see that the natural choice is:

$$\mathbf{x} = \begin{bmatrix} \Delta \mathbf{f} \\ \Delta \boldsymbol{\alpha} \\ \mathbf{s} \end{bmatrix} \in \mathbb{R}^{r+p+n} \quad (7.1)$$

7.1.2 Objective Function

All parts of the objective function, Equation (2.6), must be written in quadratic or linear terms of the optimization vector, defined in Equation (7.1). The first term of the objective

function must be rewritten in the following way:

$$\begin{aligned} & (\mathbf{f}_0 + \Delta\mathbf{f})^\top \mathbf{P}(\mathbf{f}_0 + \Delta\mathbf{f}) \\ &= \Delta\mathbf{f}^\top \mathbf{P} \Delta\mathbf{f} + 2\mathbf{f}_0^\top \mathbf{P} \Delta\mathbf{f} + \mathbf{f}_0^\top \mathbf{P} \mathbf{f}_0 \end{aligned} \quad (7.2)$$

where the last term, $\mathbf{f}_0^\top \mathbf{P} \mathbf{f}_0$, can be erased because it is constant. Applying the *quadprog* syntax in Equation (2.11) yields the \mathbf{H} matrix in Equation (A.1) and \mathbf{g} vector in Equation (A.2) in Appendix A.

The same calculations as in Equation (7.2) applies for the two last terms in objective function, Equation (4.1), for the TA with TIC solution 2. The \mathbf{g} vector is then given by Equation (A.9).

7.1.3 Constraints

Both equations (2.9) and (2.10) are constraints for $\Delta\boldsymbol{\alpha}$ because of the linearization to make the optimization problem convex. To solve this, Equation (2.9) is modified to fit the syntax in Equation (2.12):

$$\boldsymbol{\alpha}_{min} - \boldsymbol{\alpha}_0 \leq \Delta\boldsymbol{\alpha} \leq \boldsymbol{\alpha}_{max} - \boldsymbol{\alpha}_0 \Leftrightarrow \begin{cases} \Delta\boldsymbol{\alpha} \leq \boldsymbol{\alpha}_{max} - \boldsymbol{\alpha}_0 \\ -\Delta\boldsymbol{\alpha} \leq -\boldsymbol{\alpha}_{min} + \boldsymbol{\alpha}_0 \end{cases}$$

which yields the \mathbf{A} and \mathbf{b} matrices in equations (A.3) and (A.4), where the same calculations are performed on Equation (2.8).

Converting the equality constraint in Equation (2.7) to Equation (2.12) yields the vectors in equations (A.5) and (A.6).

The last inequality constraint in Equation (2.10) gives the vectors in equations (A.7) and (A.8). Here, restrictions on the change in control forces, $\Delta\mathbf{f}$, are added to incorporate the thruster dynamics into the TA. To always be able to guarantee feasibility of the optimization problem, the slack variables, \mathbf{s} , are chosen to be in the interval $(-\infty, \infty)$. In practice \mathbf{s} should be as small as possible so difference between the commanded and achieved forces and moments is as small as possible.

7.1.4 Numerical Differentiation

The partial derivative term in Equation (2.6) must be updated in every sample. Calculating the exact derivative for every sample is very expensive and time consuming. Therefore, the partial derivative is approximated using the forward-difference approximation [25]:

$$\frac{\partial h}{\partial \alpha_i} \approx \frac{h(\boldsymbol{\alpha} + \epsilon \mathbf{e}_i) - h(\boldsymbol{\alpha})}{\epsilon} \quad (7.3)$$

where $h = \frac{g}{\epsilon + \det(\mathbf{T}(\boldsymbol{\alpha})\mathbf{W}^{-1}\mathbf{T}^\top(\boldsymbol{\alpha}))}$ $\Big|_{\boldsymbol{\alpha}=\boldsymbol{\alpha}_0}$, ϵ is a small, positive scalar, \mathbf{e}_i is the i th unit vector and $i = 1, 2, \dots, n$.

7.1.5 Prioritization of Degrees of Freedom

When the ice loads are high, it can be desirable to include prioritization of DOFs to achieve predictable degradation of the performance of the TA. This can be done by putting different weights on the diagonal of the weighting matrix for the slack variables, \mathbf{Q} . For instance, if the weight of the first slack variable is twice as large as the weight of the second slack variable, the TA algorithm will penalize the first slack variable twice as hard as the second slack variable. A strategy for finding the weights of the slack variables, \mathbf{Q} , is given in Section 7.1.6.

It is important to keep the desired heading of the vessel. If the heading of the ship deviates too much against the ice drift, the control system and actuators may not be able to counteract the ice loads. A deviation in heading will in turn induce additional forces in sway, which can make it difficult to keep the desired position. To find a strategy for prioritization of the DOFs, the pendulum is used as a comparison. If the pendulum, as in Figure 7.1, is hanging straight down, the forces from the side are equal. They will therefore not push the pendulum to either of the sides. If the vessel is able to have a heading such that the ice drifts directly towards the bow of the vessel, using a weathervane strategy, the sway forces will in an ideal world be zero. Then, it is not so important to keep the desired sway forces.

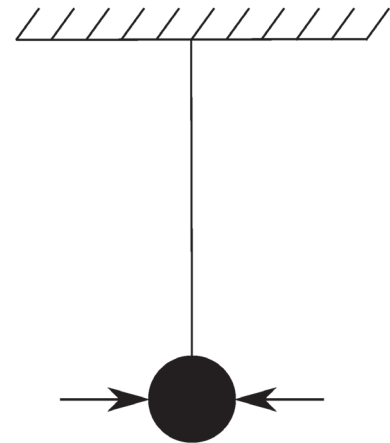


Figure 7.1: Pendulum analogy.

In an ideal world it should be possible to be on DP if the heading is perfect, which means on average no forces in sway, and the surge forces follows the desired surge forces. Using the weighting matrix for the slack variables, \mathbf{Q} , to keep this prioritization gives the largest weight on the slack in yaw and the smallest weight on the slack in sway. The weight on the slack in surge is the middle. A corresponding strategy was used in [39] when the vessel was not able to keep desired position.

7.1.6 Choice of Parameters

Several of the parameters in the TA algorithm, equations (2.6) - (2.10), are vessel specific and given in Chapter 6. This applies for the following parameters: $\mathbf{T}(\boldsymbol{\alpha})$, \mathbf{f}_{min} , \mathbf{f}_{max} , $\boldsymbol{\alpha}_{min}$, $\boldsymbol{\alpha}_{max}$, $\Delta\boldsymbol{\alpha}_{min}$ and $\Delta\boldsymbol{\alpha}_{max}$. Including thruster dynamics with restrictions on the change of control forces, $\Delta\mathbf{f}$, adds $\Delta\mathbf{f}_{min}$ and $\Delta\mathbf{f}_{max}$ to this list.

The tuning parameters in the cost function are chosen such that the TA behaves desirable. Initially, the weights of the control forces, \mathbf{P} , and change of azimuth angles, $\boldsymbol{\Omega}$, are chosen to be $diag(1, 1, 1, 1, 1, 1)$ and $diag(1, 1, 1, 1)$. $diag(x_1, x_2, \dots, x_n)$ is a diagonal matrix with x_1, x_2, \dots, x_n on the diagonal and zeros on the off-diagonal. The weights of the slack variables, \mathbf{Q} , are chosen to be in order of approximately 1000 times as large as the other weights to keep them as small as possible [30]. Including the prioritization

of DOFs, described in Section 7.1.5, the weights of the slack variables are chosen to be $diag(2500, 1000, 5000)$. This way, slack in yaw will be penalized twice as much as slack in surge, as in turn will be penalized 2.5 times as much as slack in sway. As it is stated in Section 4.2, it might be undesirable to use the tunnel thrusters. Therefore, the weights of tunnel thrusters are increased to 100. The \mathbf{P} matrix is in addition multiplied with 5 to get satisfactory performance. Also, the weights on the azimuth angle rates are increased to $diag(10, 10, 10, 10)$ to penalize change of azimuth angles harder.

In the singularity avoidance term \mathbf{W} , ρ and, ε are tuned so the term is large enough in the cost function. The weighting of the control forces, \mathbf{W} , is chosen such that the use of tunnel thrusters is penalized twice as much as the two front azimuth thrusters. In turn, the two front azimuth thrusters are penalized twice as much as the two rear azimuth thrusters. The reason for this is to force the system to use the rear azimuth thrusters rather than the front azimuth thrusters. ρ is chosen large enough so that the desirable manoeuvrability is achieved. At last, ε is chosen as a small value to avoid zero division.

Applying TIC solution 2, two additional tuning parameters are added. β is a scalar weighting the quadratic difference in control forces, $\mathbf{f} - \mathbf{f}_{ref}$, and γ is a scalar weighting the quadratic difference in azimuth angles, $\boldsymbol{\alpha} - \boldsymbol{\alpha}_{ref}$. Both variables are given sufficiently large weights to force the TA to follow the respectively references whenever possible. Simulations have shown that it is sometimes necessary to deviate from the desired azimuth angles, $\boldsymbol{\alpha}_{ref}$, to be able to resist the ice loads as well as possible.

The final values for the tuning parameters are given in equations (7.4) - (7.11).

$$\mathbf{P} = diag(500, 5, 500, 5, 5, 5) \quad (7.4)$$

$$\boldsymbol{\Omega} = diag(10, 10, 10, 10) \quad (7.5)$$

$$\mathbf{Q} = diag(2500, 1000, 5000) \quad (7.6)$$

$$\mathbf{W} = diag(4, 2, 4, 2, 1, 1) \quad (7.7)$$

$$\beta = 10^6 \quad (7.8)$$

$$\gamma = 10^{16} \quad (7.9)$$

$$\rho = 5 \cdot 10^8 \quad (7.10)$$

$$\varepsilon = 10^{-2} \quad (7.11)$$

7.2 Results Case Study

The case study consists of 5 cases, as presented in Section 6.8. The towing tank measurement data from CIV Arctic, presented in Section 6.6, consists of several data sets of multiple parameters. The parameters are drift speed, V , ice concentration, C , ice thickness, h_i , and drift angle, θ , and the data sets consist of combinations of the values presented in Table 6.3.

The results are presented using the performance methodologies described in Section 6.9. The first performance indicator, $\mathbf{s}^\top \mathbf{Q} \mathbf{s}$, is normalized between zero and one to make it easier to compare all the cases against each other. The error in produced thrust is

normalized using bis normalization, presented in Section 2.3. In the figures presenting the error, the blue lines represents the error in surge, the green lines represents the error in sway and the red lines represents the error in yaw.

For each of the cases and ice concentrations, the results will be presented in 3 figures. For all 5 cases and both ice concentration this will results in 30 figures. Only the most notable figures will be presented in sections 7.2.1 - 7.2.3. The rest will be briefly commented on in these sections, while presented in the appendix, sections B.1 - B.2. All the figures have the drift angle, θ , on the x-axis.

First, the results from the original TA algorithm will be presented in Section 7.2.1. Then, the results from adding thruster dynamics to the TA algorithm, Cases II and III, will be presented in Section 7.2.2. Finally, adding TIC to the original TA algorithm, Cases IV and V, will be presented in Section 7.2.3.

7.2.1 Thrust Allocation

In this section, the results from Case I will be presented. First for $C = 90$ [%] and then for $C = 100$ [%], for all 3 performance indicators.

Figure 7.2 presents $\mathbf{s}^\top \mathbf{Q} \mathbf{s}$ for Case I with $C = 90$ [%], and indicates a general increase in slack with increasing drift angles, θ , and ice thickness, h_i . When the ice thickness is increased for 0.5 [m] to 0.8 [m], and from 0.8 [m] to 1.2 [m], the slack term increases approximately 10 times each time. For $h_i = 0.5$ [m], the slack term decreases slightly from 0 [deg] to 5 [deg].

The slack term, for Case I with 100 [%] ice concentration, is presented in Figure 7.3. For $h_i = 0.5$ [m] and $h_i = 1.2$ the slack term does not have a distinct increase for increasing drift angles, as for $C = 90$ [%]. On the other hand, $\mathbf{s}^\top \mathbf{Q} \mathbf{s}$ for $h_i = 0.8$ follows the same development as for $C = 90$ [%], only with a magnitude approximately 10 times larger. For $h_i = 0.5$ [m], $\theta = 5$ [deg] and $h_i = 1.2$ [m], $\theta = 10$ [deg] the slack term is significant larger than for the other drift angles.

The error, sorted by ice thickness, for Case I and 90 [%] ice concentration is presented in Figure 7.4. At first glance there is no distinct development for any of the ice thicknesses. For $h_i = 0.5$ [m] and $h_i = 0.8$ [m] the error in surge is larger than the error in sway for 0 [deg] and 5 [deg], but is smaller for larger drift angles. The error for $h_i = 1.2$ [m] is approximately 0 [%] for the drift angles 0 [deg] and 5 [deg]. For 10 [deg] and 20 [deg] the error is larger and the prioritization described in Section 7.1.5 is ensured. The largest error is in sway direction for $h_i = 1.2$ [m] and $\theta = 10$ [deg], with a magnitude of 15.1 [%].

Increasing the ice concentration to 100 [%], the error for Case I, sorted by h_i , is presented in Figure 7.5. As can be seen in the figure, the error for all drift angles and ice thicknesses follows the prioritization of DOFs. Comparing it with $C = 90$ [%], the error for $h_i = 0.5$ [m] and $h_i = 0.8$ [m] is approximately in the same magnitude, but for $h_i = 1.2$ [m] the error is significant increased. For instance, for $h_i = 1.2$ [m] and $\theta = 20$ [deg] the error has increased by nearly 5 times.

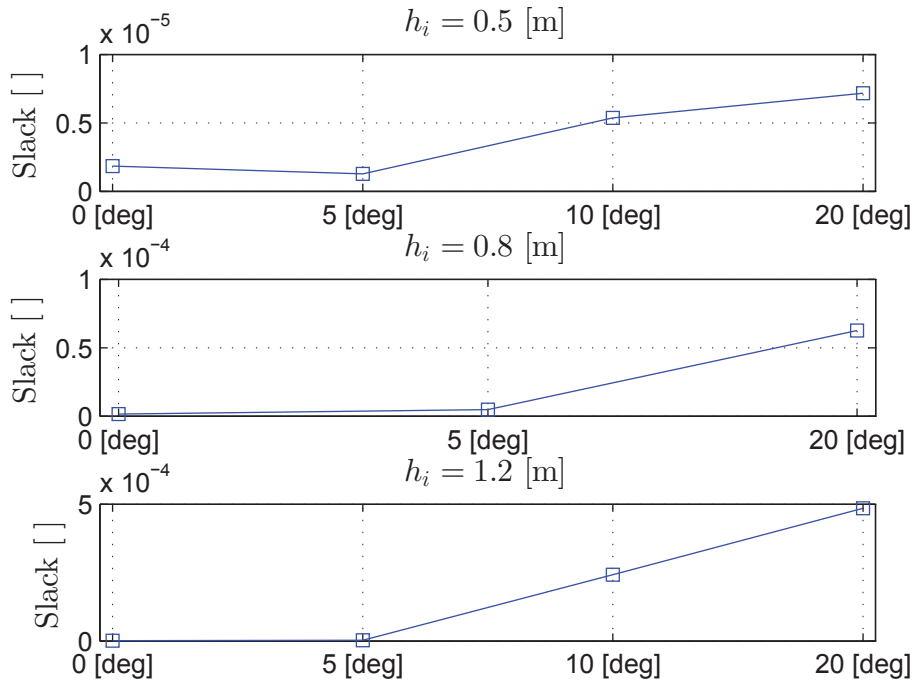


Figure 7.2: Results from Case I: $\mathbf{s}^\top \mathbf{Q} \mathbf{s}$, $C = 90$ [%].

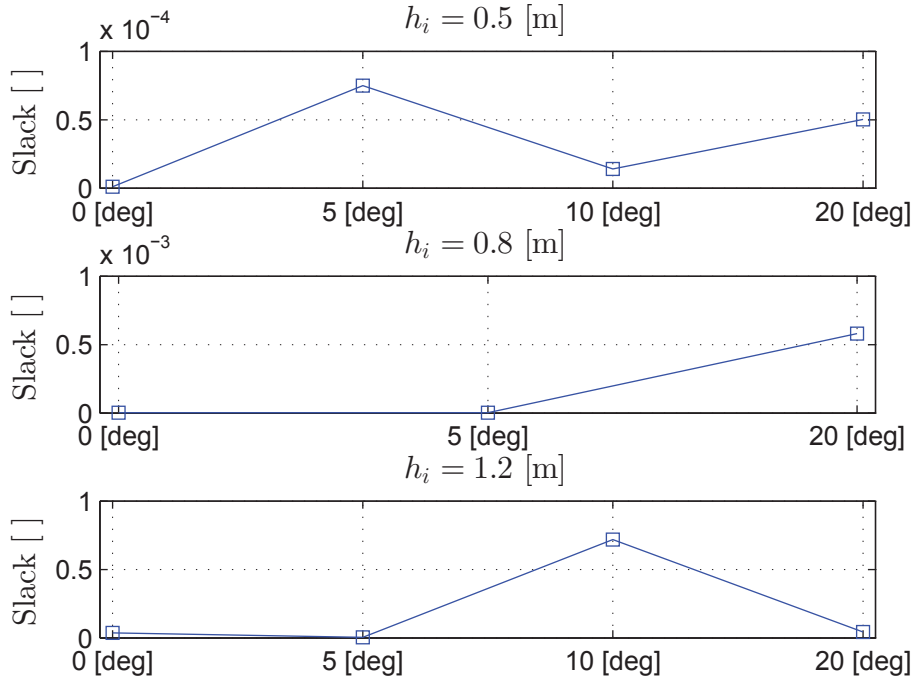


Figure 7.3: Results from Case I: $\mathbf{s}^\top \mathbf{Q} \mathbf{s}$, $C = 100$ [%].

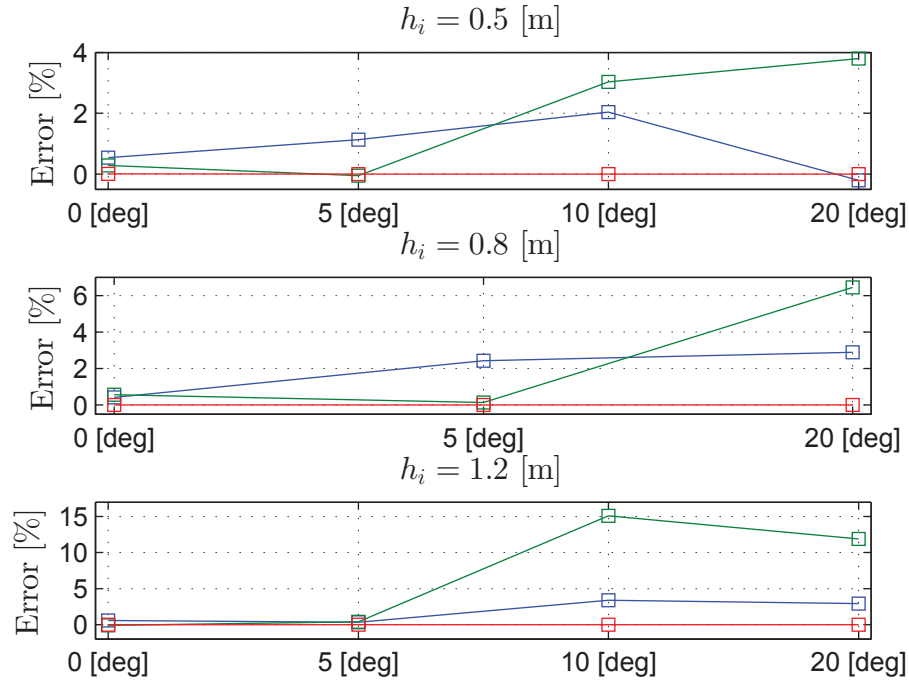


Figure 7.4: Results from Case I: Error sorted by h_i , $C = 90$ [%]. — Surge, — Sway, — Yaw.

The error, sorted by DOF, for Case I is presented in figures 7.6 and 7.7 for 90 [%] and 100 [%] ice concentration, respectively. The error for $C = 90$ [%] does not have a distinct development for the ice thicknesses. The error in yaw is significant smaller compared to surge and sway. For 100 [%] ice concentration the error for 0.5 [m] and 0.8 [m] is nearly equal and significant smaller than the error for $h_i = 1.2$ [m]. The error for $h_i = 1.2$ [m] can be approximated with a linear increase for increasing drift angles in surge and sway. For yaw, this is not the case because the error for 10 [deg] is significant larger than the other drift angles.

7.2.2 Thrust Allocation with Thruster Dynamics

Adding thruster restrictions to the TA algorithm yields the following results, in Cases II and III. The results will be presented in the same manner as in the previous section.

The control forces, \mathbf{f} , are LP filtered off-line after the optimization in Case II. The slack, \mathbf{s} , is calculated during the optimization, and the LP filter will thus not affect $\mathbf{s}^\top \mathbf{Q} \mathbf{s}$. The slack term for Case II will therefore be equal to case I, and no new information can be added. One solution to this problem can be to LP filter the control forces in the optimization loop, but this is not done in this project. It is unfortunate that no indications on the performance of the TA can be given by looking at the slack variables, but it is assumed that the error can give a good enough picture of the performance for this case.

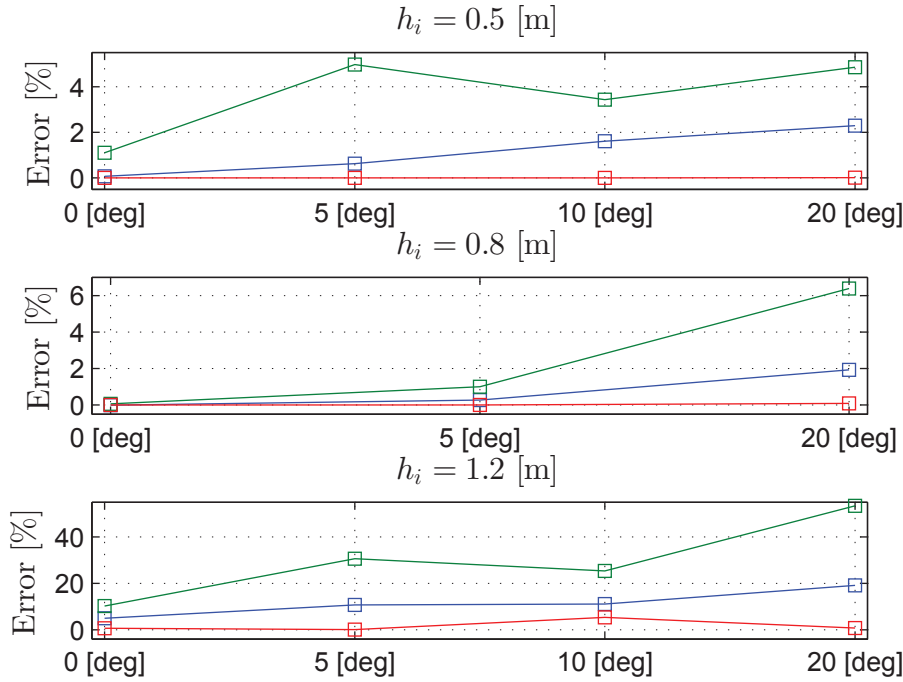


Figure 7.5: Results from Case I: Error sorted by h_i , $C = 100$ [%]. — Surge, — Sway, — Yaw.

The error, sorted by h_i , for Case II with $C = 90$ [%] is presented in Figure B.1, and is similar to Case I. An exception is a larger magnitude for $h_i = 0.5$ [m]. More interesting are the results when increasing the ice concentration to 100 [%], as is shown in Figure 7.8. For $h_i = 0.5$ [m] the error is larger compared to Case I, but the most interesting result can be seen at 0 [deg] and 20 [deg] drift angle. Here the error is -0.4 [%] and -14 [%] respectively, meaning more thrust is produced than what is required to withstand the ice loads. For $h_i = 0.8$ [m] the error in yaw is quite large, larger than the error in surge and sway for 0 [deg] and 5 [deg]. With 1.2 [m] ice thickness the error is nearly equal as it is for Case I.

Figures B.2 and B.3 presents the error, sorted by DOF, for Case II with 90 [%] and 100 [%] ice concentration, respectively. The results are not so different from Case I, except for the negative error for $h_i = 0.5$ [m] and $\theta = 20$ [deg].

$\mathbf{s}^\top \mathbf{Q} \mathbf{s}$ for Case III with $C = 90$ [%] is shown in Figure 7.9. The slack term for $h_i = 0.5$ [m] and $\theta = 5$ [deg] is significantly larger compared with the other drift angles, approximately 10 to 100 times as large. In general, $\mathbf{s}^\top \mathbf{Q} \mathbf{s}$ for $h_i = 0.8$ [m] is increasing for increasing drift angle. For $h_i = 0.8$ [m] and 5 [deg], it is nearly 80 times as large compared to Case I. Approximating the slack term for $h_i = 1.2$ [m] with a linear line from 0 [deg] to 20 [deg], it is actually decreasing with increasing drift angles. In spite of this, $\mathbf{s}^\top \mathbf{Q} \mathbf{s}$ is 1.4 times as large for $\theta = 20$ [deg] compared to Case I.

The slack term for Case III with $C = 100$ [%] is given in Figure B.4. The development for $\mathbf{s}^\top \mathbf{Q} \mathbf{s}$, with respect to drift angles, is almost the same as for Case I, only with a larger

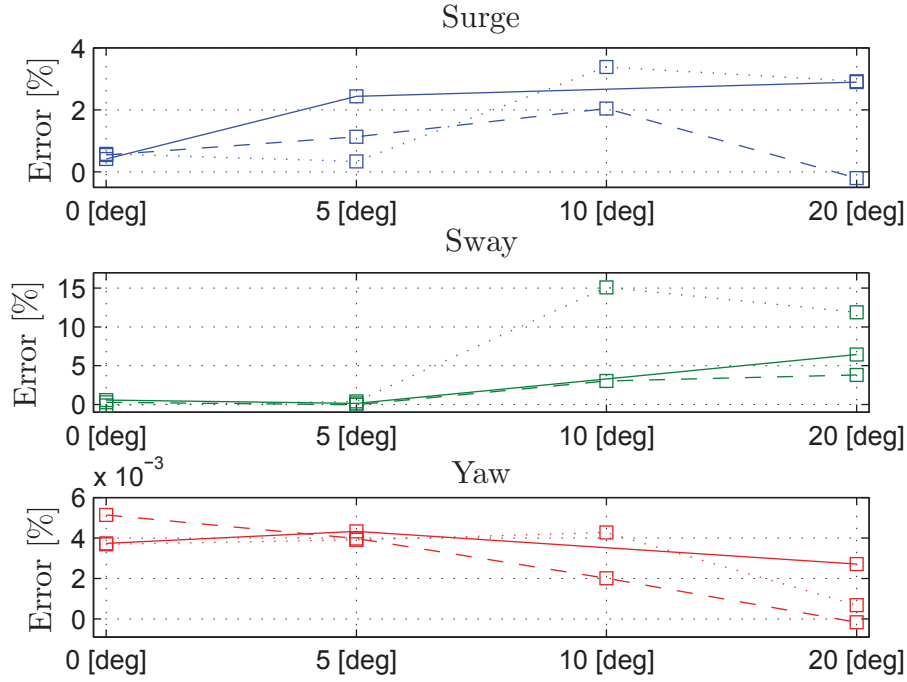


Figure 7.6: Results from Case I: Error sorted by DOF, $C = 90$ [%]. - - $h_i = 0.5$ [m], — $h_i = 0.8$ [m], \cdots $h_i = 1.2$ [m].

magnitude. An exception is for $h_i = 0.8$ [m], $\theta = 0$ [deg] where the slack term is larger than $\theta = 5$ [deg].

The error, sorted by ice thickness, for Case III is presented in figures B.5 and B.6 for $C = 90$ [%] and $C = 100$ [%], respectively. The results are not very different from Case I, except for a more linear increase in error from 5 [deg] to 20 [deg] for $h_i = 1.2$ [m], $C = 90$ [%] and a negative error in sway for $h_i = 0.5$ [m], $\theta = 0$ [deg] and $C = 100$ [%].

Figure 7.10 shows the error, sorted by DOF, for 90 [%] ice concentration. In surge direction, the largest error is for $h_i = 0.8$ [m]. In sway direction the error is nearly linear increasing from 5 [deg] to 20 [deg], and the error for $h_i = 1.2$ [m] is larger than for $h_i = 0.8$ [m] which in turn is larger than for $h_i = 0.5$ [m]. The error in yaw gives no clear indication regarding for which ice conditions the error is largest, except for $h_i = 1.2$ [m], $\theta = 0$ [deg] and $h_i = 0.5$ [m], $\theta = 5$ [deg] which is significant larger than the others.

The error, sorted by DOF, for Case III and $C = 100$ [%] is presented in Figure B.7. The results are similar to corresponding ice conditions in Case I, except that the error is a bit larger for some of the drift angles for $h_i = 1.2$ [m].

7.2.3 Thrust Allocation with Thruster Ice Clearance

The results from Case IV and V, when TIC is added to the original TA algorithm, are presented in this section. The presentation of the results is done in the same manner as

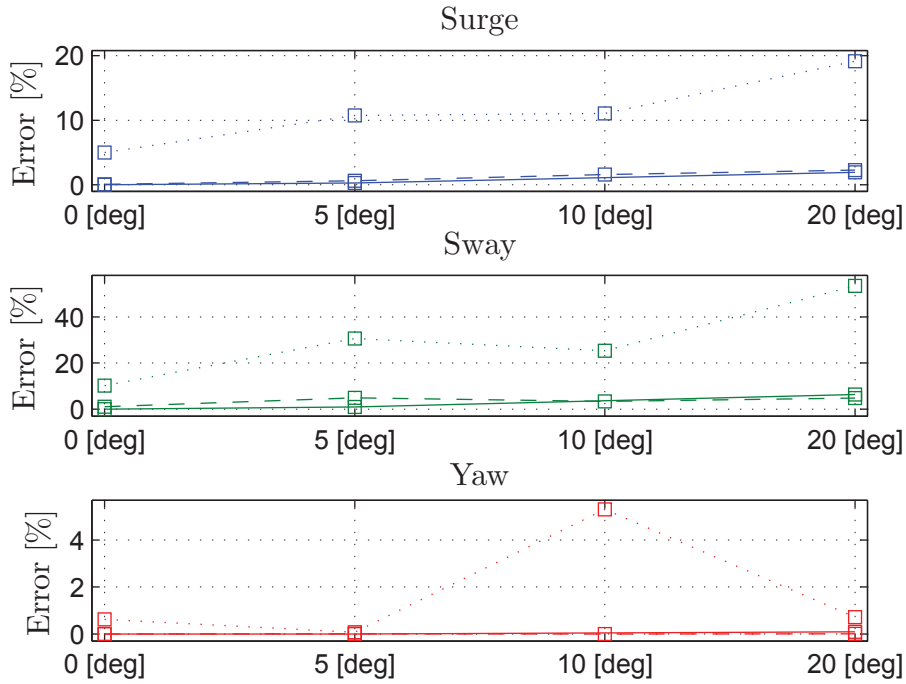


Figure 7.7: Results from Case I: Error sorted by DOF, $C = 100$ [%]. - - $h_i = 0.5$ [m], — $h_i = 0.8$ [m], \cdots $h_i = 1.2$ [m].

the two previous sections.

Figures B.8 and 7.11 presents $\mathbf{s}^\top \mathbf{Q} \mathbf{s}$ for Case IV with $C = 90$ [%] and $C = 100$ [%], respectively. The results in both figures tend to follow the same trend from Case I, except with a larger magnitude. With 100 [%] ice concentration, $h_i = 1.2$ [m] and $\theta = 10$ [deg] the slack term, $\mathbf{s}^\top \mathbf{Q} \mathbf{s}$, is the largest amongst all cases.

The error, sorted by h_i , for case IV and $C = 90$ [%] is given in Figure B.9. The results, especially for $h_i = 0.5$ [m], are similar to the results from Case I. An exception is that the error is large especially for sway.

In Figure 7.12 the error for Case IV, sorted by ice thickness, is presented. The error is significantly larger compared to Case I, and the prioritization of DOFs is maintained. For $h_i = 0.8$ [m] and 20 [deg] drift angle, the error is negative, with -1.4 [%] error.

The error for Case IV and $C = 90$ [%], sorted by DOF, is presented in Figure 7.13. It is interesting to note that the error in surge is largest for $h_i = 0.5$ [m] for all drift angles. In sway, the error is small and nearly constant from $\theta = 0$ [deg] to $\theta = 5$ [deg], and the increase in error can be linearly approximated from 5 [deg] to 20 [deg]. The error in yaw is small, compared to surge and sway, and do not follow any distinct development with respect to increasing ice thickness and drift angle.

Increasing the ice concentration to 100 [%], the error for Case IV, sorted by DOF, is shown in Figure B.10. The results are roughly the same as for Case I, only with larger magnitude.

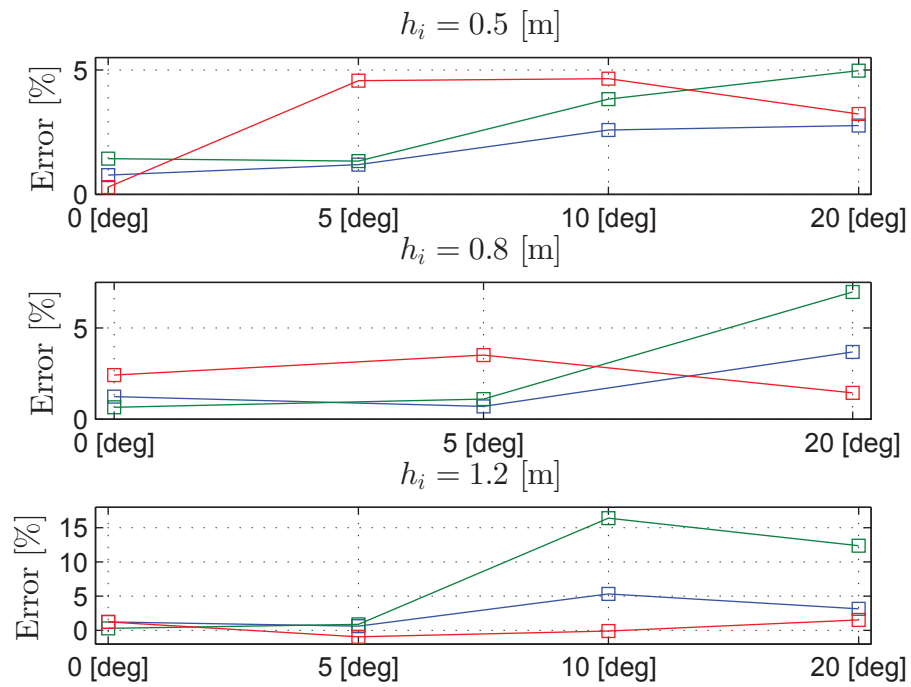


Figure 7.8: Results from Case II: Error sorted by h_i , $C = 100$ [%]. — Surge, — Sway, — Yaw.

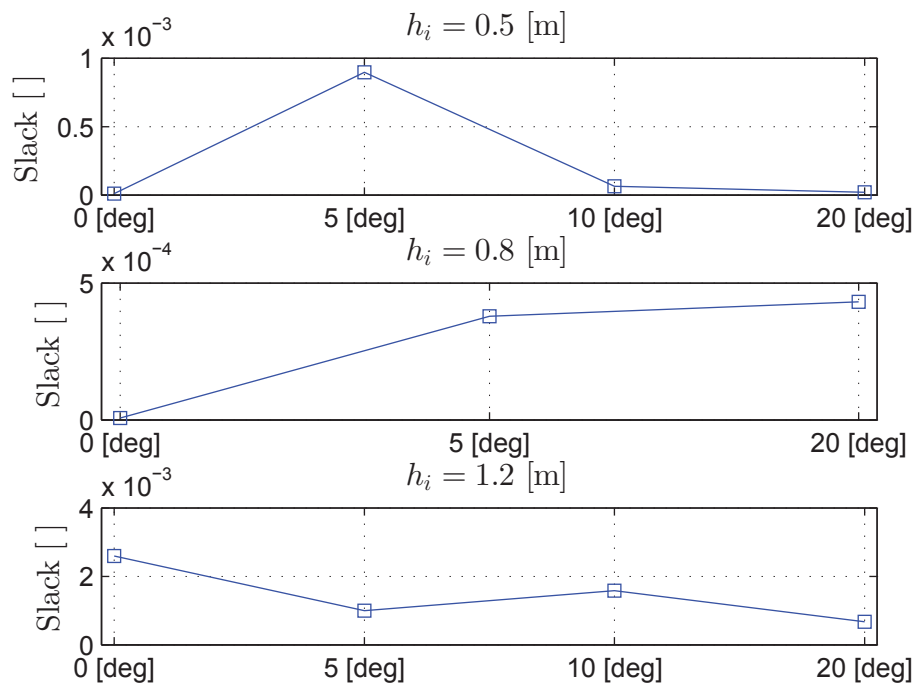


Figure 7.9: Results from Case III: $s^T Qs$, $C = 90$ [%].

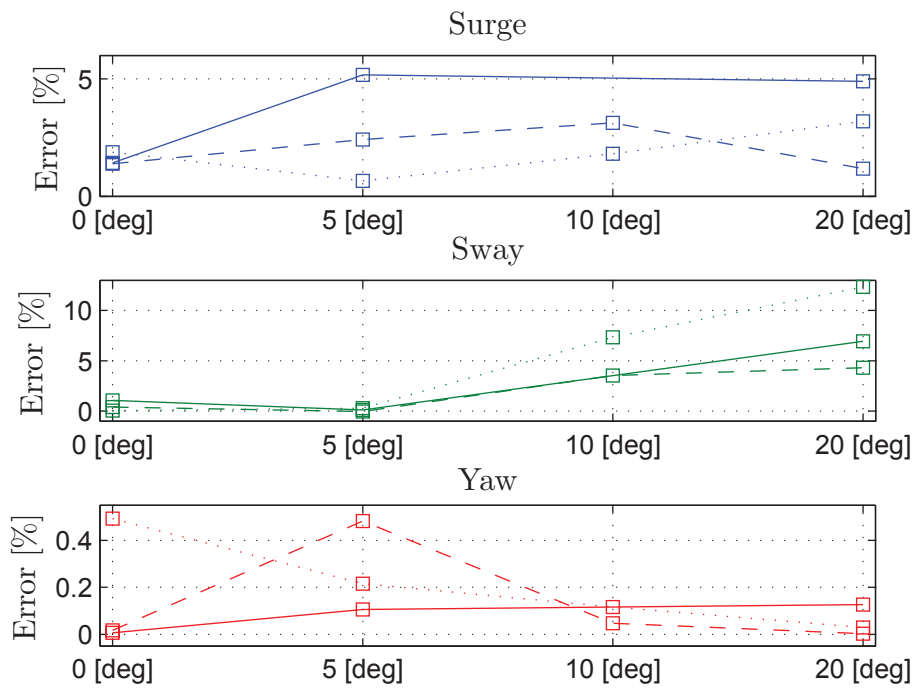


Figure 7.10: Results from Case III: Error sorted by DOF, $C = 90$ [%]. -- $h_i = 0.5$ [m], — $h_i = 0.8$ [m], \cdots $h_i = 1.2$ [m].

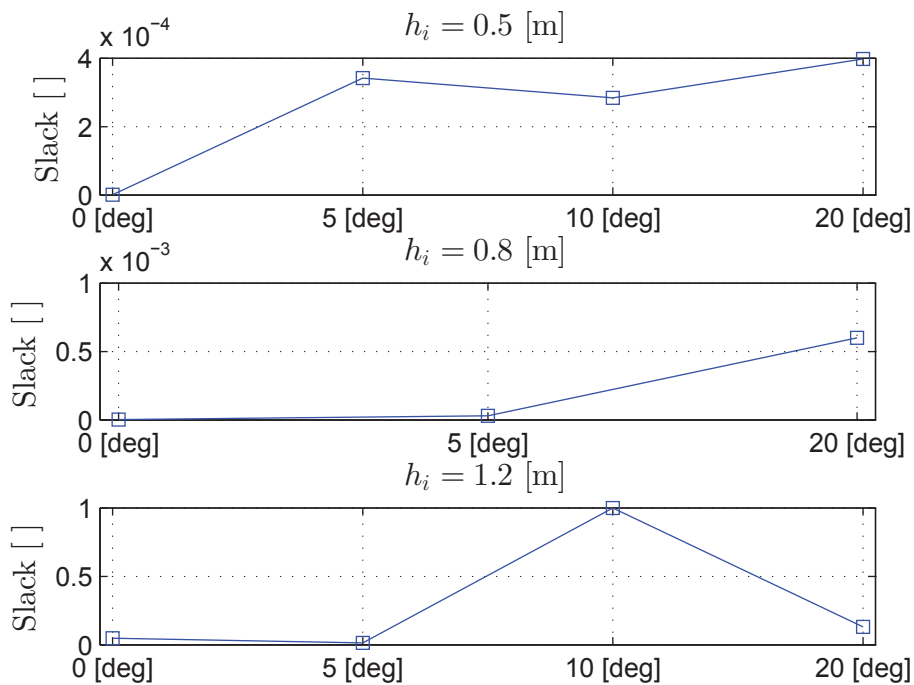


Figure 7.11: Results from Case IV: $s^T Q s$, $C = 100$ [%].

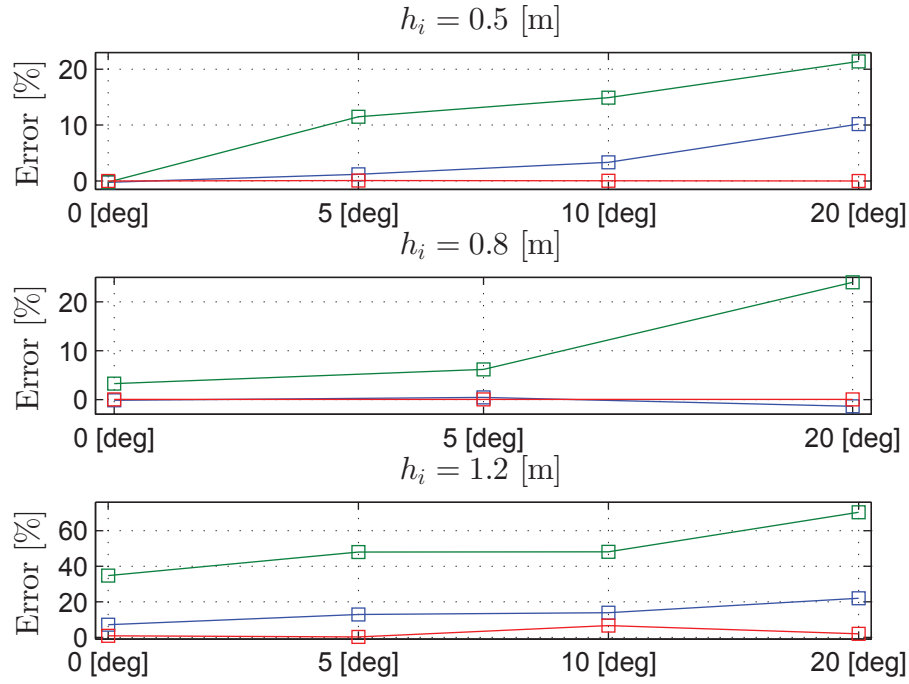


Figure 7.12: Results from Case IV: Error sorted by h_i , $C = 100$ [%]. — Surge, — Sway, — Yaw.

Figure B.11 shows the slack term for Case V with $C = 90$ [%]. The results are quite similar to the same ice conditions for Case IV, except that $\mathbf{s}^\top \mathbf{Q} \mathbf{s}$ is increasing with increasing drift angle for the smallest ice thickness and that the magnitude is larger. The same results for 100 [%] ice concentration are presented in Figure B.12. The same exceptions as for $C = 90$ [%], as described above, applies to 100 [%] ice concentration, except that the magnitude for $h_i = 1.2$ [m] is smaller for Case V compared to Case IV.

Figures B.13 and B.14 presents the error for Case V, sorted by ice thickness. Interesting observations are that the error in surge is significant negative for $C = 90$ [%], $h_i = 0.8$ [m], $\theta = 20$ [deg] and $C = 100$ [%], $h_i = 0.5$ [m], $\theta = 10$ [deg].

The error for Case V, sorted by DOF, for $C = 90$ [%] is given in Figure 7.14. In surge direction, the error is dominating for $h_i = 0.8$ [m] and negative for 20 [deg]. For sway and yaw, the error is roughly the same as for Case IV. An exception is for $h_i = 1.2$ and $\theta = 10$ [deg] where the error is significant larger than the other ice thicknesses.

Increasing the error to 100 [%], the error for Case V, sorted by DOF, is presented in Figure B.15. The results indicate that the error is approximately the same as for Case IV, only with negative errors for some of the ice conditions in surge.

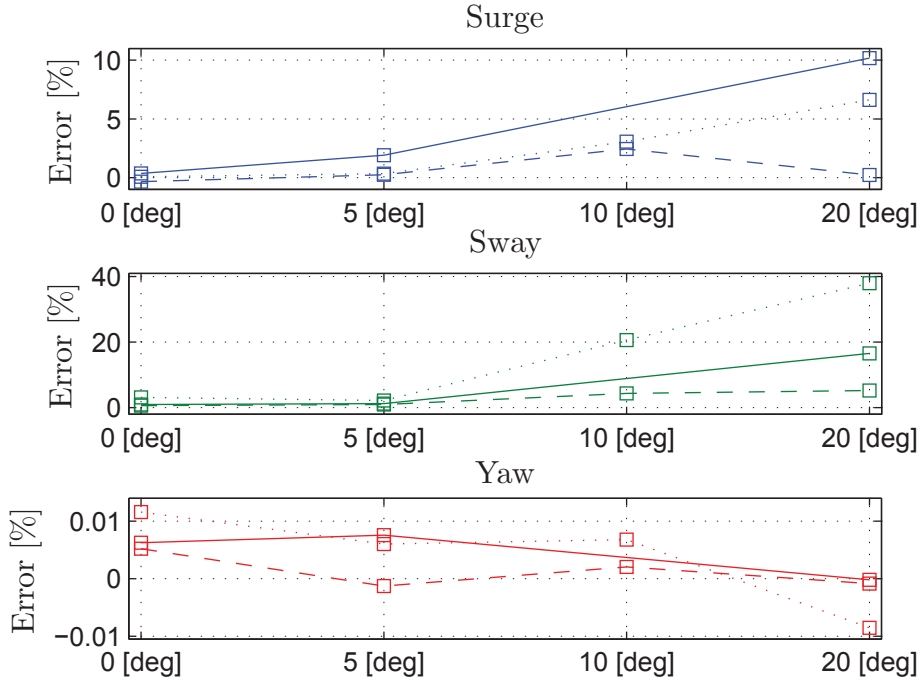


Figure 7.13: Results from Case IV: Error sorted by DOF, $C = 90$ [%]. - - $h_i = 0.5$ [m], — $h_i = 0.8$ [m], \cdots $h_i = 1.2$ [m].

7.3 Results Energy Considerations

In the energy considerations, the energy of the remaining control forces, \mathbf{f}_{diff} and the ice loads the TA were not able to counteract for, $\boldsymbol{\tau}_{diff}$, is calculated and compared. A complete overview of all the cases as a function of all the ice conditions is given in tables C.1 - C.5. The energy of \mathbf{f}_{diff} and $\boldsymbol{\tau}_{diff}$ are summed up over the time axis and subtracted from each other. This way, the results in tables C.1 - C.5 give an overall indication of the ability to avoid drift-offs all together over the time axis. There might be cases where the vessel will drift off in small periods of time and then come back into position, but simulations showed that for most of the cases the TA was either able to prevent drift-offs or not. An exception is for $h_i = 1.2$ [m], $C = 90$ [%] and $\theta = 20$ [deg] where the energy of \mathbf{f}_{diff} and $\boldsymbol{\tau}_{diff}$ were similar, and only minor difference resulted in a positive result for surge and negative for sway.

Simulations for Cases I - III, presented in tables C.1 - C.3, indicated that the vessel was able to withstand the ice loads for all ice conditions with 0.5 [m] and 0.8 [m] of ice. For $h_i = 1.2$ [m] the TA started to have problems with withstanding the ice loads in sway for $C = 90$ [%] and $\theta = 20$ [deg]. For 100 [%] ice concentration, the results indicated that the TA was not able to withstand the ice loads in surge and sway. For Case IV, presented in Table C.4, the results indicated that the TA also failed to withstand the ice loads for sway for $\theta = 20$ [deg] with 0.5 [m] of ice and 100 [%] ice concentration, in addition to both ice concentrations for 0.8 [m] of ice. For Case V, presented in Table C.5, the indications on

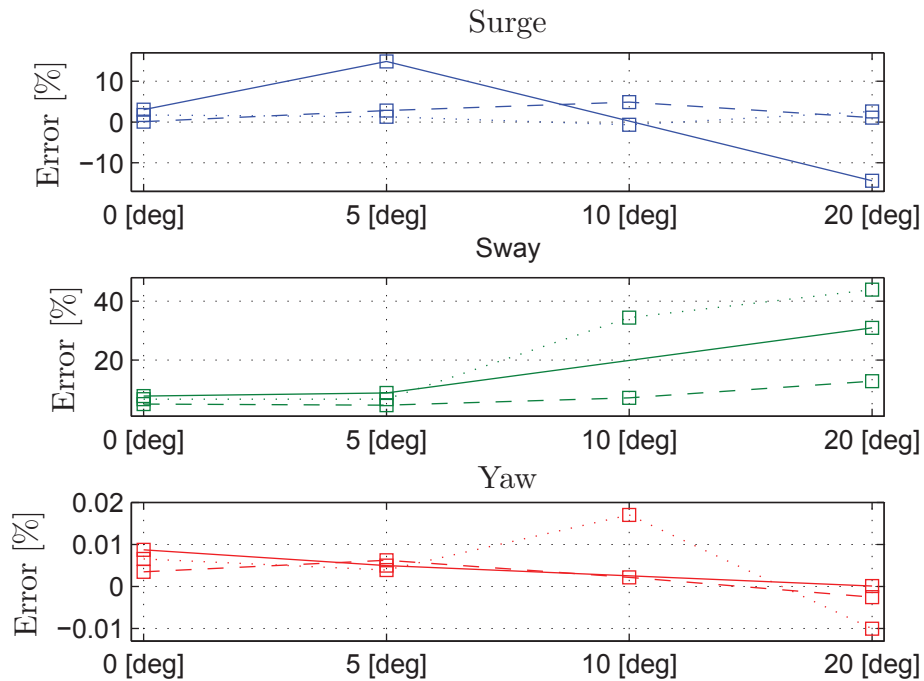


Figure 7.14: Results from Case V: Error sorted by DOF, $C = 90$ [%]. - - $h_i = 0.5$ [m], — $h_i = 0.8$ [m], \cdots $h_i = 1.2$ [m].

Table 7.1: Possible drift-offs in sway, Case V.

h_i [m]	C [%]	θ [deg]
0.5	100	10
		20
0.8	90	20
	100	20
	90	10
		20
1.2	100	0
		5
		10
		10
		20

failure to withstand the ice loads in sway apply to the ice conditions presented in Table 7.1. It is also worth noticing that the TA was able to withstand the ice loads in yaw for all of the cases.

To give some examples of the energy analysis, it is chosen to present the results for surge direction for the lightest ice condition and the toughest ice condition. In Figure 7.15, the difference in the energy of f_{diff} and τ_{diff} is plotted in the time domain. For the time

intervals at around 15 [s], 410 - 480 [s], around 920 [s] and around 1180 [s] the error is nearly 0, meaning that little of the control forces are left to withstand the ice loads. For this ice condition this happens only for small periods of time, and the remaining control forces are quite large the rest of the time. The energy of the \mathbf{f}_{diff} and $\boldsymbol{\tau}_{diff}$ are plotted separately in the frequency plane in Figure 7.16. The same results are presented, and it is easy to see that the energy of \mathbf{f}_{diff} is larger than the energy of $\boldsymbol{\tau}_{diff}$ in the whole frequency plane. Note that the y-axis shows the power spectral density (PSD) of the energy signals.

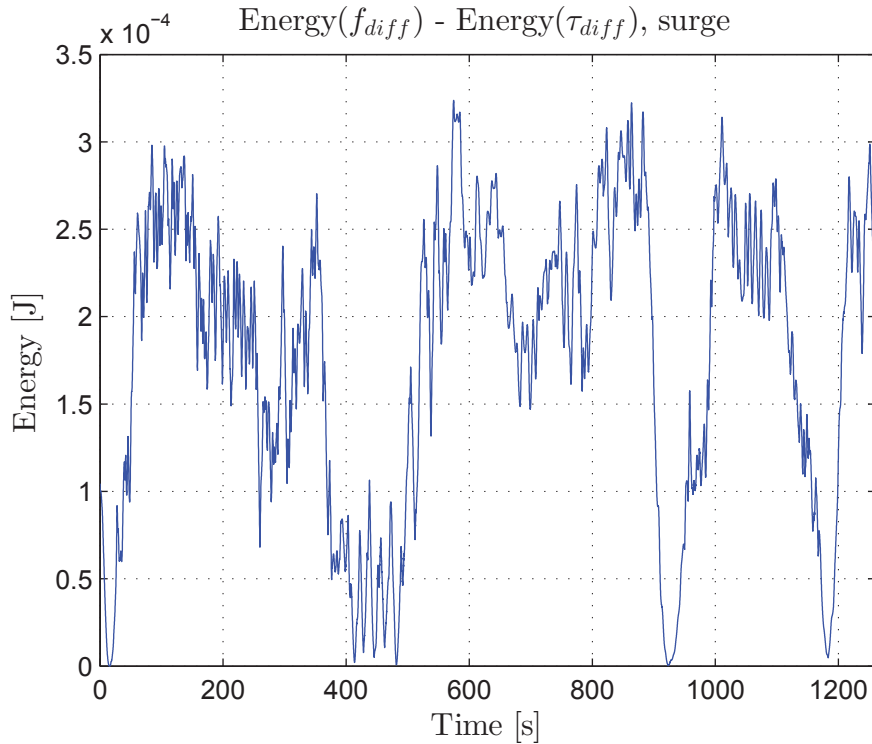


Figure 7.15: Energy of \mathbf{f}_{diff} subtracted energy of $\boldsymbol{\tau}_{diff}$ for lightest ice condition, surge direction.

The results for the toughest ice condition are presented in figures 7.17 and 7.18, in the time and frequency domain, respectively. In Figure 7.17 it can be seen that the energy of $\boldsymbol{\tau}_{diff}$ is larger than the energy of \mathbf{f}_{diff} for most of the time, and it is likely that the vessel will not be able to come back into position in the small periods when the difference is positive. In the frequency plane, the energy of the ice loads that the TA is not able to withstand, $\boldsymbol{\tau}_{diff}$, larger than the energy of the remaining control forces, \mathbf{f}_{diff} , except for small frequencies. For some of the small frequencies, below approximately 0.5 [Hz], the two signals seem to be on top of each other, but the difference becomes significant quite soon.

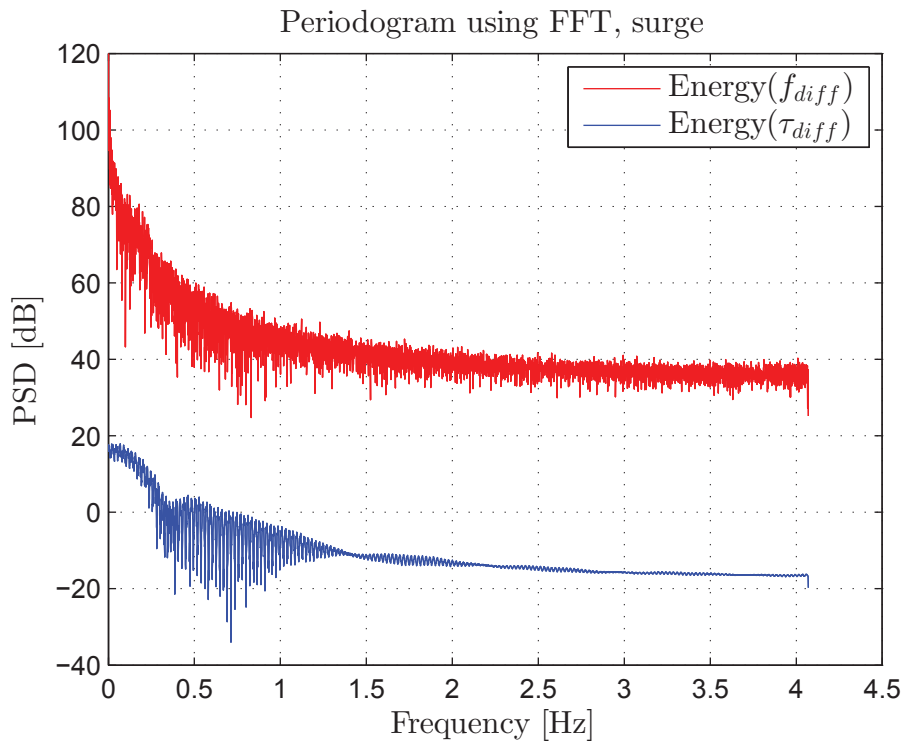


Figure 7.16: Frequency analysis of the energy of f_{diff} and τ_{diff} for the lightest ice condition, surge direction.

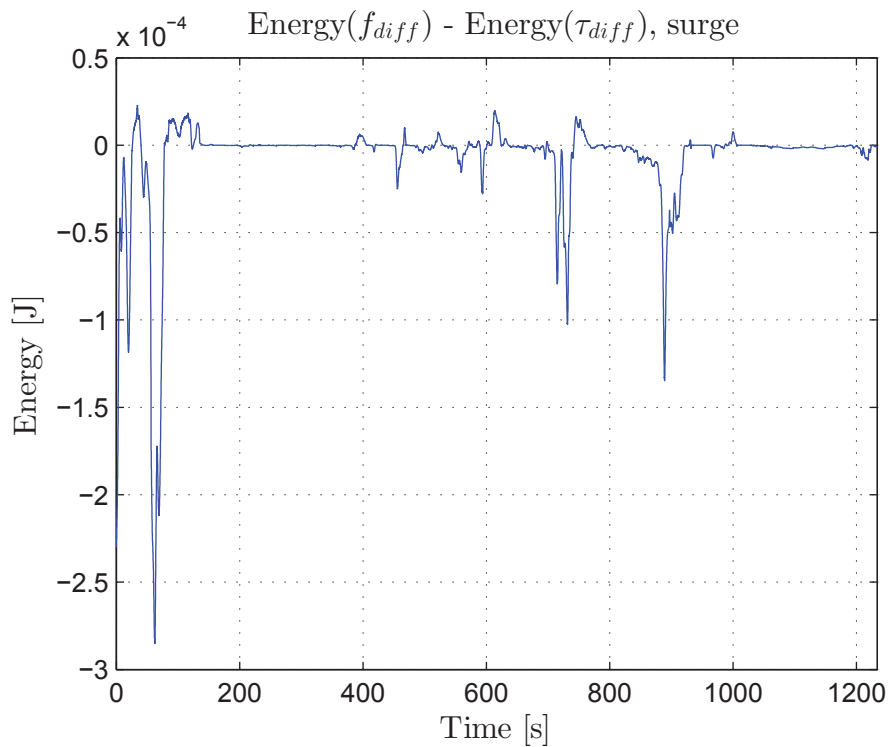


Figure 7.17: Energy of f_{diff} subtracted energy of τ_{diff} for toughest ice condition, surge direction.

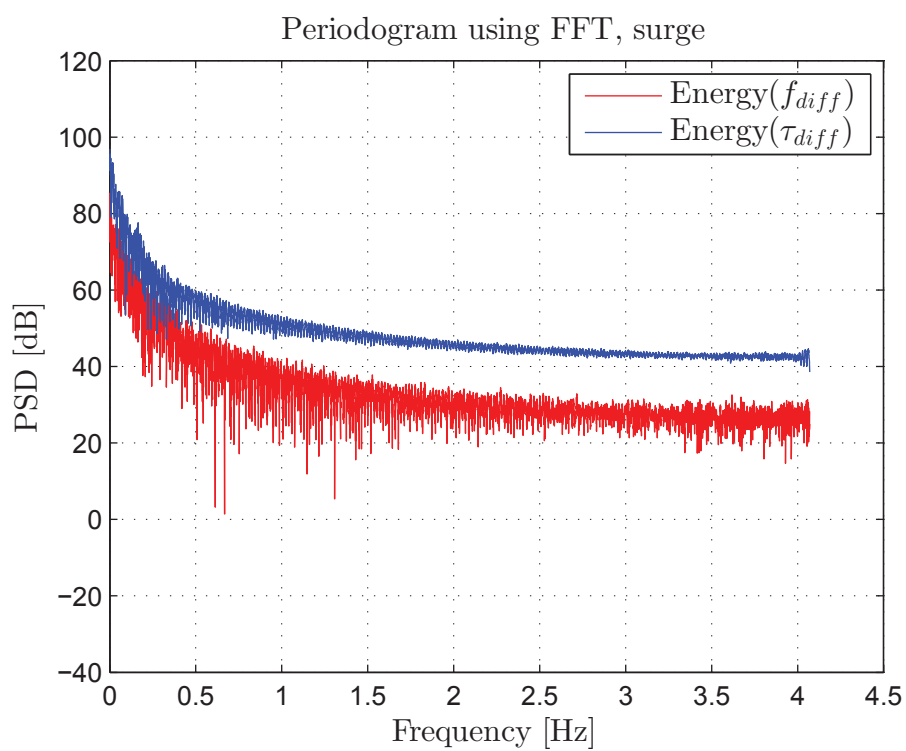


Figure 7.18: Frequency analysis of the energy of f_{diff} and τ_{diff} for the toughest ice condition, surge direction.

Chapter 8

Discussion

The main objectives of this study were to implement and test an optimization based TA including thruster dynamics and TIC, suggest suitable methods for illustrating the performance and implementing prioritization of DOFs. A case study was carried out using towing tank measurement data from CIV Arctic and the results were illustrated using the methodology described in Section 6.9. A brief discussion of the results will be given in Section 8.1, along with drawbacks of the towing tank measurement data, parameter tuning and the prioritization of DOFs. A more detailed discussion of the results, along with the methods used, is presented in sections 8.2 - 8.4. The results from the energy considerations are discussed in Section 8.5.

8.1 General Discussion

In general, $\mathbf{s}^\top \mathbf{Q} \mathbf{s}$ increased with increasing ice thickness. Increasing the ice concentration from 90 [%] to 100 [%] increased $\mathbf{s}^\top \mathbf{Q} \mathbf{s}$ as well, for instance with a magnitude of approximately 10 times for $h_i = 0.5$ [m] and $h_i = 0.8$ [m] in Case I. When the ice thickness was increased to 1.2 [m], the slack term increased significantly. For all cases, except Case III, $\mathbf{s}^\top \mathbf{Q} \mathbf{s}$ increased with approximately 1000 times from $h_i = 0.8$ [m] to $h_i = 1.2$ [m] for $C = 100$ [%]. In real life, this means that by reducing the ice concentration from 100 [%] to 90 [%], for instance by IM, it is more likely that the vessel is able to be on DP. Also, the results indicated that 1.2 [m] of ice may be too much for the DP control system to handle.

Investigating the error, for light ice conditions, such as $C = 90$ [%] and the two smallest ice thicknesses, it did not have any distinct increase with respect to drift angle. Two exceptions are for Cases IV and V, when TIC was added to the TA, and the error was larger compared to the previous cases. For 100 [%] ice concentration, the error was larger than for 90 [%] ice concentration, and the prioritization of DOFs was more visible. Sorting the error by DOFs showed a clear picture that the error for $h_i = 1.2$ [m] was in general larger than the other ice thicknesses. There are some exceptions, for instance for some of the drift angles for Case V with $C = 100$ [%]. For 90 [%] ice concentration the error was

not so large and the prioritization of DOFs not that clear.

For $C = 100$ [%], $h_i = 1.2$ [m] and $\theta = 10$ [deg], $\mathbf{s}^\top \mathbf{Q} \mathbf{s}$ was significantly larger compared to the other drift angle for all cases. Looking further into the ice loads, τ_{ice} , applied to the TA, it seemed like the TA was not able to counteract all the ice loads in the beginning if they were too large. As seen in Figure 8.1, the TA was not able to counteract for the ice loads the first approximately 100 [s]. In this ice condition, the ice loads in the beginning were too large for the TA to withstand and the error became large. Some of the reason may be that the TA needed some time to stabilize the thruster levels and azimuth angles to desired values. Later in the time series for sway, it can be seen several times that the TA was not able to counteract for sway forces. This is assumed to be due to the prioritization of DOFs.

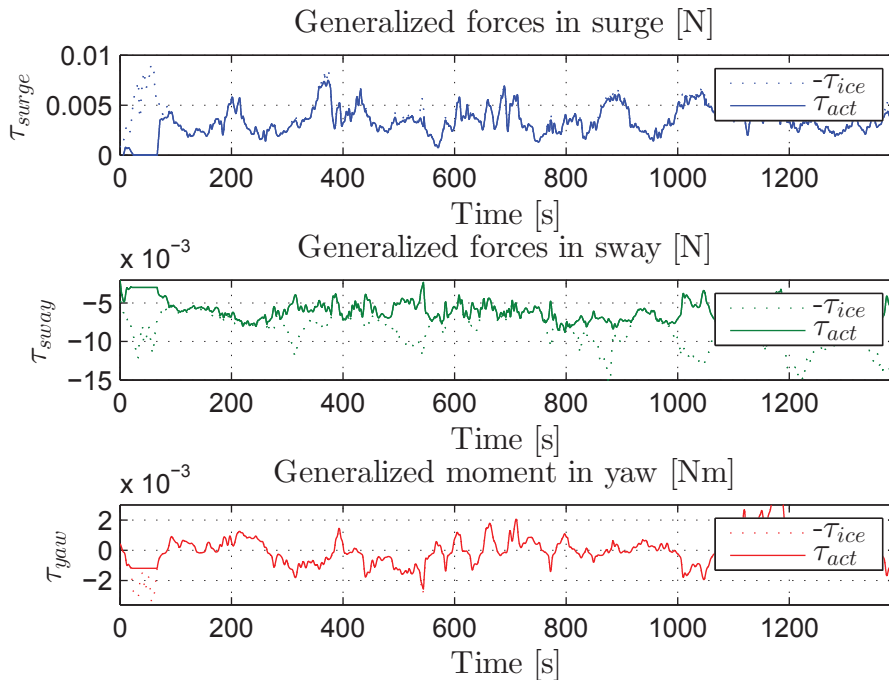


Figure 8.1: τ_{ice} and τ_{act} for Case I with $C = 100$ [%], $h_i = 1.2$ [m] and $\theta = 10$ [deg].

In the case study, towing tank measurement data from CIV Arctic were used as input to the TA. It is difficult and expensive to gather real life measurement data, so model test data is believed to be adequate in the design of DP systems [11]. Drawbacks with model tests in ice are for instance that the ice floes are preformed into squares, which are not realistic, and the effects from the basin walls. At the side of the basin at least two of the ice floes did not move when the ship was towed through the ice sheet, and it is therefore believed that the width of the basin did not affect the measurement data. But at the end of the model basin, the ice tended to pack together and might give a higher ice concentration. The measurement data were stopped when this before this was noticeably, but it might have had some effect. In the towing tests, the vessel was towed through the model basin, without running propulsion, with restrictions on movement in surge, sway

and yaw. In practice, the vessel will only have limited amount of power, and for heavy ice conditions the velocity of the vessel will decrease before the ice splits. Compared to real life measurement data, the peaks in ice loads, from the towing tank measurement data, might not be as large. Even though there are some large peaks in the towing tank measurement data, the DP system would perhaps not be able to react on them. This can be because they change too fast [11, 39], and will only push the vessel a little out of position. This is an interesting subject, and what the energy analysis in Chapter 5 tries to shed light on.

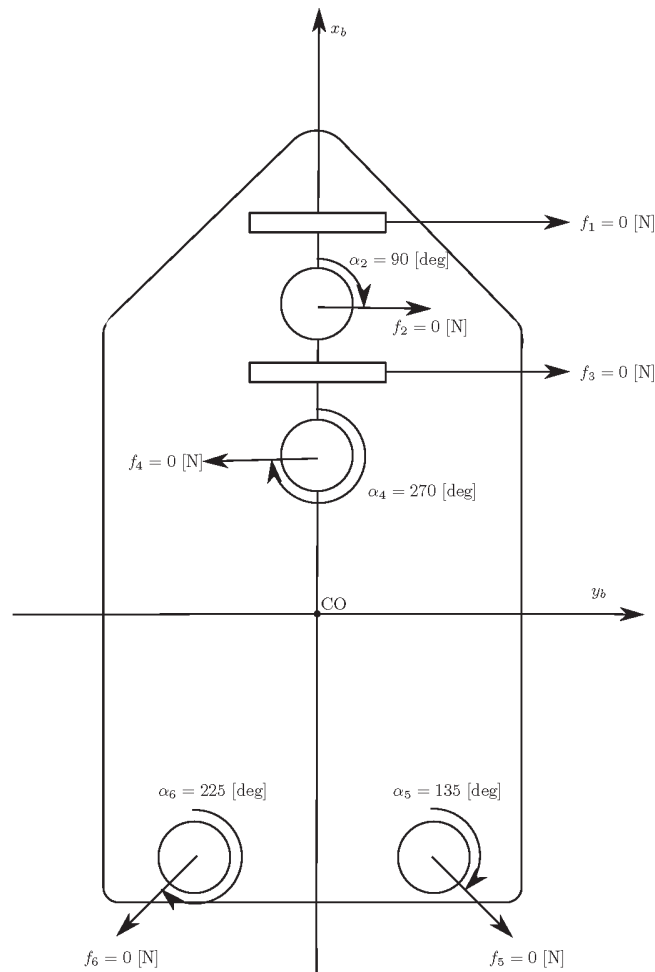


Figure 8.2: Initial values for the case study vessel.

The number of tuning parameters in the TA algorithm is substantial. Equations (7.4) - (7.11) contain a total of 23 parameters to be tuned for satisfactory performance. Some guidelines for tuning are given in Section 7.1.6, but it is likely that the parameters can be tuned even better. This may be challenging because experience from tuning of the TA algorithm has shown that small change in parameters and initial values will affect the performance of the TA. The initial values for the control forces, \mathbf{f} , and the azimuth angles, $\boldsymbol{\alpha}$, for the case study is presented in Figure 8.2. For DP applications this initial thruster configuration seemed to be good because the angles of the azimuth thrusters were well distributed around 360 [deg]. The slack variables, \mathbf{s} , were initialised to 0. The scope

of this work did not include finding optimal tuning parameters, but rather to implement and test a TA algorithm with satisfactory performance. For that reason, more effort should be put into finding optimal tuning parameters, for instance to avoid near singular configurations as mentioned in [43].

To achieve predictable degradation of the TA's performance when the ice loads are too high, prioritization of DOFs was implemented using the weights of the slack variables, \mathbf{Q} . As presented in Section 7.1.5, the main priority is to keep the desired moments in yaw. Then, the vessel will ideally be bow first straight towards the ice and the sway forces will be zero. The results presented in sections 7.2 and 7.3 indicated that for though ice conditions the prioritization of DOFs was followed. This means that the largest error was in sway and the smallest in yaw.

8.2 Thrust Allocation

The TA algorithm chosen for this work was the most advanced, including for instance restrictions on azimuth angle rates and singularity avoidance. It was based on numerical optimization, and was on a form such that QP could be used, but since it is so advanced the number of tuning parameters was found to be extensive.

The results presented in Section 7.2.1 indicated relatively small errors and slack for Case I, compared to the other cases. When the ice loads were large, from approximately $\theta = 10$ [deg] and above for $C = 90$ [%] and for all ice conditions for $C = 100$ [%], the error followed the prioritization of DOFs, as described in Section 7.1.5. Reducing the ice concentration from 100 [%] to 90 [%], for instance by using IM, resulted in a smaller slack term. In Figure 7.2 it can be seen that for two of the ice conditions $\mathbf{s}^T \mathbf{Q} \mathbf{s}$ was significantly larger than the others. For $C = 100$ [%], $h_i = 0.5$ [m] and $\theta = 5$ [deg] the magnitude of the slack variable was $7.49 \cdot 10^{-5}$. By investigating the error for this ice condition, Figure 7.5 reveals that most of the error comes from sway direction. Looking into the time series of τ_{ice} and τ_{act} for sway it was noticed that the error was substantial in the period between approximately 950 [s] and 1200 [s], as seen in Figure 8.3. The TA was not able to withstand the sway forces of the ice loads in this period of time, because the available control forces were used to withstand the yaw moments and most of the surge forces. This was according to the prioritization of DOFs and was expected. The other large slack term was for $C = 100$ [%], $h_i = 1.2$ [m] and $\theta = 10$ [deg]. The reason for this is partly explained above, in Section 8.1. Another reason can be that the error in yaw was quite large, as seen in Figure 7.7, which was due to the error in the first 100 [s], as seen in figure 8.1. Multiplying the slack in yaw, quadratically, with the weight of the slack in yaw, $\mathbf{Q}_{yaw} = 5000$, the results will be very large.

8.3 Thrust Allocation with Thruster Dynamics

To make the TA more realistic, thruster dynamics were added to the optimization problem. Two strategies were tried out to approximate the physical dynamics of the thrusters. First,

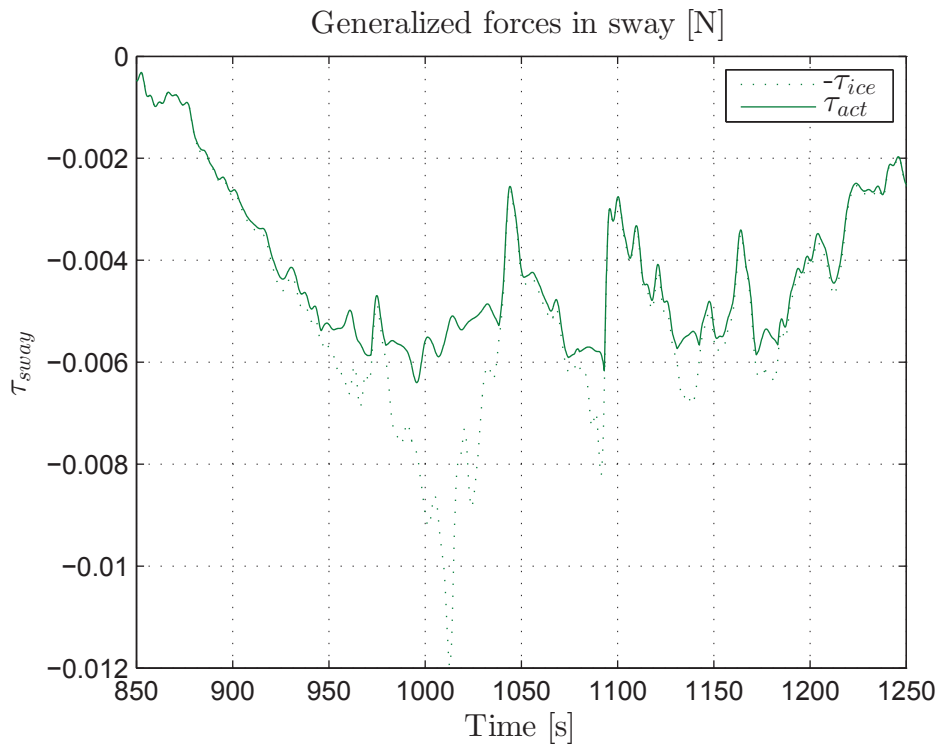


Figure 8.3: τ_{ice} and τ_{act} between 870 [s] and 1250 [s] for Case I with $C = 100$ [%], $h_i = 0.5$ [m] and $\theta = 5$ [deg].

a LP filter was included. A disadvantage with the LP filter is that the TA algorithm does not know of it, and since only the control forces were LP filtered the slack variables were equal to the ones in Case I. The results may have been better if the control forces were LP filtered on-line, but this was not considered in this report because the second way of approximating the thruster dynamics was found to be a better solution. Including restrictions on the control forces, implicitly in the TA algorithm, enables the optimization problem to be solved with constraints on the control force rates. In the original TA algorithm, this was already included for azimuth angle rates, and easy to include for the control forces.

Unfortunately, $\mathbf{s}^\top \mathbf{Q} \mathbf{s}$ for Case II was not able to provide new information about the slack, due to reasons described above. For Case III, on the other hand, $\mathbf{s}^\top \mathbf{Q} \mathbf{s}$ indicated that the slack was larger when adding thruster dynamics. With 100 [%] ice concentration and 1.2 [m] of ice, the slack term was very large for Case I and did not increase very much for Case III. For the same ice concentration, but with $h_i = 0.8$ [m], the slack term increased significant, with approximately 5000 for 0 [deg] drift angle as an example.

At first glance, the error in yaw for Case II was quite large. For several of the ice conditions the error in yaw was larger than for surge and sway, and did not follow the prioritization of DOFs. The error in surge and sway were not that different from Case I, but the error in yaw was quite different. For some of the ice conditions, it was actually negative, meaning that the TA produced more thrust than what was required to withstand the ice loads. This can have something to do with that the control forces were LP filter after

the optimization, but this must be looked further into. For Case III, with $C = 100$ [%], $h_i = 0.5$ [m] and $\theta = 0$ [deg], the error was also negative. Another reason for the negative error can be that the TA must produce too much forces in sway to keep the desired forces and moments in surge and yaw. The negative error seemed to happen more frequently for Case II. It can be that the off-line LP filtering worsens the error compared to Case III, when thruster dynamics was included implicitly in the TA algorithm. Finally, the error for Case III was very different compared to Case I. For $C = 90$ [%], the error did not follow the prioritization of the DOFs, and in magnitude it was larger. But increasing the ice concentration to 100 [%] did not result in a significant increase of error, except for $h_i = 0.5$ [m].

8.4 Thrust Allocation with Thruster Ice Clearance

In Section 4.2, two solutions were proposed for implementing TIC. For both solutions, sectors were defined for the azimuth thrusters to apply control forces within. In the first solution, the TA algorithm decided which azimuth angles were best within these sectors, and a minimum limit of control forces were applied to the thrusters in those directions. For the second approach, two terms were added to the objective function to let the azimuth thrusters follow predefined references in control forces and azimuth angles. The first approach was simple and minor changes were needed in the optimization problem to make it work. The downside was that the vessel operator will have little control with the directions the azimuth thrusters applied forces. The second approach aimed to let the vessel operator have more control of the behaviour of the azimuth thrusters used for TIC. Two additional tuning parameters were introduced, but it is believed that the second solution give a more predictable behaviour. The first solution can roughly be converted into the second solution by making the sectors very narrow and change the directions of the sectors, but the second solution is considered as a better design.

Judging by the slack term, adding TIC to the TA followed roughly the same development with respect to drift angle as for Case I. Exceptions are that the magnitude was larger, and for Case V with $C = 100$ [%], $h_i = 0.5$ [m] where the slack term changed to be approximately linear increasing.

The error for Case IV looked similar to Case I, only with a larger magnitude, except for $C = 90$ [%] and $h_i = 0.5$ [m] which is nearly equal to Case I. For 100 [%] ice concentration the error was largest for 1.2 [m] of ice and the prioritization of DOFs was ensured. For the second solution of TIC the development of the error was not so clear. Compared to Case I and IV, the error was in general larger for Case V. The error for $C = 100$ [%] and $h_i = 1.2$ [m] did not increase significantly with respect to θ , and the error sorted by DOFs was not that clearly dominated by $h_i = 1.2$ [m] as in previous cases. This is not because the error for $h_i = 1.2$ [m] was smaller, but because the error for the other ice thicknesses had become larger. The prioritization of DOFs was still followed for most of the ice conditions, but some of the errors were negative. The reason for the negative error can be that the TA tries to follow the reference in control forces, \mathbf{f}_{ref} , and therefore produces more thrust than needed to withstand the ice loads.

8.5 Energy Considerations

The results presented in Section 7.3, with primary focus on Table C.1 - C.5, gave indications on possible drift-offs. The results indicated that adding thruster dynamics to the TA did not increase to the possibility for not being able to keep desired position and heading. This means that the possibility for drift-offs did not increase by making the TA algorithm more realistic by adding thruster dynamics. By adding TIC to the original TA algorithm, the results indicated that the possibility for drift-offs were present for lighter ice conditions than for the previous cases. The energy considerations indicated that by letting the TA decide the azimuth angles, on the azimuth thrusters used for TIC, it was able to withstand the ice loads for more of the ice conditions, compared to forcing them to follow predefined references. On the other hand, these negative results in the energy consideration were only for sway.

Comparing the results for Case I with results from CIV Arctic [39], the TA presented in this report was able to withstand more of the ice conditions. With the same prioritization of DOFs, the TA in the CIV Arctic report was not able to withstand the ice loads in sway for $h_i = 0.5$ [m], $C = 100$ [%], $\theta = 5$ [deg] and for 1.2 [m] of ice with $C = 90$ [%], $\theta = 5$ [deg]. For $h_i = 1.2$ [m], $C = 100$ [%] and $\theta = 0$ [deg] the TA in the CIV Arctic report was not able to withstand the ice loads in surge and sway. For the other ice conditions the results were equal. Note that the TA used in the CIV Arctic report was simplified by clustering the thrusters together in one place at front and rear. Comparing the results, for Case I, to a constrained nullspace-based TA [17], where the same vessel and input data was used, the results were the same. For sway, the TA was not able to withstand the ice loads for the same ice conditions. The three cases where the ice loads in surge was the problem, [17] showed that it can be possible. In tables C.1 - C.5 it is only shows possible or not possible drift-offs, but in [17] the results are presented in detail. Even though the results gave positive results, they can be very close to negative and a more detailed way of presenting the result could have been considered.

Chapter 9

Conclusion

In this final chapter, some conclusions based on previous presented material will be given. Some conclusions on the choice of the TA algorithm, including design choices for thruster dynamics and TIC, will be drawn out, with a subsequent conclusion on the results. Then, some conclusions regarding the energy considerations, and how the results can say anything about the DP capability, will be presented. Finally, some suggestions for further work will be given.

9.1 Concluding Remarks

Based on the discussion in Chapter 8, the error of the TA was in general reduced when the ice concentration was reduced from 100 [%] to 90 [%]. In real life, use of IM will achieve this. To check the performance of the TA algorithm, the results showed that first looking at the slack term, $\mathbf{s}^\top \mathbf{Q} \mathbf{s}$, gave a first impression. But to be able to look into the reason for the slack variable, the error in produced thrust should be looked into in more detail. Also, when the ice loads became too high, the prioritization of DOFs was present.

Conclusion based on the methods and results will be carried out below in the same manner as the results and discussions were presented.

9.1.1 Thrust Allocation

The TA algorithm chosen for implementation was the most advanced one described in Section 2.1.2. It is based on numerical optimization and includes features such as singularity avoidance and physical constraints on azimuth thrusters. Even though the number of tuning parameters is large, it is assumed that this TA algorithm is the best with respect to real life performance because of the included features.

For light ice conditions, the results indicated that the case study vessel using the developed TA was able to withstand the ice loads. For larger ice loads, in the other hand, the error

between the ice loads and produced thrust became large and the possibility for drift-offs increased.

9.1.2 Thrust Allocation with Thruster Dynamics

One thing that was not included in the TA algorithm, given in equations (2.6) - (2.10), was the dynamics of the control forces. To make the algorithm better for real life performance, thruster dynamics were added. Two solutions were purposed, LP filtering and adding new restrictions implicitly in the TA algorithm. It is believed that the second solution is the best because then the TA algorithm know of the thruster dynamics while doing the optimization, as was already done for the azimuth angle rates in Equation (2.10). The resulting optimization is given in equations (3.2) - (3.7).

Based on the results in Section 7.2.2, the TA with restrictions on change of control forces performed well compared to Case I. The error in yaw was smaller compared to Case II, and the degradation of performance follows the prioritization of DOFs, as presented in Section 7.1.5, well for heavy ice conditions. Adding thruster dynamics to the TA did not increase the error very much, except for Case II where the error in yaw was quite significant.

9.1.3 Thrust Allocation with Thruster Ice Clearance

Based on the discussion in Section 8.4, the second solution for including TIC into the TA algorithm is considered the best choice. A positive factor for the first solution is that the TA chooses the best azimuth angles to withstand the ice loads, and the all over performance of the TA seems to be better judging by the results in Section 7.2.3. Even though the error was larger, the second solution is considered the best way of solving the TIC, because it gives better control over the azimuth thrusters. The IM performed by the Finnish ice breaker "MSV Fennica", which used the thruster wakes to clear the ice shows a great potential for TIC [3], and perhaps the DP system can be enhanced by incorporating it in the TA.

Looking at the results in Section 7.2.3, the performance for Case IV was better for some of the ice conditions compared to Case V, which might be because the TA chooses the best azimuth angles to withstand the ice loads. This applies primarily to $h_i = 0.5$ [m] and $h_i = 0.8$ [m], because the error for $h_i = 1.2$ [m] was quite the same for both cases. Compared to case I, the error was not very different for $C = 90$ [%], $h_i = 0.5$ [m]. For larger ice conditions the error increased significantly from Case I to Cases IV and V.

9.1.4 Energy Considerations

Using energy considerations, and looking at the difference in energy of the ice loads the TA was not able to counteract for and the energy of the remaining control forces after the optimization, some indications on possible drift-offs can be given. The results do not

give a clear picture of whether the vessel is able to be on DP, but rather an indication of possible drift-offs over time. This is based on how much control forces are left after the optimization to counteract for the ice loads the TA did not withstand.

Based on the results in Section 7.3 and discussions in Section 8.5, it can be concluded that the TA was able prevent drift-offs for all $h_i = 0.5$ [m] and $h_i = 0.8$ [m], except for large drift angles for Cases IV and V. For $h_i = 1.2$ [m], $C = 100$ [%] the energy consideration indicated possible drift-offs for drift angles from 5 [deg] and above. Including thruster dynamics did not affect the possibility for drift-offs, but by adding TIC the possibility for drift-offs was present for lighter ice conditions compared to Case I.

The primary goal for the prioritization of DOFs was to use more effort to withstand the ice loads in yaw, and it was achieved by the energy considerations always giving a positive result for the moments in yaw.

9.2 Future Work

This study has focused on optimizing the TA for Arctic conditions, and included thruster dynamics and TIC. Some ideas have been implemented and simulated in the case study, but more can still be done to give better performance of the TA. Some recommendations for further work are:

- The results from the case study give an indication of the performance of the TA. The whole DP control system, as in Figure 1.2, should be simulated to investigate how well the DP vessel in ice performs with the TA algorithm including thruster dynamics and TIC.
- Test the TA on a real vessel.
- In the second way of including thruster dynamics, the restrictions on change of control forces can be divided into 3 steps, as described in Section 3.2.
- Integrate the PMS in the thruster dynamics with restrictions on change of control forces. The restrictions can be dependent on the states of the engines and information can be passed between the modules.
- Use mathematical models to investigate automatic activation of TIC based on model prediction.
- Further improvement of the reference signals used in TIC solution 2. Both how fast the azimuth thrusters should flush back and forth and how large the references in control forces should be. Adaptation, based on mathematical models of the ice, can be included.
- Investigate how wide the azimuth sectors for TIC should be, and possible time-varying dependent on the ice conditions.
- Do a more detailed analysis of the energy considerations to investigate how close the TA is to possible drift-offs. Also, investigate when in the time series this might

happen.

- Include a more sophisticated way of defining forbidden thruster zones for the azimuth thrusters to avoid thruster losses, for instance thruster-thruster losses [33].
- Better tuning of parameters to improve performance.
- Investigate the negative errors.

Bibliography

- [1] ABB. Azipod® VI Series Product Introduction. [http://www05.abb.com/global/scot/scot293.nsf/veritydisplay/f524ca488f88beb2c12576e3004a96d8/\\$file/Azipod_VI_project_guide_v5.pdf](http://www05.abb.com/global/scot/scot293.nsf/veritydisplay/f524ca488f88beb2c12576e3004a96d8/$file/Azipod_VI_project_guide_v5.pdf). Accessed: October 12th 2012.
- [2] International Marine Contractors Association. Specification for DP Capability Plots, IMCA M 140 Rev 1, 2000.
- [3] T. Berg. Untraditional Ice Management. Arctic Shipping Forum, Helsinki, 2013.
- [4] T.E. Berg, B.O. Berge, S. Hanninen, R.A. Suojanen, and H. Borgen. Design Considerations for an Arctic Intervention Vessel. In *OTC Arctic Technology Conference*, 2011.
- [5] Det Norske Veritas. *Rules for Classification of Ships: Dynamic Positioning Systems - Enhanced Reliability DYNPOS-ER, Part 6, Chapter 26*. Veritasveien 1, N-1322 Høvik, Norway, January 2011.
- [6] Det Norske Veritas. *Rules for Classification of Ships: Dynamic Positioning Systems, Part 6, Chapter 7*. Veritasveien 1, N-1322 Høvik, Norway, July 2011.
- [7] K.J. Eik. *Ice Management in Arctic Offshore Operations and Field Development*. PhD thesis, Norwegian University of Science and Tehcnology (NTNU), 2010.
- [8] T.I. Fossen. *Handbook of Marine Craft Hydrodynamics and Motion Control*. Wiley, 2011.
- [9] T. Heideman and S. Hänninen. Propulsion in Ice. In *Marine Technology*, pages 23–27. SNAME Magazine, USA, January 2011.
- [10] S.A. Hughes. *Physical Models and Laboratory Techniques in Coastal Engineering*, volume 7. World Scientific Publishing Company Incorporated, 1993.
- [11] N.A. Jenssen, S. Muddesitti, D. Phillips, and K. Backstrom. DP In Ice Conditions. In *Dynamic Positioning Conference*, 2009.
- [12] T.A. Johansen, T.I. Fossen, and S.P. Berge. Constrained Nonlinear Control Allocation with Singularity Avoidance using Sequential Quadratic Programming. *Control Systems Technology, IEEE Transactions on*, 12(1):211–216, 2004.

- [13] K. Juurmaa, T. Mattsson, and G. Wilkman. The development of the new double acting ships for ice operation. In *16th International Conference on Port and Ocean Engineering under Arctic Conditions (POAC'01)*, Ottawa, 2001.
- [14] M. Juva and K. Riska. On the power requirement in the Finnish-Swedish ice class rules. *Winter Navigation Research Board*, 53, 2002.
- [15] A.J. Keinonen. Ice Management for Ice Offshore Operations. Houston, Texas, May 5-8 2008. Arctic Technology Conference.
- [16] Ø.K. Kjerstad. personal communication, November 6th 2013.
- [17] Ø.K. Kjerstad, R. Skjetne, and B.O. Berge. Constrained nullspace-based thrust allocation for heading prioritized stationkeeping of offshore vessels in ice. In *In Proceedings of the 22th International Conference on Port and Ocean Engineering under Arctic Conditions*, Helsinki, Finland, 2013.
- [18] MARINTEK. *Fact Sheet. ShipX - Station Keeping*, January 2012.
- [19] MARINTEK CIV Arctic KMB. CIV Arctic. <http://www.sintef.no/Projectweb/CIV-Arctic/>. Accessed: March 9th 2013.
- [20] MathWorks. butter - Butterworth filter design. <http://www.mathworks.se/help/signal/ref/butter.html>. Accessed: March 14th 2013.
- [21] MathWorks. filter - 1-D digital filter. <http://www.mathworks.se/help/matlab/ref/filter.html>. Accessed: March 14th 2013.
- [22] MathWorks. quadprog - Quadratic programming, R2012b Documentation. <http://www.mathworks.se/help/optim/ug/quadprog.html>. Accessed: September 24th 2012.
- [23] I. Metrikin, S. Løset, N.A. Jenssen, and S. Kerkeni. Numerical Simulation of Dynamic Positioning in Ice. In *DP Conference, Houston, USA, October*, pages 9–10, 2012.
- [24] K. Moran, J Backman, and J.W. Farrell. Deepwater drilling in the arctic ocean's permanent sea ice. In *Proceedings of the Integrated Ocean Drilling Program*, volume 302, 2006.
- [25] J. Nocedal and S.J. Wright. *Numerical Optimization*. Springer, 2nd edition, 2006.
- [26] Norwegian University of Science and Technology. KMB Arctic DP. <http://www.marin.ntnu.no/arctic-dp>. Accessed: March 9th 2013.
- [27] International Bureau of Weights, Measures, and Barry N Taylor. *The international system of units (SI)*. US Department of Commerce, Technology Administration, National Institute of Standards and Technology, 2001.
- [28] L.D. Paarmann. *Design and Analysis of Analog Filters: A Signal Processing Perspective*. The Springer International Series in Engineering and Computer Science. Springer, 2001.
- [29] K. Riska. Design of Ice Breaking Ships. *Course material NTNU*, 2011.

- [30] E. Ruth. *Propulsion control and thrust allocation on marine vessels*. PhD thesis, Norwegian University of Science and Tehcnology (NTNU), 2008.
- [31] R. Schwandt. Ice-Breaking with Streerable Thrusters. In *Dynamic Positioning Conference*, 2005.
- [32] SNAME. Nomenclature for Treating the Motion of a Submerged Body Through a Fluid. *The Society of Naval Architects and Marine Engineers, Technical and Resarch Bulletin No. 1-5*, 1950.
- [33] A.J. Sørensen. *Marine Control Systems: Propulsion and Motion Control of Ocean Structures*. Department of Marine Technology, NTNU, 2012.
- [34] A.J. Sørensen, A.K. Ådnanes, T.I. Fossen, and J.P. Strand. A new method of thruster control in positioning of ships based on power control. *4th IFAC Conference on Manoeuvring and Control of Marine Craft (MCMC'97), Brijuni, Croatia, 172*, 179, 1997.
- [35] Statoil. Statoil stepping up in the Arctic. http://www.statoil.com/en/NewsAndMedia/News/2012/Pages/28aug_Arctic.aspx. Accessed: October 15th 2012.
- [36] B. Su, Ø.K. Kjerstad, R. Skjetne, and T.E. Berg. Ice-going capability assessment and DP-Ice Capability Plot for a double acting intervention vessel in level ice. In *In Proceedings of the 22th International Conference on Port and Ocean Engineering under Arctic Conditions*, Helsinki, Finland, 2013.
- [37] United States Geological Survey. 90 Billion Barrels of Oil and 1,670 Trillion Cubic Feet of Natural Gas Assessed in the Arctic. <http://www.usgs.gov/newsroom/article.asp?ID=1980>. Accessed: October 15th 2012.
- [38] U.S. Energy Information Administration. Data Highlights. <http://www.eia.gov/>. Accessed: May 27th 2013.
- [39] V. Valtonen. Analysis of ice loads affecting on vessel in DP, based on ice model test measurements, AARC report number K-151. Technical report, Aker Arctic Technology Inc., 2011.
- [40] A. Veksler and H.L. Lundeberg. personal communication, April 9-11 2013.
- [41] G. Wilkman and Aker Arctic Technology Inc. Experience of Air Bubbling System in Ice Navigation and Future Possibilities. Houston, Texas, February 7-9 2011. Arctic Technology Conference.
- [42] G. Wilkman, R. Suojanen, S. Saarinen, T. Mattson, and T. Leiviskä. DP In Ice Conditions - Challenges and Opportunities. *Marine Technology Society, Houston, US*, 2009.
- [43] H.E. Wold. Optimal thrust allocation in Arctic DP with thruster ice clearance. Technical report, Norwegian University of Science and Technology (NTNU), 2012.
- [44] Capt P. Zahalka. Bollard Pull. Technical report, Association of Hanseatic Marine Underwriters, 2008.

Appendix A

quadprog Matrices

An overview of the matrices used in *quadprog* is:

$$\mathbf{H} = \begin{bmatrix} 2\mathbf{P} & 0_{6 \times 4} & 0_{6 \times 3} \\ 0_{4 \times 6} & 2\mathbf{\Omega} & 0_{4 \times 3} \\ 0_{3 \times 6} & 0_{3 \times 4} & 2\mathbf{Q} \end{bmatrix} \in \mathbb{R}^{r+p+n \times r+p+n} \quad (\text{A.1})$$

$$\mathbf{g} = \begin{bmatrix} 2\mathbf{P}\mathbf{f}_0 \\ \left[\frac{\partial}{\partial \boldsymbol{\alpha}} \left(\frac{\rho}{\varepsilon + \det(\mathbf{T}(\boldsymbol{\alpha})\mathbf{W}^{-1}\mathbf{T}^\top(\boldsymbol{\alpha}))} \right) \Big|_{\boldsymbol{\alpha}=\boldsymbol{\alpha}_0} \right]^\top \\ \mathbf{0}_{n \times 1} \end{bmatrix} \in \mathbb{R}^{r+p+n} \quad (\text{A.2})$$

$$\mathbf{A} = \begin{bmatrix} \mathbf{I}_{r \times r} & \mathbf{0}_{r \times p} & \mathbf{0}_{r \times n} \\ -\mathbf{I}_{r \times r} & \mathbf{0}_{r \times p} & \mathbf{0}_{r \times n} \\ \mathbf{0}_{p \times r} & \mathbf{I}_{p \times p} & \mathbf{0}_{p \times n} \\ \mathbf{0}_{p \times r} & -\mathbf{I}_{p \times p} & \mathbf{0}_{p \times n} \end{bmatrix} \in \mathbb{R}^{2r+2p \times r+p+n} \quad (\text{A.3})$$

$$\mathbf{b} = \begin{bmatrix} \mathbf{f}_{max} - \mathbf{f}_0 \\ -\mathbf{f}_{min} + \mathbf{f}_0 \\ \boldsymbol{\alpha}_{max} - \boldsymbol{\alpha}_0 \\ -\boldsymbol{\alpha}_{min} + \boldsymbol{\alpha}_0 \end{bmatrix} \in \mathbb{R}^{2r+2p} \quad (\text{A.4})$$

$$\mathbf{A}_{eq} = [\mathbf{T}(\boldsymbol{\alpha}_0) \quad \frac{\partial}{\partial \boldsymbol{\alpha}} (\mathbf{T}(\boldsymbol{\alpha})\mathbf{f}) \Big|_{\boldsymbol{\alpha}=\boldsymbol{\alpha}_0, \mathbf{f}=\mathbf{f}_0} \quad \mathbf{I}_{3 \times 3}] \in \mathbb{R}^{n \times r+p+n} \quad (\text{A.5})$$

$$\mathbf{b}_{eq} = \boldsymbol{\tau} - \mathbf{T}(\boldsymbol{\alpha}_0)\mathbf{f}_0 \in \mathbb{R}^n \quad (\text{A.6})$$

$$\mathbf{lb} = \begin{bmatrix} \Delta \mathbf{f}_{min} \\ \Delta \boldsymbol{\alpha}_{min} \\ -\infty_{n \times 1} \end{bmatrix} \in \mathbb{R}^{r+p+n} \quad (\text{A.7})$$

$$\mathbf{ub} = \begin{bmatrix} \Delta \mathbf{f}_{max} \\ \Delta \boldsymbol{\alpha}_{max} \\ \infty_{n \times 1} \end{bmatrix} \in \mathbb{R}^{r+p+n} \quad (\text{A.8})$$

where

$$\begin{aligned}
\mathbf{P} &= \mathbf{P}^\top \in \mathbb{R}^{r \times r} \\
\mathbf{\Omega} &= \mathbf{\Omega}^\top \in \mathbb{R}^{p \times p} \\
\mathbf{Q} &= \mathbf{Q}^\top \in \mathbb{R}^{n \times n} \\
\mathbf{T}(\boldsymbol{\alpha}) &\in \mathbb{R}^{n \times r} \\
\mathbf{W} &= \text{diag}(w_1, w_2, \dots, w_r) \in \mathbb{R}^{r \times r} \\
\boldsymbol{\tau} &\in \mathbb{R}^n
\end{aligned}$$

For TIC solution 2, the \mathbf{g} vector is given by:

$$\mathbf{g} = \begin{bmatrix} 2\mathbf{P}(\mathbf{f}_0 - \begin{bmatrix} 0 \\ \mathbf{f}_{ref}(1) \\ 0 \\ \mathbf{f}_{ref}(2) \\ 0 \\ 0 \end{bmatrix}) \\ \begin{bmatrix} sa(1) + 2\gamma(\boldsymbol{\alpha}_0(1) - \boldsymbol{\alpha}_{ref}(1)) \\ sa(2) + 2\gamma(\boldsymbol{\alpha}_0(2) - \boldsymbol{\alpha}_{ref}(2)) \\ sa(3) \\ sa(4) \\ \mathbf{0}_{n \times 1} \end{bmatrix} \end{bmatrix} \in \mathbb{R}^{r+p+n} \quad (\text{A.9})$$

because of the two added terms including the references, \mathbf{f}_{ref} and $\boldsymbol{\alpha}_{ref}$. The variable sa is the singularity avoidance term, given by $\left[\frac{\partial}{\partial \boldsymbol{\alpha}} \left(\frac{\rho}{\varepsilon + \det(\mathbf{T}(\boldsymbol{\alpha})\mathbf{W}^{-1}\mathbf{T}^\top(\boldsymbol{\alpha}))} \right) \Big|_{\boldsymbol{\alpha}=\boldsymbol{\alpha}_0} \right]^\top \in \mathbb{R}^p$.

Appendix B

Appendix Results

The case study resulted in numerous figures, and not all of them could be presented in the report. The most notable figures were presented in section 7.2.1 - 7.2.3, and the rest will be presented below in sections B.1 - B.2.

B.1 Thrust Allocation with Thruster Dynamics

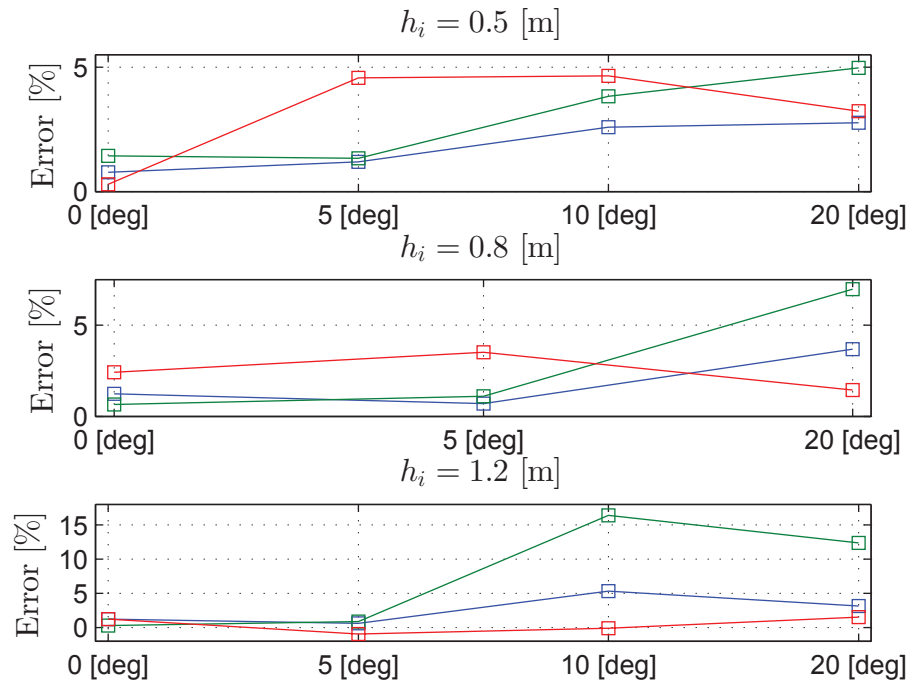


Figure B.1: Results from Case II: Error sorted by h_i , $C = 90$ [%]. — Surge, — Sway, — Yaw.

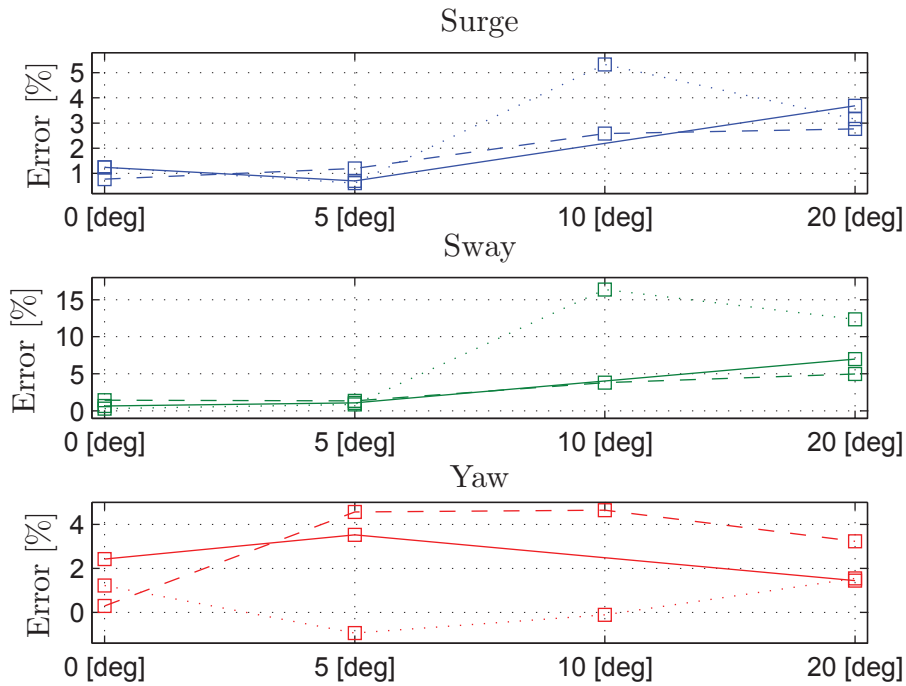


Figure B.2: Results from Case II: Error sorted by DOF, $C = 90$ [%]. -- $h_i = 0.5$ [m], — $h_i = 0.8$ [m], \cdots $h_i = 1.2$ [m].

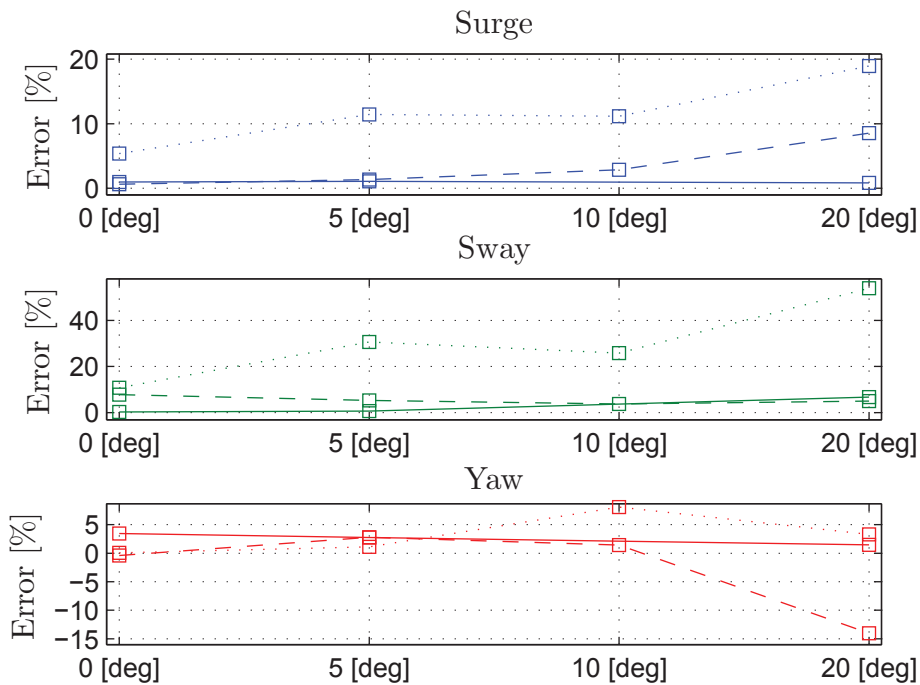


Figure B.3: Results from Case II: Error sorted by DOF, $C = 100$ [%]. -- $h_i = 0.5$ [m], — $h_i = 0.8$ [m], \cdots $h_i = 1.2$ [m].

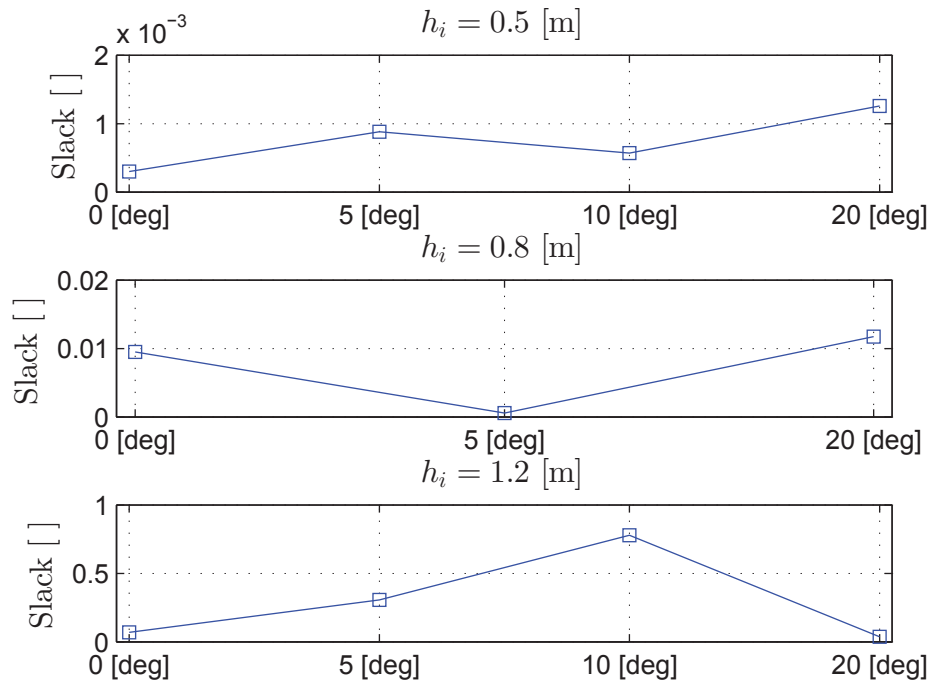


Figure B.4: Results from Case III: $s^\top Qs$, $C = 100$ [%].

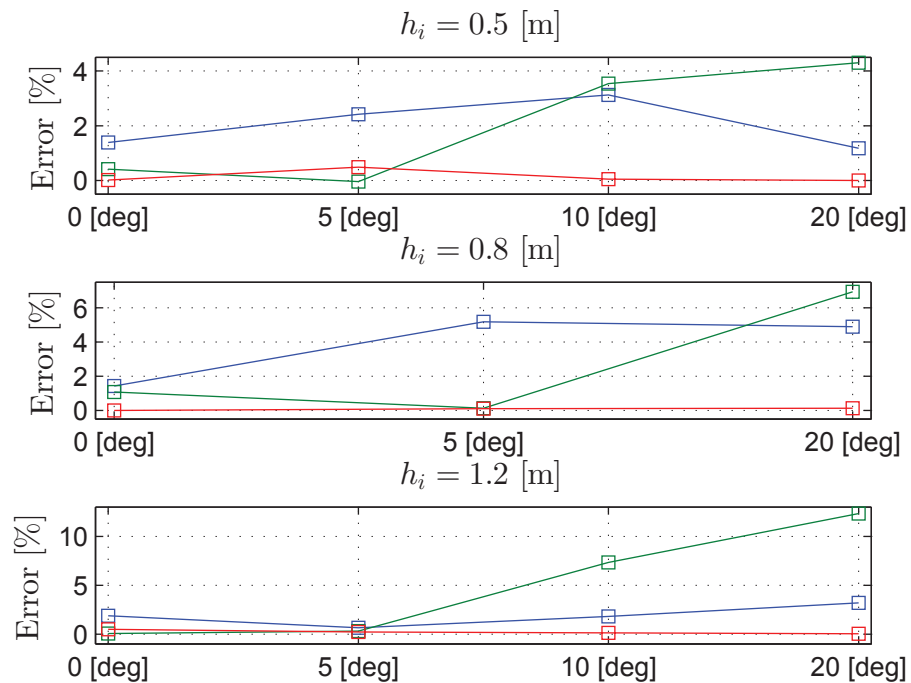


Figure B.5: Results from Case III: Error sorted by h_i , $C = 90$ [%]. — Surge, — Sway, — Yaw.

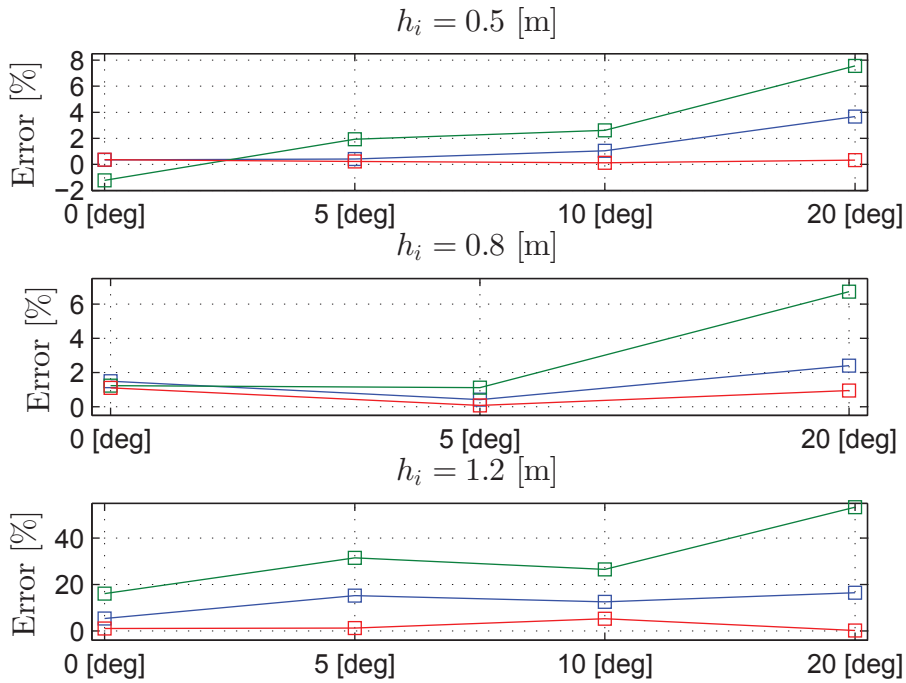


Figure B.6: Results from Case III: Error sorted by h_i , $C = 100$ [%]. — Surge, — Sway, — Yaw.

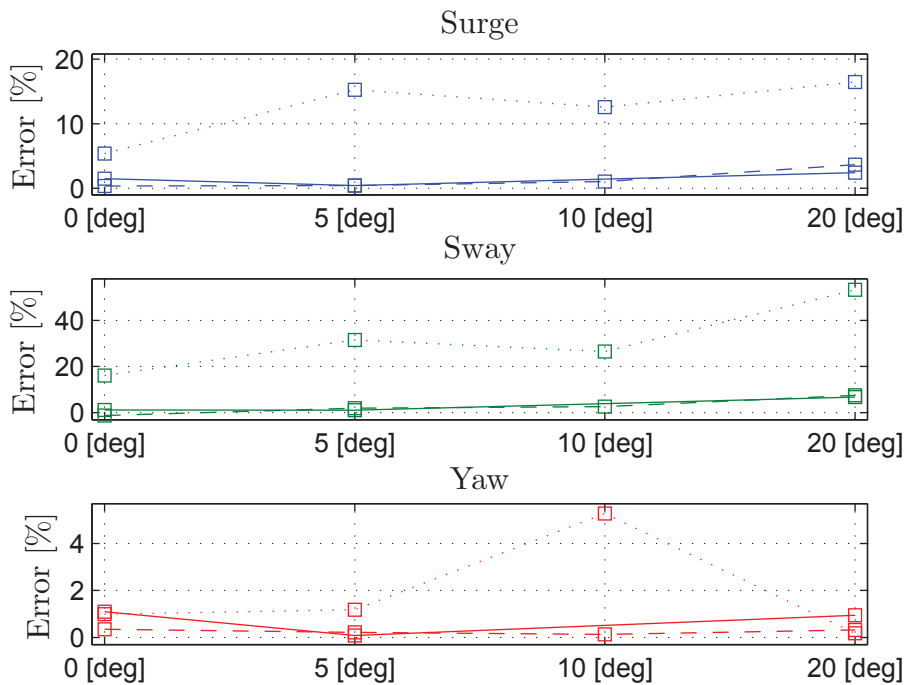


Figure B.7: Results from Case III: Error sorted by DOF, $C = 100$ [%]. - - $h_i = 0.5$ [m], — $h_i = 0.8$ [m], \cdots $h_i = 1.2$ [m].

B.2 Thrust Allocation with Thruster Ice Clearance

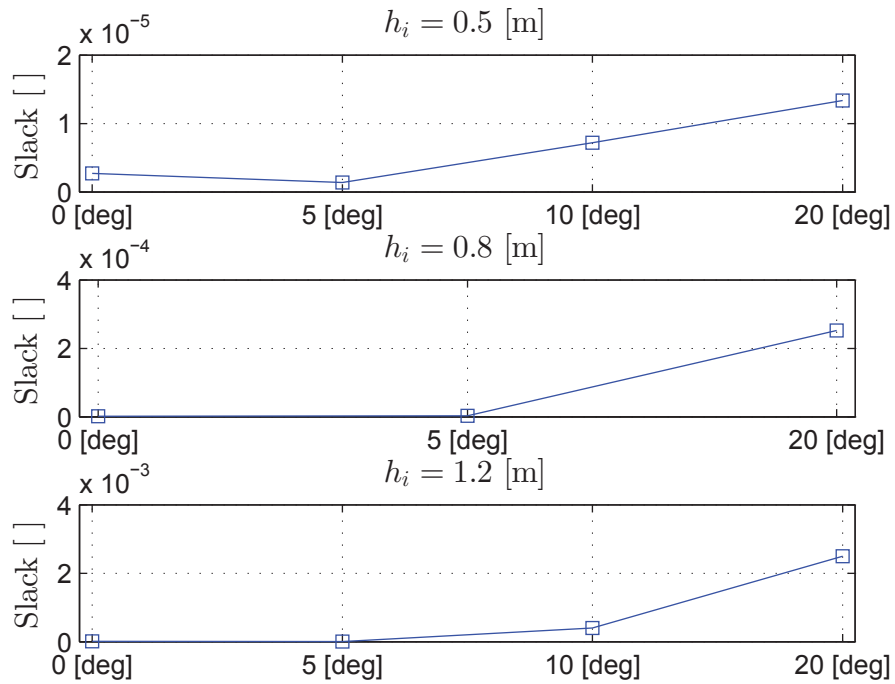


Figure B.8: Results from Case IV: $\mathbf{s}^\top \mathbf{Q} \mathbf{s}$, $C = 90$ [%].

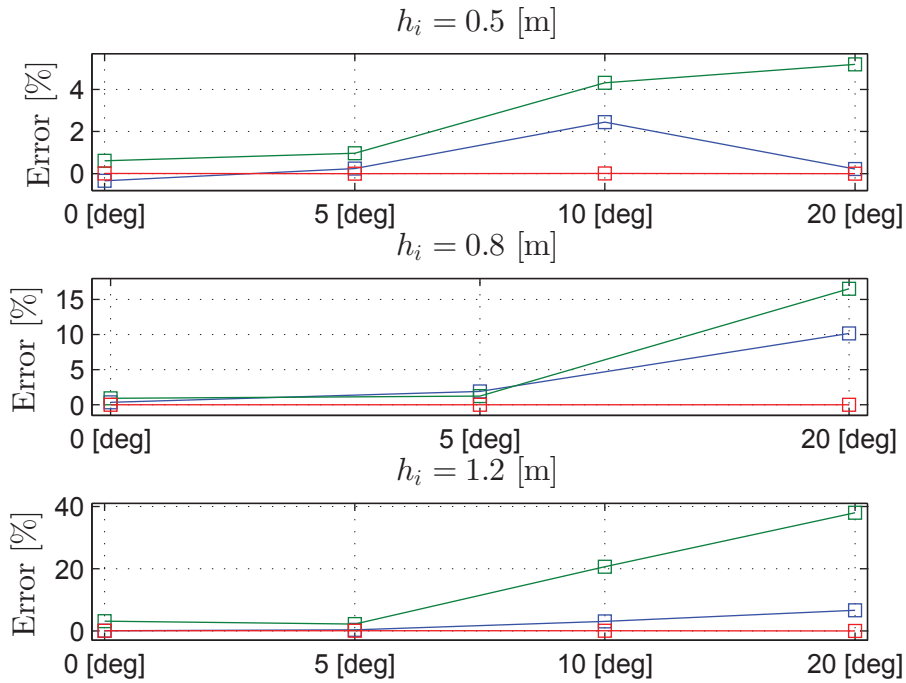


Figure B.9: Results from Case IV: Error sorted by h_i , $C = 90$ [%]. — Surge, — Sway, — Yaw.

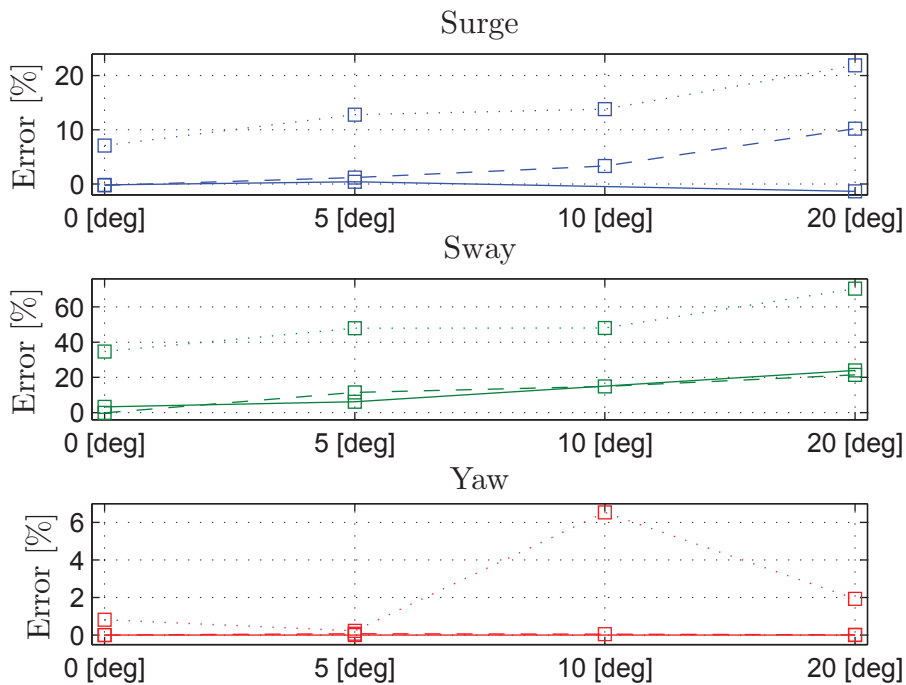


Figure B.10: Results from Case IV: Error sorted by DOF, $C = 100$ [%]. - - $h_i = 0.5$ [m], — $h_i = 0.8$ [m], \cdots $h_i = 1.2$ [m].

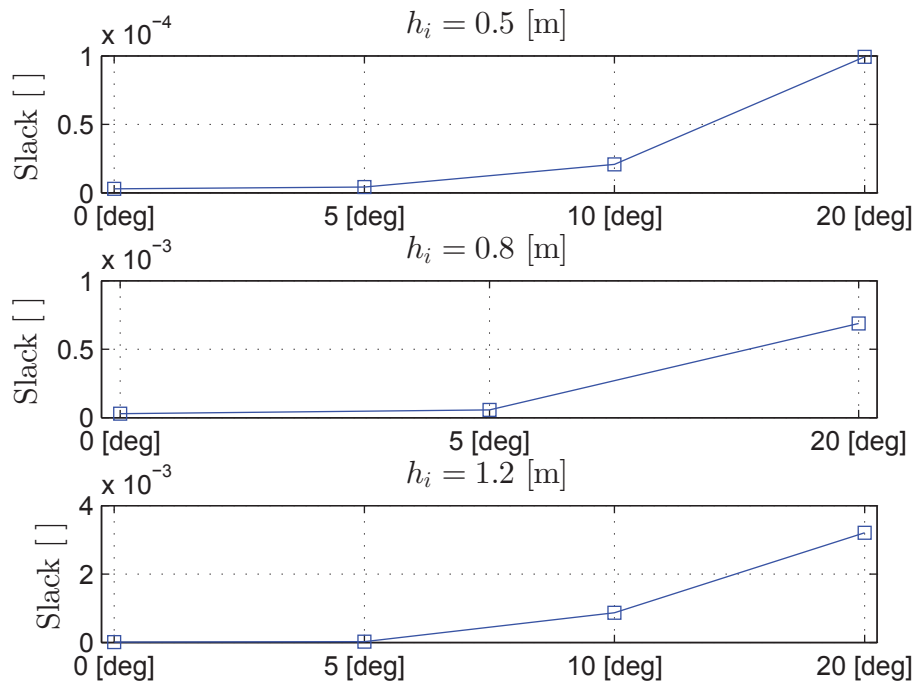


Figure B.11: Results from Case V: $s^\top Qs$, $C = 90$ [%].

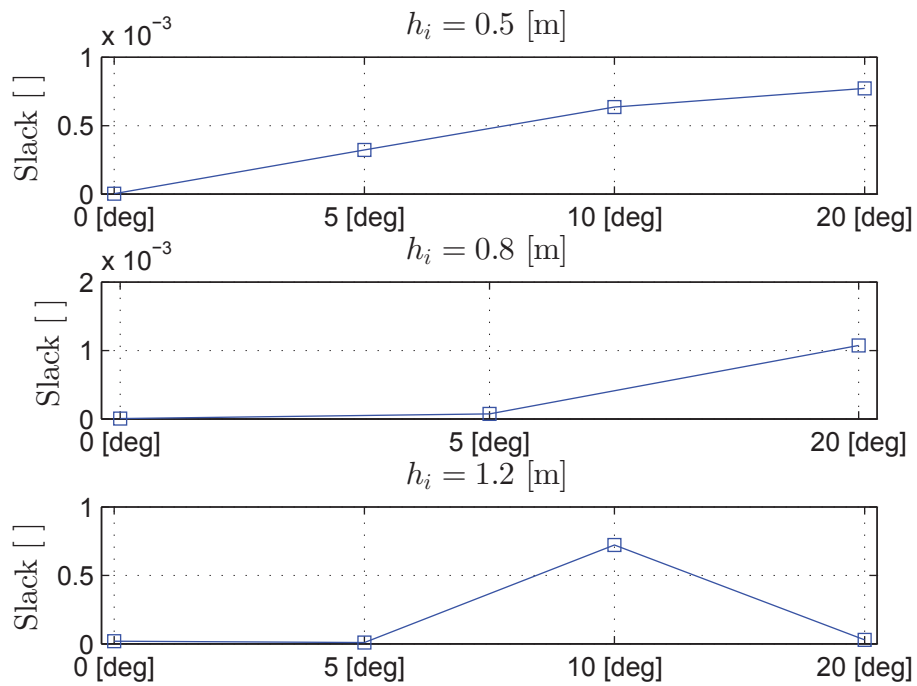


Figure B.12: Results from Case V: $s^\top Qs$, $C = 100$ [%].

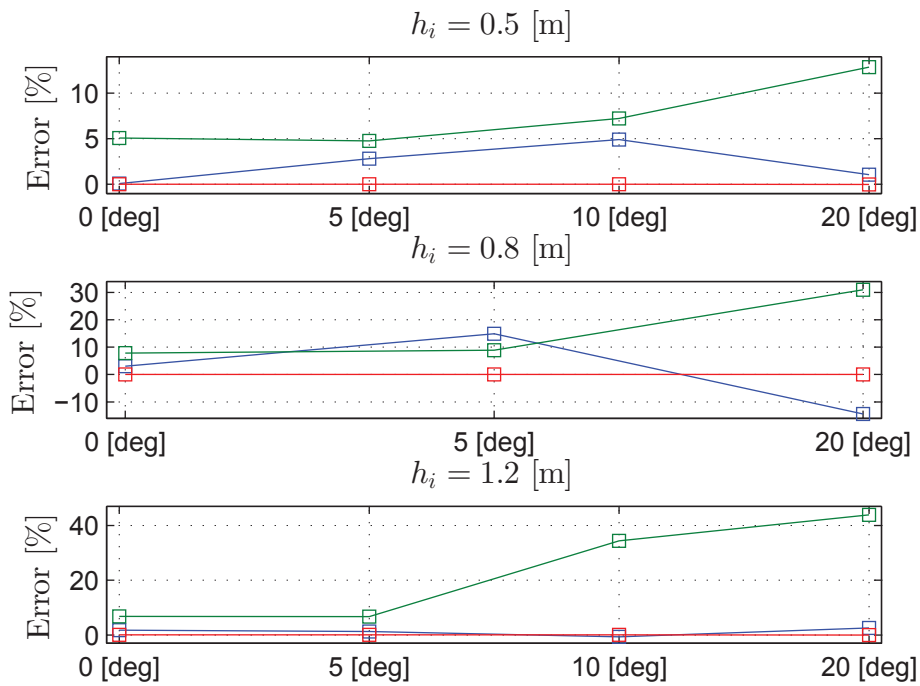


Figure B.13: Results from Case V: Error sorted by h_i , $C = 90$ [%]. — Surge, — Sway, — Yaw.

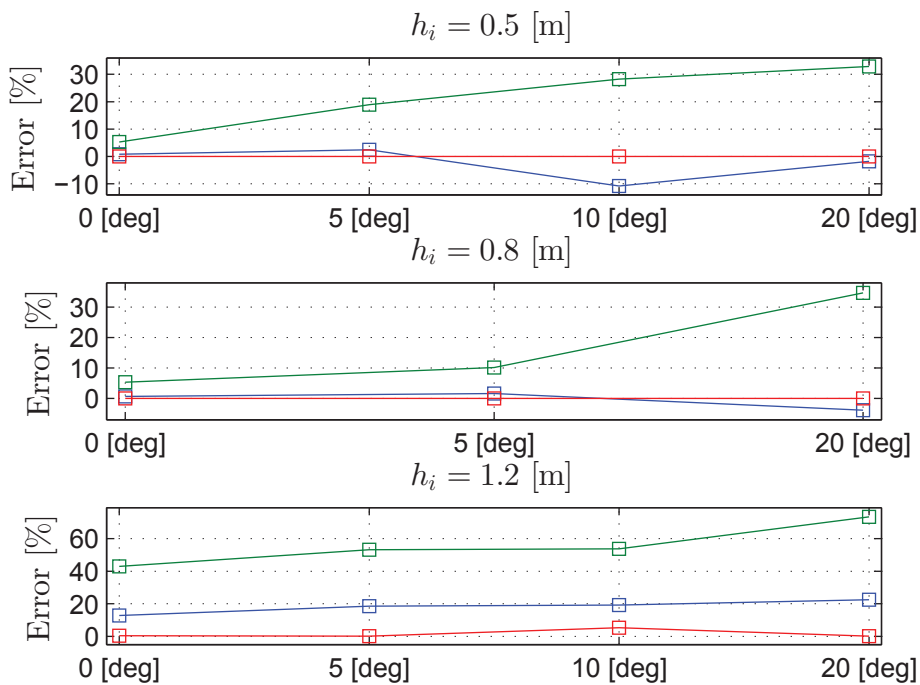


Figure B.14: Results from Case V: Error sorted by h_i , $C = 100$ [%]. — Surge, — Sway, — Yaw.

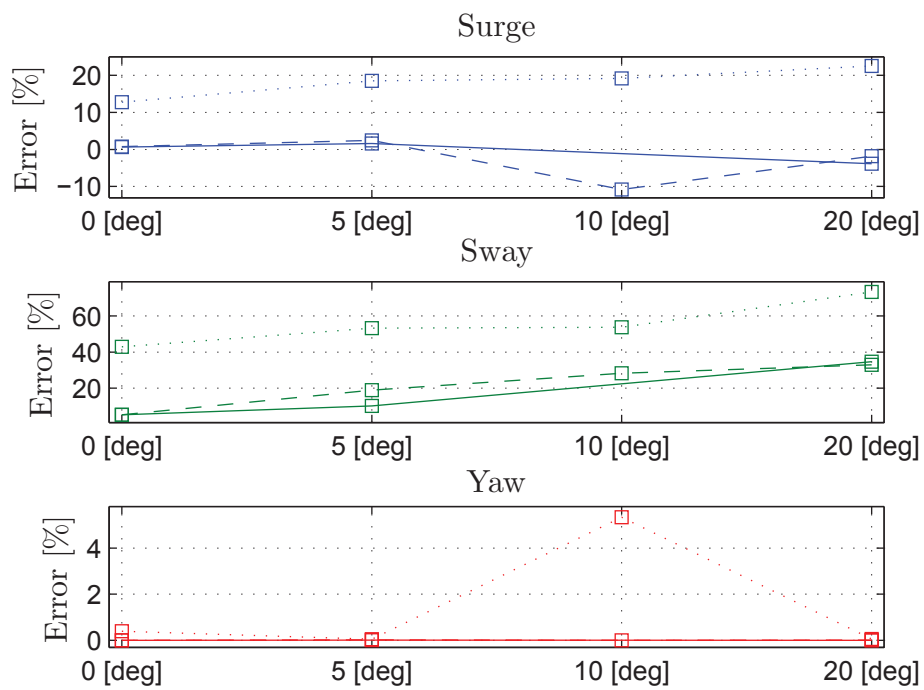


Figure B.15: Results from Case V: Error sorted by DOF, $C = 100$ [%]. - - $h_i = 0.5$ [m], — $h_i = 0.8$ [m], \cdots $h_i = 1.2$ [m].

Appendix C

Energy Consideration Tables

Tables C.1 - C.5 give an indication of if the vessel was able to keep the desired position and heading for the Cases I - V, based on the energy considerations. The energy of τ_{diff} and f_{diff} , for each DOF, were summed up over the time axis and subtracted from each other. If the result was positive, it indicated that the vessel was able to withstand the ice loads over the whole time axis. A negative result indicated the opposite. A positive result is represented with a green check mark and a negative result with a red cross in the tables below.

Table C.1: Results energy considerations, Case I.

h_i [m]	C [%]	θ [deg]	Surge	Sway	Yaw
0.5	90	0	✓	✓	✓
		5	✓	✓	✓
		10	✓	✓	✓
		20	✓	✓	✓
	100	0	✓	✓	✓
		5	✓	✓	✓
		10	✓	✓	✓
		20	✓	✓	✓
0.8	90	0	✓	✓	✓
		5	✓	✓	✓
		20	✓	✓	✓
	100	0	✓	✓	✓
		5	✓	✓	✓
		20	✓	✓	✓
1.2	90	0	✓	✓	✓
		5	✓	✓	✓
		10	✓	✓	✓
		20	✓	✗	✓
	100	0	✓	✓	✓
		5	✗	✗	✓
		10	✗	✗	✓
		20	✗	✗	✓

Table C.2: Results energy considerations, Case II.

h_i [m]	C [%]	θ [deg]	Surge	Sway	Yaw
0.5	90	0	✓	✓	✓
		5	✓	✓	✓
		10	✓	✓	✓
		20	✓	✓	✓
	100	0	✓	✓	✓
		5	✓	✓	✓
		10	✓	✓	✓
		20	✓	✓	✓
0.8	90	0	✓	✓	✓
		5	✓	✓	✓
		20	✓	✓	✓
	100	0	✓	✓	✓
		5	✓	✓	✓
		20	✓	✓	✓
1.2	90	0	✓	✓	✓
		5	✓	✓	✓
		10	✓	✓	✓
		20	✓	✗	✓
	100	0	✓	✓	✓
		5	✗	✗	✓
		10	✗	✗	✓
		20	✗	✗	✓

Table C.3: Results energy considerations, Case III.

h_i [m]	C [%]	θ [deg]	Surge	Sway	Yaw
0.5	90	0	✓	✓	✓
		5	✓	✓	✓
		10	✓	✓	✓
		20	✓	✓	✓
	100	0	✓	✓	✓
		5	✓	✓	✓
		10	✓	✓	✓
		20	✓	✓	✓
0.8	90	0	✓	✓	✓
		5	✓	✓	✓
		20	✓	✓	✓
	100	0	✓	✓	✓
		5	✓	✓	✓
		20	✓	✓	✓
1.2	90	0	✓	✓	✓
		5	✓	✓	✓
		10	✓	✓	✓
		20	✓	✗	✓
	100	0	✓	✓	✓
		5	✗	✗	✓
		10	✗	✗	✓
		20	✗	✗	✓

Table C.4: Results energy considerations, Case IV.

h_i [m]	C [%]	θ [deg]	Surge	Sway	Yaw
0.5	90	0	✓	✓	✓
		5	✓	✓	✓
		10	✓	✓	✓
		20	✓	✓	✓
	100	0	✓	✓	✓
		5	✓	✓	✓
		10	✓	✓	✓
		20	✓	✗	✓
0.8	90	0	✓	✓	✓
		5	✓	✓	✓
		20	✓	✗	✓
	100	0	✓	✓	✓
		5	✓	✓	✓
		20	✓	✗	✓
1.2	90	0	✓	✓	✓
		5	✓	✓	✓
		10	✓	✓	✓
		20	✓	✗	✓
	100	0	✓	✓	✓
		5	✗	✗	✓
		10	✗	✗	✓
		20	✗	✗	✓

Table C.5: Results energy considerations, Case V.

h_i [m]	C [%]	θ [deg]	Surge	Sway	Yaw
0.5	90	0	✓	✓	✓
		5	✓	✓	✓
		10	✓	✓	✓
		20	✓	✓	✓
	100	0	✓	✓	✓
		5	✓	✓	✓
		10	✓	✗	✓
		20	✓	✗	✓
0.8	90	0	✓	✓	✓
		5	✓	✓	✓
		20	✓	✗	✓
	100	0	✓	✓	✓
		5	✓	✓	✓
		20	✓	✗	✓
1.2	90	0	✓	✓	✓
		5	✓	✓	✓
		10	✓	✗	✓
		20	✓	✗	✓
	100	0	✓	✗	✓
		5	✗	✗	✓
		10	✗	✗	✓
		20	✗	✗	✓